Influence of the Ligand Architecture on Reactivity of High-Valent Non-Heme Metal Intermediates

A Thesis Submitted in Partial Fulfillment of the
Requirements for the degree of

DOCTOR OF PHILOSOPHY

Submitted By

Prasenjit Barman

(Roll No. 11612237)

Department of Chemistry

Indian Institute of Technology Guwahati, India

Guwahati-781039

Assam, India

14th September , 2016

Dedicated to

Maa Kamakhya

&

My Family

Contents

Statement

I hereby declare that the matter embodied in this thesis is result of investigations carried out by me in the Department of Chemistry, Indian Institute of Technology Guwahati, India under the guidance of Dr. Chivukula V. Sastri. In keeping with the general practice of reporting scientific observations, due acknowledgements have been made wherever the work described is based on the findings of other investigators.

Prasenjit Barman

Certificate

This is to certify that Prasenjit Barman has been working under my supervision since July 2011 as a regular registered Ph. D. student. I am forwarding his thesis entitled **"Influence of the Ligand Architecture on Reactivity of High-Valent Non-Heme Metal Intermediates"** for being submitted for the Ph. D. (Science) degree of this institute. I certify that he has fulfilled all the requirements according to the rules of this institute regarding the investigations embodied in his thesis and this work has not been submitted elsewhere for a degree.

14th September, 2016.

Dr. Chivukula V. Sastri

Supervisor

Department of Chemistry

Indian Insitute of Technology Guwahati

ACKNOWLEDGEMENT

I express my sincere gratitude to my supervisor, ***Dr. Chivukula V. Sastri*** *(Department Chemistry, Indian Institute of Technology Guwahati) for his meaningful guidance. I earnestly thank him for his guidance, inspiration, priceless suggestions and support, which helped me carry out my Ph.D thesis with utmost success.*

I am also very thankful to my doctoral committee chairman and members Prof. Gopal Das, Dr. M. Qureshi and Dr. Debapratim Das for sparing their precious time to evaluate the progress of my work. I would also like to thank the Head of the Department and the other faculty members for their kind help in carrying out this work. I am also grateful to all the members of the research and technical staff of the department without whose help I could not have completed this thesis.

I would like to acknowledge the Department Of Chemistry, Indian Institute of Technology Guwahati, for providing me the facilities that were necessary to pursue my thesis and all the faculty members for their constant assistance and support.

I would like to thank IIT Guwahati for financial support and all the facilities that were made available to me. I thank CIF, IIT Guwahati for providing the facility of LC-MS, Mr. K. Singh for their help.

I would like to thank my lab senior Dr. Anil KumarVardhaman. He was always present as a friend and guide, always inspired and motivated me from my master's program. Without his help it would not have been possible to achieve my goals. I would also thank my lab juniors: Sayanta and Gourab for their help.

My sincere thanks to my seniors, friends and other research scholars in the department, especially Dr. Babulal Das, Dr. Laxminarayana, Dr. Ziyauddin Khan, Dr. Mohan lal, Dr. Himanshu Sekhar Jena, Dr. Ch. Nagesh, Dr. Srimanta Guin, Dr. Saroj Kumar Rout, Dr. Arghya Banerjee, Dr. Satyapriya Bhandari, Dr. Md Palashuddin Sk, Julu, Samir, Sourav, Sahoo, Anup, Arghya, Sumon, Bhowmik, Bhaswati, Deka, Somnathda, Sujit, Subhasisda, Utpal, Barun, Shilaj, Manas, Buddha, Ganesh, Soumen and Suranjan.

Last but not least: I thank my parents Basudeb-Sulata, my sister Shrabanti, brother-in-law Bibhas, Krittika and Chhanda for their endless moral support and motivation

especially at difficult times. My Ph.D endeavors would not have been completed without their blessings. I express my sincere gratitude to them. I would like to thank all others who are associated with my work directly or indirectly at IIT Guwahati for their help.

Place: IIT GUWAHATI *Sincerely*

Date: 14/09/2016 *(Prasenjit Barman)*

Abstract

Reactivities of the high-valent non-heme metal intermediates have also been investigated exhaustively in past few decades in various oxidation reactions. It has also seen that the reactivities of the high-valent intermediates are highly influenced by primary and secondary coordination spheres along with spin states, solvents, pH etc. In a quest for an efficient biomimetic catalyst with high selectivity and reactivity, one have to understand the factors that control reactivities of non-heme metal complexes in various oxidation reactions. The ligand structure around the central metal ion is one of the important factors that influence these reactivities.

In the present work, the reactivity studies towards S-oxidation, C-H activation, aldehyde deformylation, ClO_2 formation with high-valent Mn(IV)-oxo, Mn(III)-peroxo, Fe(IV)-oxo and Fe(IV)-imido species supported by pentadentate ligands have been evaluated. These reactivity studies provide remarkable insights into the mechanistic pathway of these intermediates with changing ligand architecture.

The reactivities of two isomeric bispidine Mn(IV)-oxo complexes were compared in oxidation reaction and observed that one of the isomer was more reactive and also showing an opposite reactivity pattern with corresponding Fe^{IV}=O complexes. Deformylation reaction by Mn(III)-peroxo has been evaluated and was found that it reacts through hydrogen atom abstraction reactions instead of the commonly proposed nucleophilic addition reaction. Reaction bifurcation was observed with changing ligand structure during the formation of chlorine dioxide. Steric factor at terminal oxidants plays a crucial role in Fe(IV)-oxo and Fe(IV)-imido complexes towards alcohol oxidation reaction.

Graphical Abstract of the Thesis

CHAPTER-III

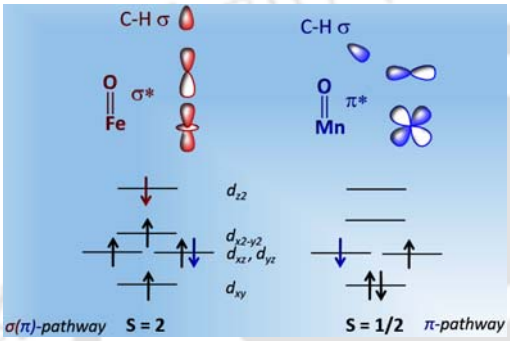

Angew. Chem. Int. Ed. **2015**

CHAPTER-IV

Angew. Chem. Int. Ed. **2016**

CHAPTER-V

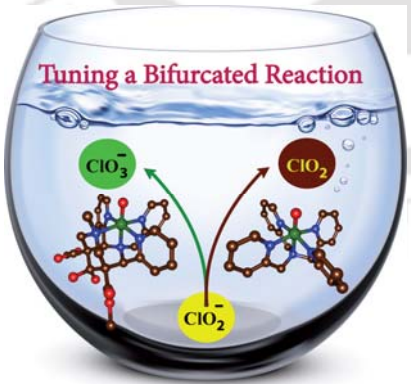

Inorg. Chem. **2016**

CHAPTER-VI

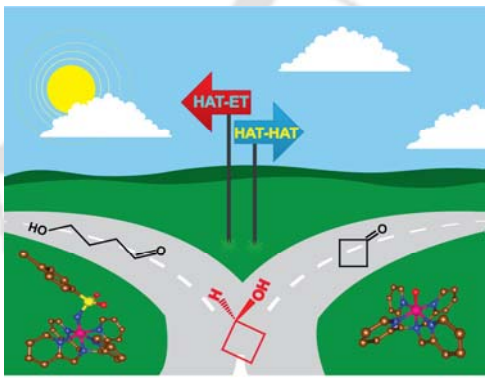

J. Am. Chem. Soc. **2014**

List of Tables

List of Figures and Schemes

Abbreviations

α-KG	α-ketoglutarate
BLM	Bleomycin
DFT	Density functional theory
Bn-Tpen	N-benzyl-N,N',N'-tris(2-pyridylmethyl)-1,2-diaminoethane
CAN	Cerium (IV) ammonium nitrate
CHD	1,4-cyclohexadiene
KO_2	Potassium superoxide
DBT	Dibenzothiophene
DHA	9,10-dihydroanthracene
DMSO	Dimethyl sulphoxide
$EDTA^{4-}$	Ethylenediaminetetraacetate
ESI-MS	Electrospray ionization mass spectrometry
EXAFS	Extended x-ray absorption fine structure
KIE	Kinetic isotope effect
LMCT	Ligand to metal charge transfer
m-CPBA	meta chloro per benzoicacid
MeCN	Acetonitrile
MeOH	Methanol
NADH	Nicotinamide adenine dinucleotide Hydride
N4Py	N-bis(2-pyridylmethyl)-N-bis(2-pyridyl)methylamine

NMR	Nuclear magnetic resonance
BPMCN	N,N'-bis(2-pyridylmethyl)-N,N'-dimethyl-trans-1,2-diaminocyclohexane
OTf	Triflate
PCET	Proton coupled electron transfer
PhIO	Iodosylbenzene
PhINTs	[N-(p-tolylsulfonyl)-imino)]phenyliodinane
PPh_3	Triphenylphosphine
TAML	tetraamidomacrocyclic ligand
TauD	taurine/α-KG dioxygenase
BQCN	N,N'-dimethyl-N,N'-bis(8-quinolyl) cyclohexanediamine
$[H_3buea]^{3-}$	tris[(*N'-tert*-butylureaylato)-Nethylene]aminato
^{H,Me}Pytacn	1-[(6-methyl-2-pyridyl)methyl]-4,7-dimethyl-1,4,7-triazacyclono nane
$[H_2bupa]^{3-}$	bis[(N'-t-butylurealy)-N-ethyl](6-pivalamido-. 2-pyridylmethyl)-aminato
TMC	Tetramethylcyclam
TMG_3tren	1,1,1-tris{2-[N^2-(1,1,3,3-tetramethylguanidino)]ethyl}amine
TPA	tris(2-pyridylmethyl)amine

Compounds Abbreviations by Chapter

Chapter 3

3	$[Mn^{IV}(O)(L^{1})]^{2+}$
4	$[Mn^{IV}(O)(L^{2})]^{2+}$

Chapter 4

5	$[Mn^{III}(O_2)(L^{1})]^{2+}$

Chapter 6

6	$[Fe^{IV}(O)(N4Py)]^{2+}$
7	$[Fe^{IV}(NTs)(N4Py)]^{2+}$

Synopsis

The thesis entitled **"Influence of the Ligand Architecture on Reactivity of High-valent Non-Heme Metal Intermediates"** deals with exploring novel reactivities of high-valent metal intermediates towards various substrates that incorporate well characterized pentadentate ligands viz. N4Py and Bispidine (N4Py = N,N-bis(2-pyridylmethyl)-N-bis(2-pyridyl)methylamine) (Bispidine = dimethyl-2,4-di(2-pyridyl)-3-methyl/benzyl-7-(pyridin-2-ylmethyl)-3,7-diazabicyclo[3.3.1]nonan-9-one-1,5-dicarboxylate).

Enzymes plays key role in most of the biological functions. Nature has taken advantage of the special properties of the metal ions and tuned them by encapsulation with different protein matrices to perform a large variety of specific functions associated with life processes. Metals play roles in approximately one-third of the known enzymes. Metals may be a co-factor or they may be incorporated into the molecule, and these are known as metalloenzymes.

Biologically relevant metals like Mn, Fe, Co, Ni, Cu and Zn are the obvious working examples for biomimetic chemistry. Iron is one of the most essential elements for life, found in the active site of many proteins and enzymes and plays key roles in many biological processes. Manganese also found in many enzymes active site, including manganese superoxide dismutase, manganese catalase, and manganese ribonucleotide reductase. The iron containing proteins are broadly classified into two categories: heme and non-heme. The metalloproteins bearing a porpyrin submit are classified as heme systems and the rest of the metalloproteins having non-porphyrin subunits are classified as non-heme proteins.

Oxygen-containing mononuclear metal (Fe, Mn, Ni, Co) species like metal(III)–peroxo, metal(III)–hydroperoxo, metal(III/II)-superoxo and metal(IV)–oxo are key intermediates in the catalytic activation of dioxygen by metalloenzymes. Many non-heme Fe/Mn containing enzymes act by catalyzing the activation of dioxygen (O_2) in many metabolically important functions. Oxygen-coordinating metal intermediates, such as metal superoxo, peroxo, hydroperoxo and oxo species, play central roles in many biological and catalytic processes. In all the iron catalyzed biochemical reactions the suspected intermediates are describe below in Figure 1.

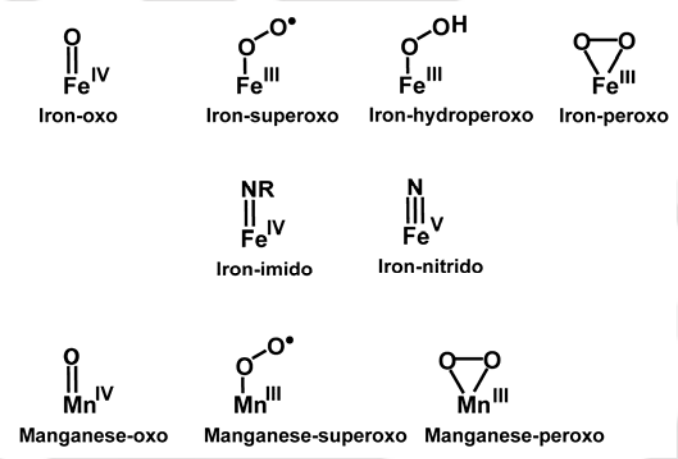

Figure 1. Plausible high-valent Iron and Manganese intermediates with Oxygen and Nitrogen.

The work embodied in this thesis has been divided into six Chapters. A brief, Chapter-wise account of the results is presented below.

Chapter-1. Introduction

In this chapter, recent literature relevant to metal(IV)-oxo, metal(III)-hydroperoxo, metal(III)-peroxo and metal(IV)-imido complexes with iron as well

as manganese and their reactivity studies have been reviewed as function of their spectroscopic and structural information, kinetics, reactivity trends and mechanistic insights. Recent developments taken place by high-valent non-heme iron complexes are also discussed.

Chapter-2. Material and Methods

A general description of the synthesis of various precursor compounds and high-valent non-heme metal complexes as well as the spectroscopic, ESI-MS and NMR techniques employed during the research work is presented in this chapter.

Chapter-3. Influence of Ligand Architecture on Oxidation Reactions by High-valent Manganese-Oxo Complexes Using Water as a Source of Oxygen

The non-heme manganese chemistry of biomimetic systems and enzymes led to the characterization of a number of high-valent Mn^{IV}=O intermediates in electrophilic oxygenation reactions. Here in, report, a mononuclear non-heme Mn^{IV}=O complexes with two isomers of a bispidine ligand that are synthesized and characterized by various spectroscopic methods. The Mn^{IV}=O complexes show reactivity in oxidation reactions (hydrogen abstraction, HAT, and sulfoxidation). Interestingly, one of the isomers (L^1) is significantly more reactive than the other (L^2), while in the corresponding iron(IV)-oxo based oxidation reactions the L^2–based system was previously found to be more reactive than the L^1–based catalyst.

$[Mn^{II}(L^1)(ClO_4)_2]$ (**1**) and $[Mn^{II}(L^2)(ClO_4)_2]$ (**2**) (L^1 = dimethyl-2,4-di(2-pyridyl)3-(pyridin-2-ylmethyl)-7-benzyl-3,7-diaza-bicyclo[3.3.1] nonan-9-one-1,5-dicarboxylate, L^2 = dimethyl-2,4-di(2-pyridyl)3-benzyl-7-(pyridin-2-

ylmethyl)-3,7-diaza-bicyclo[3.3.1] nonan-9-one-1,5-dicarboxylate) were prepared in acetonitrile were structurally characterized with various spectroscopic methods. The high-valent Mn^{IV}=O intermediates, $[Mn^{IV}(O)L^{1}]^{2+}$ (**3**; 2 mM) and $[Mn^{IV}(O)L^{2}]^{2+}$ (**4**; 2 mM) were generated from their Mn^{II} precursors, using cerium(IV) ammonium nitrate (CAN) (8 mM) as a one electron oxidant in acetonitrile/water (9:1) or acetone/water (9:1) at 5 ºC. The addition of Ce^{IV} to the colorless solution of the Mn^{II} complexes produced pale green solutions. Complex **3** exhibits absorption spectra with an intense band at 545 nm ($\varepsilon \approx 400$ $M^{-1}cm^{-1}$), with a weak absorption in the near IR region at 970 nm ($\varepsilon \approx 35$ $M^{-1}cm^{-1}$). Similarly, complex **4** has electronic transitions at 570 nm ($\varepsilon \approx 400$ $M^{-1}cm^{-1}$) and at 975 nm ($\varepsilon \approx 103$ $M^{-1}cm^{-1}$, Figure 2). The electro-spray ionization mass spectra (ESI-MS) of **3** and **4** exhibit prominent peaks with *m/z* ≈ 332, and the isotope patterns show that these correspond to $[Mn^{IV}(O)L^{1,2}]^{2+}$.

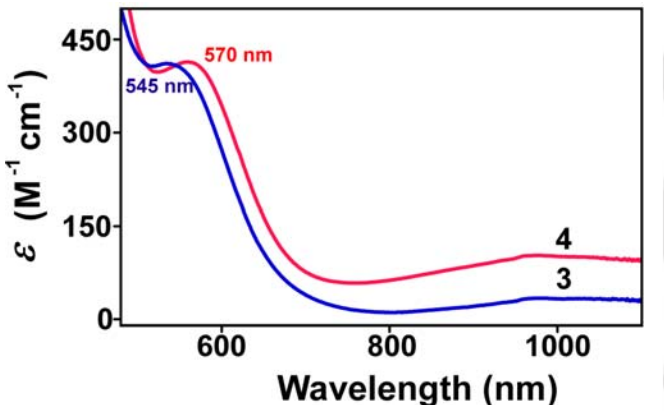

Figure 2. UV/Vis spectra of **3** (blue line) and **4** (red line), generated in the reactions of **1** (2 mM) and **2** (2 mM) with CAN (8 mM) in CH_3CN / H_2O (9:1) at 5 ºC.

The reactivity of **3** and **4** was carried out in the presence of 2-electron oxidation substrates such as oxidation of sulphur of thioanisole. Upon the addition of thioanisole to the corresponding intermediate solution at 5 ºC , the

intermediate decayed immediately to yield methyl-phenyl sulfoxide as a major product . The second-order rate constant, determined by pseudo-first-order fitting of the kinetic data for the decay of **3** and **4** respectively, increased linearly with increasing thioanisole concentration, giving second-order rate constants of **3** and **4** as about 1.2 x 10^{-1} M^{-1} s^{-1} and 1.2 x 10^{-2} M^{-1} s^{-1} respectively (Figure 3). It appears, therefore, that the $[Mn^{IV}(O)(L^1)]^{2+}$ complex *reacts with thioanisole with rate constants that are about ten times higher than those found for the* $[Mn^{IV}(O)(L^2)]^{2+}$ *complex.* It is interesting to note that previously it was reported that in case of iron(IV)-oxo the L^2 based ligand is more reactive than L^1. In order to further elucidate the reaction pathway, second-order rate constants (k_X) for the oxidation of various *para* substituted thioanisole substrates (k_H is the second order rate constant for thioanisole) with the oxidant **4** were also determined: a plot of the logarithm of the rate constant ratio [$\log(k_X/k_H)$] against the one-electron oxidation potentials (E^0_{OX}) of the sulfides gave a linear correlation with a slope of -10.8. Similar large slope values were also obtained in Hammett correlations. Such a large negative slope implies that the electron transfer from the sulfides to **4** rather than a group transfer are the rate-determining step.

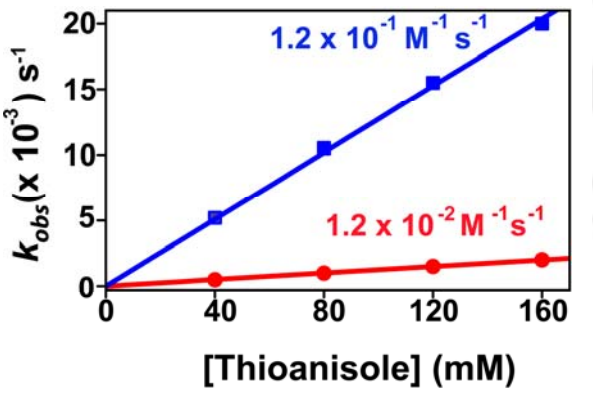

Figure 3. Second order rate constants determined in the reaction of 2 mM of **3** (■) and **4** (●) in CH_3CN / H_2O (9:1) against various concentrations of thioanisole at 5 ºC.

The reactivity of **3** and **4** was investigated kinetically in hydrogen atom abstraction reaction of 2,4-di-*tert*-butylphenol at -40 ºC. In this case the **3** *shows a high reactivity at about 40 times greater than that of* **4**. To further substantiate the H-atom abstraction reaction with phenol, evaluated the corresponding second-order rate constants with series of *para* substituted 2,6-di-*tert*-butylphenol substrates. A plot of the logarithm of the rate constant ratio [$\log(k_X/k_H)$] as a function of σ_p^+ shows an excellent Hammett correlation with a ρ value of -1.6. Such a linear relationship has been used as evidence for an H-atom abstraction pathway in the oxidation of phenol O-H bonds. As further support, also plotted $\log(k_X/k_H)$ values against the phenol O-H bond dissociation energy (BDE), which afforded a good correlation with a slope of -0.40. That indicates the H-atom abstraction in the rate determine step.

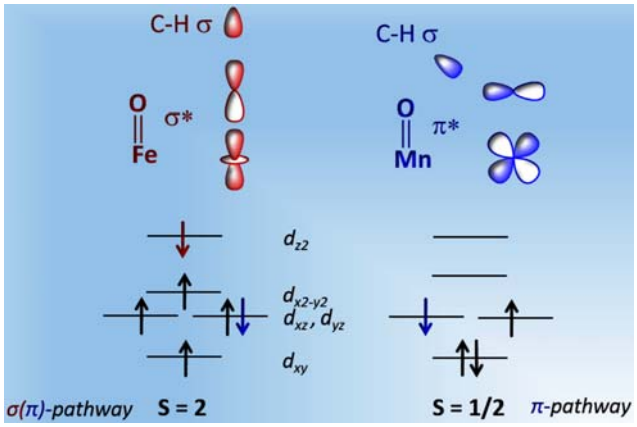

Mn(II) complexes of ligand L^1 and L^2 has been successfully synthesized and well characterized by spectroscopic techniques. Generation of high-valent Mn^{IV}=O complexes using water as an oxygen source by reacting Mn(II) complexes with Ce(IV) in CH_3CN / H_2O (9:1) at 5 ºC. The reactivity and mechanistic pathway of oxygen atom transfer reactions with thioanisole and various *para* substituted

thioanisole and proved that Mn^{IV}=O complex of L^1 shows 10 times faster reactivity than L^2 and reaction proceed by an electron transfer pathway. Where as in hydrogen atom abstraction reaction Mn^{IV}=O of L^1 complex shows 40 times more reactive than L^2. Interestingly Mn^{IV}=O complexes were showing an opposite reactivity pattern with recently reported corresponding Fe^{IV}=O complexes. This inversion of reactivity is discussed on the basis of DFT and molecular mechanics (MM) model calculations, which indicate that the order of reactivities are primarily due to a switch of reaction channels (σ vs.π) and concomitant steric effects.

Chapter-4. Deformylation Reaction by a Non-heme Manganese(III)-Peroxo Complex via Initial Hydrogen Atom Abstraction

Manganese-dioxygen adduct have been postulated to be a key intermediate to small molecule activation as well as manganese containing enzyme. A varied range of Mn^{III} intermediates were generated and studied with different set of ligands using various spectroscopic techniques, including UV/Vis with variable temperature, electron paramagnetic resonance (EPR), and X-ray absorption, magnetic circular dichroism (MCD), variable-temperature, variable-field (VTVH) MCD. Metal-peroxo intermediates are key species in the catalytic cycles of non-heme metalloenzymes, but their chemical properties and reactivity patterns are still poorly understood. The synthesis and characterization of a manganese(III)-peroxo complex with a pentadentate bispidine ligand system and its reactivity with aldehydes has been studied.

Manganese(II) complex, $[Mn^{II}(L^1)(ClO_4)_2]^{2+}$ (**1**), (L^1 = dimethyl-2,4-di(2-pyridyl)3-(pyridin-2-ylmethyl)-7-benzyl-3,7-diaza-bicyclo[3.3.1] nonan-9-one-1,5-dicarboxylate) was synthesized by reacting $Mn^{II}(ClO_4)_2 \cdot 2CH_3CN$ with the pentadentate bispidine ligand (L^1) in CH_3CN under an argon atmosphere.

Addition of 10 equivalents of H_2O_2 to a colorless solution containing $[Mn^{II}(L^1)(ClO_4)_2]^{2+}$ (**1**; 2 mM) and triethylamine (TEA; 2.5 equivalents) in an acetonitrile solution at 15 ºC afforded a blue intermediate (**5**) with an absorption band at 605 nm ($\varepsilon \approx 270$ M^{-1} cm^{-1}; with a half-life ~60 minutes). The blue intermediate is characterized with various spectroscopic techniques including UV-vis, electrospray ionization-mass spectrometry (ESI-MS). The ESI mass spectra of **5** exhibit a prominent ion peak with *m/z* = 678.31 whose isotopic distribution pattern corresponds to $[Mn^{III}(L^1)(O_2)]^+$. The nucleophilic and electrophilic character of **5** was then investigated in a reaction with 2-PPA as a substrate. Previous work showed that manganese(III)-peroxo complexes react with aldehydes to give the corresponding deformylated products by attacking the carbonyl group in a nucleophilic reaction. Addition of 2-PPA to **5** in CH_3CN at 15 ºC, the intermediate decayed immediately and led to acetophenone as product (Figure 4a). The pseudo-first-order rate constant of the decay of **5** increased linearly with increasing 2-PPA concentration, thus giving a second-order rate constant of 2.74×10^{-2} M^{-1} s^{-1} (Figure 4b).

To establish whether the mechanism proceeds through a nucleophilic attack on the carbonyl group, 2-methyl-2-phenylpropionaldehyde (2-Me-2-PPA) used as a mechanistic probe. Upon addition of 2-Me-2-PPA to **5** at 15 ºC, the intermediate decays at the rate of its natural decay. However, when the reaction solutions were analyzed with ESI-MS no deformylated products were observed. These results demonstrate that the manganese(III)-peroxo does not react with 2-PPA through a nucleophilic attack on the carbonyl group. In order to find out, whether an alternative pathway was possible starting with an initial hydrogen atom abstraction, decided to investigate the reaction with α-[D_1]-PPA.

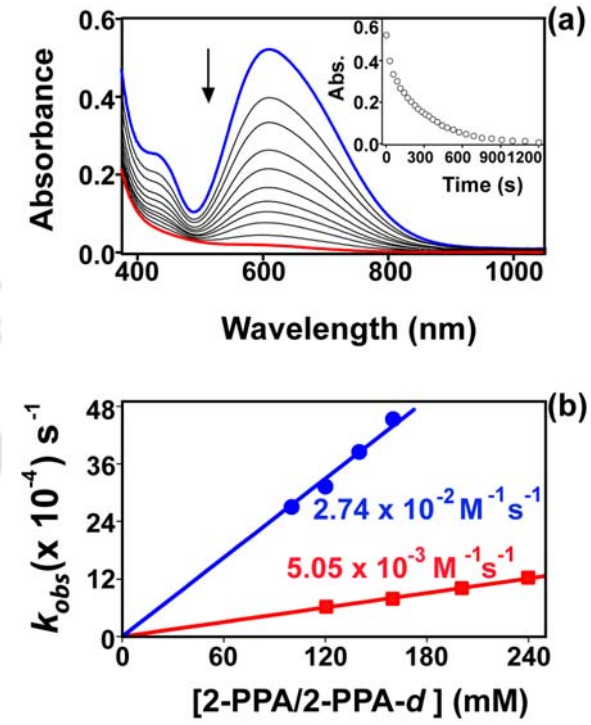

Figure 4. Kinetics of the reaction of **5** with 2-PPA: a) UV/Vis spectral changes of **5** (2 mM) upon addition of 2-PPA (160 mM) in the presence of TEA (5 mM) and hydrogen peroxide (20 mM) in CH_3CN at 15 ºC. Inset shows the time course of the absorbance at 605 nm. b) Plot of k_{obs} against the concentration of 2-PPA and α-[D_1]-PPA (~90%, D enriched) and the derived second-order rate constant for the reaction of 2 mM **5** with substrate at various concentrations in CH_3CN at 15 ºC for 2-PPA (•) and α-[D_1]-PPA (■).

Thus, upon addition of α-[D_1]-PPA (~90%, D enriched) to **5** in CH_3CN at 15 ºC determined a second-order rate constant of 5.05 × 10^{-3} M^{-1} s^{-1} (Figure 4b).Therefore, our kinetics studies establish the manganese(III)-peroxo complex to react with 2-PPA via a rate determining hydrogen atom abstraction reaction from the α-position with a kinetic isotope effect (KIE) of 5.4. To find further evidence of this novel reaction mechanism, performed a radical trapping experiment with bromotrichloro-methane. Addition of 2-PPA to intermediate **5** in

the presence of excess CCl_3Br (or CBr_4) in CH_3CN at 15 ºC, leads to the formation of α-brominated product of the 2-PPA exclusively.

Manganese(III)-peroxo complex with a pentadentate bispidine ligand system has been synthesized and characterized and studied its reactivity with aldehydes. Manganese(III)-peroxo can react through hydrogen atom abstraction reactions instead of the commonly proposed nucleophilic addition reaction. Evidence of the mechanism comes from experiments which identify a primary kinetic isotope effect of 5.4 for the deformylation reaction. For the help of density functional theory, found that the side-on manganese-peroxo with bispidine ligand system will preferentially react via hydrogen atom abstraction rather than nucleophilic addition with aldehydes through its availability of low-energy metal 3d orbitals that can pick up an electron from the peroxo group.

Chapter-5. Influence of Ligand Architecture in Tuning Reaction Bifurcation Path-ways for Chlorite Oxidation by Non-heme Iron Complexes

Reaction bifurcation processes are often encountered in the oxidation of substrates by enzymes and generally lead to a mixture of products. One particular bifurcation process that is common in biology relates to electron transfer versus oxygen atom transfer processes by high-valent iron(IV)-oxo complexes, which Nature uses for the oxidation of metabolites and drugs. In biomimicry and bioremediation an important reaction relates to the detoxification of ClO_x^- in water, which can lead to a mixture of products through bifurcated reactions. Bioremediation of oxido anions of chlorine (ClO_x^-) is important for the generation of clean drinking water. However, efficient and cheap catalysts for this process with iron are rare. Three water soluble iron(II) complexes for the production of chlorine dioxide from chlorite under ambient temperature at physiological pH has been studied.

Ligands, N4Py = N,N-bis(2-pyridylmethyl)-bis(2-pyridyl) methylamine, L^1 = dimethyl 2,4-di(2-pyridyl)3-(pyridin-2-ylmethyl)-7-methyl-3,7-diazabicyclo [3.3.1]nonan-9-one-1,5-dicarboxylate and L^2 = dimethyl 2,4-di(2-pyridyl)-3-methyl-7-(pyridin-2-ylmethyl)-3,7-diazabicyclo[3.3.1]nonan-9-one-1,5-dicarboxylate and its corresponding Fe(II) complexes were prepared and characterized by spectroscopic methods. The reactivity of sodium chlorite with nonheme iron(II) complexes with pentadentate ligands N4Py, L^1 and L^2 was investigated in acetate buffer (50 mM) at pH=5.0 at 25 °C. Addition of the iron(II) complexes to solutions of sodium chlorite ($NaClO_2$), there is an increase in absorbance at 360 nm, characteristic for the formation of chlorine dioxide. Figure 5a shows the spectral changes for the reaction of $[Fe^{II}(L^1)]^{2+}$ with ClO_2^-, whereas those involving the $[Fe^{II}(L^2)]^{2+}$ and $[Fe^{II}(N4Py)]^{2+}$ complexes where the

same spectral changes are observed. Negative ion mode ESI-MS of a diethyl ether extract of the reaction mixture (Inset of Figure 5a) shows a signal with an isotopic pattern consistent with ClO_2 formation (*m/z* = 67.14). The reaction reaches a maximum in conversion within 40 min with oxidant loading of 10 μM at 25ºC and pH 5.0. The first-order rate constants as a function of oxidant concentration for the reaction of ClO_2^- with $[Fe^{II}(N4Py)]^{2+}$, $[Fe^{II}(L^1)]^{2+}$ and $[Fe^{II}(L^2)]^{2+}$ were determined. The second-order rate constants of k_2 = 10 M^{-1} s^{-1} and 32 M^{-1} s^{-1}, respectively, for $[Fe^{II}(L^1)]^{2+}$ and $[Fe^{II}(L^2)]^{2+}$ (Figure 5b) were determined from the dependence of the rate of generation of ClO_2 on the initial concentrations of the iron(II) complexes.

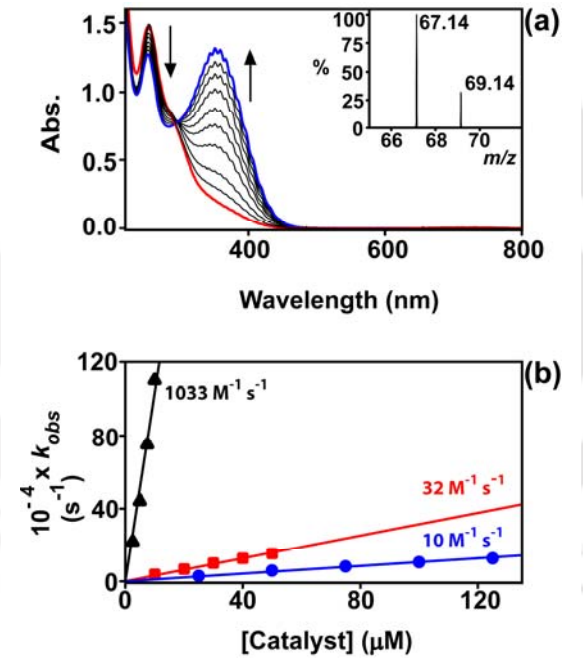

Figure 5. Spectroscopic and kinetics studies for the reaction of iron(II) complexes with ClO_2^-. (a) Changes in the UV/Vis absorption spectra at a scan interval of every 180s upon the addition of 8.0 mM $NaClO_2$ to 50 μM $[Fe^{II}(L^1)]^{2+}$ in an acetate buffer. Inset shows ESI-MS of products obtained. (b) Second order rate constants obtained for the reaction of ClO_2^- with $[Fe^{II}(N4Py)]^{2+}$ (▲), $[Fe^{II}(L^1)]^{2+}$ (●) and $[Fe^{II}(L^2)]^{2+}$ (■).

These reaction rates correspond to a maximum yield of 13 and 10% with respect to iron for $[Fe^{II}(L^1)]^{2+}$ and $[Fe^{II}(L^2)]^{2+}$, respectively. In comparison to the bispidine-type complexes, addition of 10 μM $[Fe^{II}(N4Py)]^{2+}$ to chlorite (4 mM) resulted in the immediate appearance of an absorption band at 360 nm with second-order rate constants of k_2 = 1033 M^{-1} s^{-1} (Figure 5b) and maximum yield of 16%. In order to prove the bifurcation pathway in the reaction mixture, an assay experiment with both the complexes has been studied. The content of ClO_3^- in the product mixture was determined using *o*-tolidine. It should be noted that *o*-tolidine reacts with ClO_3^- but not with either ClO_2^- or ClO_2. Reaction of the iron(II) bispidine complexes with $NaClO_2$ in acetate buffer in the presence of *o*-tolidine at ambient temperature results in the appearance of a band at 442 nm corresponding to 3,3′-dimethyl-4-amino-4′-nitrobiphenyl (Figure 6a). The ESI-MS spectrum (after extraction) shows a signal at *m/z* = 242.24 corresponding to the oxidized product. In addition, a signal at *m/z* = 227.07 corresponding to the partially oxidized nitroso intermediate is observed (Figure 6b). In contrast, the reaction with $[Fe^{II}(N4Py)]^{2+}$ did not result in the formation of products associated with the reaction of *o*-tolidine with ClO_3^-. Instead a peak at 388 nm was observed in the UV/Vis absorption spectrum indicating the presence of ferric species (Figure 6a). ESI-MS analysis of the organic extracted phase did not show significant formation of the nitro derivate, which may be a consequence of subsequent reaction in the oxidation of ClO_2^-. Hence, the bispidine based complexes, $[Fe^{II}(L^1)]^{2+}$ and $[Fe^{II}(L^2)]^{2+}$ react via oxygen atom transfer processes with the formation of ClO_3^- products as the dominant pathway, whereas $[Fe^{II}(N4Py)]^{2+}$ reacts to yield ClO_2 and related products through a one-electron transfer process.

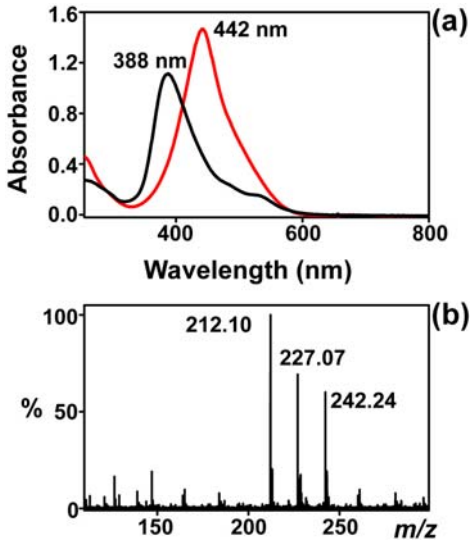

Figure 6. (a) UV/Vis absorption spectra of $[Fe^{II}(N4Py)]^{2+}$ (10 μM, 388 nm) and $[Fe^{II}(L^2)]^{2+}$ (10 μM, 442 nm) after reaction with 4.0 mM $NaClO_2$ with *o*-tolidine (40 μM) in acetate buffer. (b) ESI-MS spectra of products obtained from the reaction of $NaClO_2$ with $[Fe^{II}(L^2)]^{2+}$.

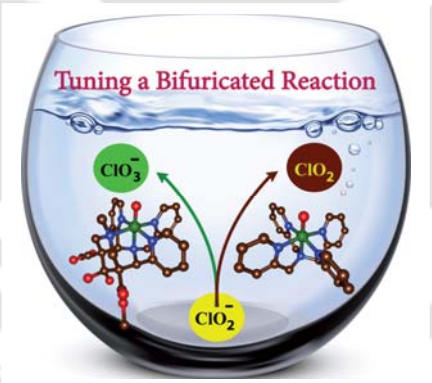

In summary, first experimental results of detoxification of chlorite to chlorine dioxide selectively have been studied using non-heme iron complexes. With the help of Density functional theory, found that the reaction can proceed via competitive pathways (oxygen atom transfer as well as proton coupled electron transfer), whereby the nature of the ligand system and its binding affinity

of ClO_x^- substrates determine the driving force of each reaction step.There is a iron(IV)-oxo formation in the first step, which can go further reaction with two pathways either oxygen atom transfer or proton coupled electron transfer to give chlorine dioxide. In $[(N4Py)Fe^{II}]^{2+}$ its going mainly via proton coupled electron transfer (PCET) pathway but $[(L^1)Fe^{II}]^{2+}$ and $[(L^2)Fe^{II}]^{2+}$ going via oxygen atom transfer pathway.

Chapter-6. Long-Range Electron Transfer Triggers Mechanistic Differences between Iron(IV)-Oxo and Iron(IV)-Imido Oxidants

The results obtained and discussed in Chapters 5 reveal novel reactions that could be explored to understand the reaction mechanism of high-valent iron intermediates. By contrast to iron(IV)-oxo complexes, which have been extensively studied over the years, only few studies have been reported on its closely related iron(V)-nitrido species ($Fe^V{\equiv}N$) or the iron(IV)-imido ($Fe^{IV}{=}NR$) species. In principle, these high-valent metal-nitrido/imido complexes should have strong oxidative power and capable to catalyze isolobal amination reactions. During the past decade, the chemistry of metal-catalyzed aziridination of alkenes and aminidation of aliphatic C–H bonds using iminoiodane reagents has been studied by several groups. In recent years, the putative metal-nitrogen multiple bonded species have been isolated and spectroscopically characterized, which led to significant progress on the understanding of its fundamental chemical properties. However, details on its potential as nitrogen atom transfer agent are lacking and little knowledge exists in its relative reactivity with respect to the well-known iron(IV)-oxo species.

In non-heme iron chemistry, the aromatic amination of ligands by an iron-nitrido complex was reported by several groups, and recently, the spectroscopic

characterization of the iron(IV)-tosylimido (tosylimido^{2-} = NTs) complex with pentadentate N4Py ligand (N4Py = *N*,*N*-bis(2-pyridylmethyl)-*N*-bis(2-pyridyl) methylamine), $[Fe^{IV}(NTs)(N4Py)]^{2+}$, was described. As this species was shown to have a relatively long lifetime, it makes it highly suitable for reactivity studies, especially since the iron(IV)-oxo analogue can be studied in tandem. In this chapter reactivity study of $[Fe^{IV}(O)(N4Py)]^{2+}$ (**6**) and $[Fe^{IV}(NTs)(N4Py)]^{2+}$ (**7**) towards alcohol oxidation was evaluated.

In pursuit of mechanistic pathway for Fe^{IV}=NR species in the presence of organic substrates, a comparative reactivity study of $[Fe^{IV}(NTs)(N4Py)]^{2+}$ (**7**) and $[Fe^{IV}(O)(N4Py)]^{2+}$ (**6**) were carried out. For the two electron oxidation reactions (thioanisole oxidation), **7** was found to be a better oxidant with a second order rate constant higher by a magnitude of five times. A detailed investigation into the mechanistic pathway using substituted thioanisoles showed for sulfoxidation reactions with **7** proceed via step wise electron transfer process which is contrary to a group transfer oxidation pathway by **6**. Previously it was found that **7** perform organic substrate oxidation (sulfoxidation, HAT) via an electron transfer pathway with a low KIE and small Hammett value. With keeping in mind, have further extended the reactivity of **6** and **7** in alcohol oxidation.

The second order rate constant, k_2, obtained for benzyl alcohol at 25 ^{o}C was determined to be 1.48×10^{-2} M^{-1} s^{-1} for $[Fe^{IV}(NTs)(N4Py)]^{2+}$, whereas a value of 8.20×10^{-2} M^{-1} s^{-1} was found for $[Fe^{IV}(O)(N4Py)]^{2+}$. Therefore, the $[Fe^{IV}(O)(N4Py)]^{2+}$ complex reacts with benzyl alcohol with rate constants that are almost six times larger than those found for the $[Fe^{IV}(NTs)(N4Py)]^{2+}$ complex (Figure 7b). To gain more insight into the details of the hydrogen atom abstraction mechanism, repeated the experiments with benzyl alcohol-d_7 ($C_6D_5CD_2OH$). These studies established a kinetic isotope effect (KIE) of 7.0, which is relatively low for typical hydrogen atom abstraction reactions but can

still be considered as a rate determining HAT step in the reaction mechanism (Figure 7b). In the case of HAT of fluorene by **6** and **7**, also a KIE = 7 for the iron(IV)-tosylimido complex was established, whereas a value of 30 was obtained for the iron(IV)-oxo species. Clearly, there are fundamental differences in reactivity between iron(IV)-oxo and iron(IV)-tosylimido that lead to this dramatic lowering of the kinetic isotope effects.

To gain insight into the intrinsic details of the reaction mechanism of benzyl alcohol with **6** and **7**, decided to study *para* substituted benzyl alcohols and create a Hammett plot. Reaction of $[Fe^{IV}(O)(N4Py)]^{2+}$ with *para* substituted benzyl alcohol indicates that the reaction rates are not greatly dependent on the *para* substituent and either electron-withdrawing or electron-donating group give similar reaction rates. When plot the reaction rate as a function of σ_P of the substituent a small Hammett ρ value ~ -0.1 is found by contrast to the reaction of **6** with benzyl alcohol, the same reaction with **7** gives a dramatic change in substituent effect with a Hammett ρ value of ~ -1.71 (Figure 7c). This large Hammett value indicates that during the hydrogen atom abstraction from the substrate there is a considerable amount of positive charge built-up in the transition state. To unequivocally establish that the rate-determining step is indeed one-electron transfer did a subsequent set of experiments with cyclobutanol as mechanistic probe. In the oxidation of cyclobutanol by **7** observe 4-hydroxybutyraldehyde as the major products; hence the reaction of **6** with aliphatic substrates proceeds via a dominant radical pathway. By contrast, cyclobutanol reacts with **6** to yield cyclobutanone product after a specific C–H bond cleavage.

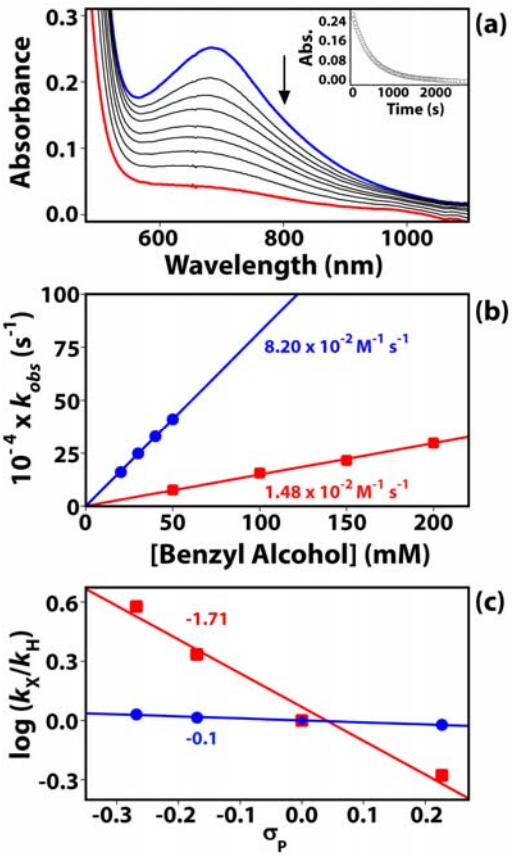

Figure 7. (a) UV-vis. spectral changes of **7** (1 mM, blue line) upon the addition of *para*-H-benzyl alcohol (150 equiv. diluted in 50 μL of CH_3CN) in CH_3CN at 298 K. Inset shows decay profile of 660 nm band. (b) Second-order rate constants determined in the reactions of 1 mM of **6** (●) and **7** (■) in CH_3CN solution against various concentrations of benzyl alcohol at 298 K. (c) Plot of log (k_X/k_H) against σ_p values of *para*-X-benzyl alcohol in reaction with **6** (●) and **7** (■) at 298 K. The k_X and k_H are the second order rate constants of *para*-X-benzyl alcohol at 298 K.

In summary, this chapter present here the first comparative study on the reactivity patterns of non-heme iron(IV)-oxo versus iron(IV)-imido. This chapter explained that due to the larger electron affinity of the oxidant the iron(IV)-imido is a better oxidant of sulfoxidation reactions than iron(IV)-oxo. By contrast, these trends are

reversed for stepwise one-electron transfer reactions, such as, hydrogen atom abstraction reactions where stereochemical interactions upon substrate approach determine the relative rate constants. However, the opposite trend is found for HAT reactions from, e.g. *para*-X-benzyl alcohol and fluorene. Subsequent DFT calculations confirmed the experimentally observed trends and gave smaller barriers for HAT by iron(IV)-oxo complexes relative to iron(IV)-imido, whereas the reverse trend is found for heteroatom transfer. The origin of the rate reversal was investigated through a thermochemical analysis of the bond breaking and electron transfer processes. It was found that the electron affinity of $[Fe^{IV}(NTs)(N4Py)]^{2+}$ is so high that it accepts electrons from HAT substrates at a large distance, which was due to differences in orbital interactions as compared to the iron(IV)-oxo species.

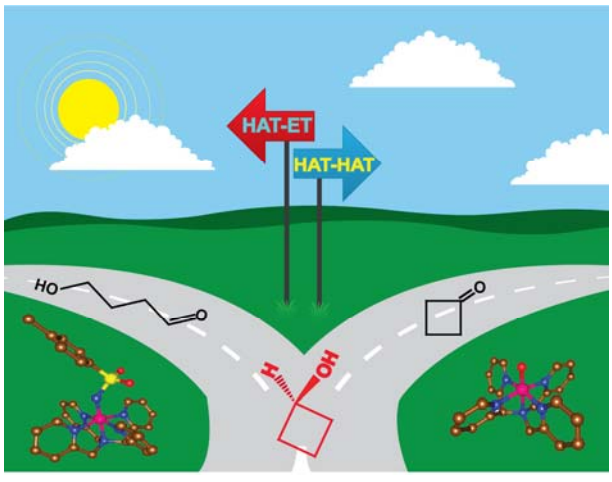

List of publications:

1. A. K. Vardhaman, **P. Barman,** C.V. Sastri, D. Kumar, S. P. de Visser, Mechanisitic Insights to Halide Oxidation by Non-Heme Iron Complexes. Haloperoxidase versus Halogenase. *Chem. Commun.* **2013**, *49*, 10926-10928.
2. A. K. Vardhaman, **P. Barman,** C.V. Sastri, D. Kumar, S. P. de Visser, Comparison of the Reactivity of Non-heme Iron(IV)-Oxo versus Iron(IV)-Imido Complexes: Which is the Better Oxidant? *Angew. Chem. Int. Ed.* **2013**, *52*, 12288-12292.
3. S. Kumar, A. S. Faponle, **P. Barman,** A. K. Vardhaman, C.V. Sastri, D. Kumar, S. P. de Visser, Long-range Electron Transfer Triggers Mechanistic Differences between Iron(IV)-Oxo and Iron(IV)-Imido oxidants. *J. Am. Chem. Soc.* **2014**, *136*, 17102-17115.
4. **P. Barman,** A. K. Vardhaman, B. Martin, S. J. Wörner, C. V. Sastri, P. Comba, Influence of Ligand Architecture on Oxidation Reactions by High-Valent Non-heme Manganese-Oxo Complexes Using Water as a Source of Oxygen. *Angew. Chem. Int. Ed.* **2015**, *54*, 2095-2099.
5. **P. Barman,** P. Upadhyay, A. S. Faponle, J. Kumar, S. S. Nag, D. Kumar, C. V. Sastri, S. P. de Visser, Deformylation Reaction by a Non-Heme Manganese(III)-Peroxo Complex via Initial Hydrogen Atom Abstraction. *Angew. Chem. Int. Ed.* **2016**, *55*, 11091–11095 (**VIP article**).
6. **P. Barman,** A. S. Faponle, A. K. Vardhaman, D. Angelone, A.-M. Rensland, W. R. Browne, P. Comba, C. V. Sastri, S. P. de Visser, Influence of Ligand Architecture in Tuning Reaction Bifurcation Pathways for Chlorite Oxidation by Non-heme Iron Complexes. *Inorg. Chem.* **2016**, *55,* 10170–10181.

CHAPTER-I

Introduction

1.1 Introduction

Enzymes are biological catalysts that can accelerate the rates of chemical reactions manifold compared to the corresponding non-enzymatic reactions. The catalytic ability of enzymes originated not only from the peptidyl residues constituting the active sites, but also from the presence of redox active metal ions in it. Such metal ions are responsible for the catalytic capability by allowing enzymes to bind selectively with substrates and stabilize intermediates and transition states along the reaction coordinate. Furthermore, metal ions can also afford chemical transformations and reactivities that are not possible with the amino acids alone. Therefore, metal ion containing enzymes add sizeable flavour to the types of chemistry observed in biochemical systems.

Enzymes play key role in most of the biological functions. Nature has taken advantage of the special properties of the metal ions and tuned them by encapsulation with different protein matrices to perform large variety of specific functions associated with life processes.

There are 13 metals, namely, Na, K, Mg, Ca (from the alkali and alkaline-earth metals) and V, Cr, Mn, Fe, Co, Ni, Cu, Zn and Mo (from the d-block transition metals) that are considered to be essential for the biological function of humans as well as other living systems. Biologically relevant metals like Mn, Fe, Co, Ni, Cu and Zn are the obvious working examples for biomimetic chemistry. Iron is one of the most essential elements for life, found in the active site of many proteins (like methane monoxygenase, bleomycin, chloroperoxidase, cytochrome P450) and plays key role in many biological processes (Table 1.1). Apart from iron, manganese is also found in many enzyme's active sites, including manganese superoxide dismutase, manganese catalase, and manganese ribonucleotide reductase (Table 1.2). The enzymes are broadly classified into two categories: heme and non-heme proteins.

Table 1.1. Selected iron containing enzymes

Enzyme	Substrate Activity
Methane monoxygenase 	Methane to methanol
Bleomycin 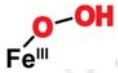	DNA cleavage and oxygenation of hydrocarbons
Chloroperoxidase 	Halogenation
Cytochrome P450 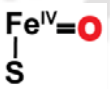	Hydrogen atom transfer

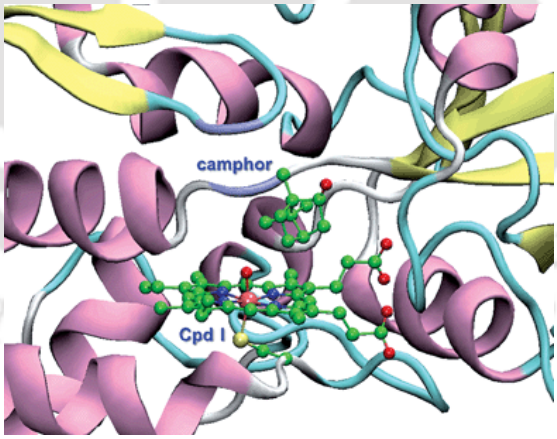

Figure 1.1. Compound I (the active species) of P450cam produced from the X-ray structure (PDB code: 1DZ9).[1, 2]

Table 1.2. Selected manganese containing enzymes

Enzyme	**Substrate Activity**
Mn-Superoxide Dismutase (MnSOD)	Superoxide disproportionation
Mn-Catalase (MnCAT)	H_2O_2 disproportionation
Mn-Ribonucleotide Reductase (MnRNR)	Conversion of ribo- to deoxyribonucleotides
Mn-dependant Catechol Oxyganase (MndD)	Oxidation of aromatics
Oxygen Evolving Complex (OEC)	Formation of O_2 from H_2O
Oxalate Oxidase (OxOx)	Conversion of oxalate to formate

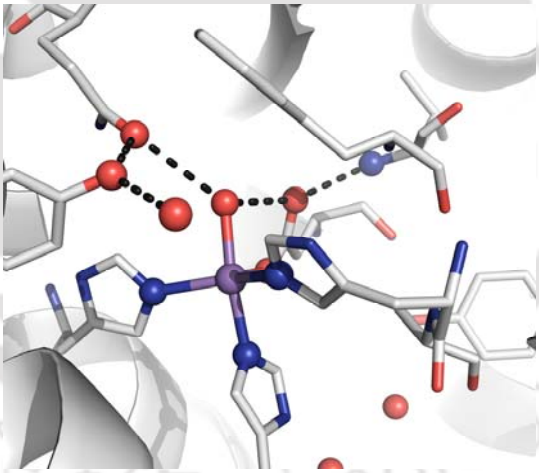

Figure 1.2. Active site for manganese Superoxide Dismutase.

A large, functionally and mechanistically diverse family of enzymes utilize similar, mononuclear non-heme metal centers to couple the activation of oxygen and the oxidation of substrates.[3-7]In most cases, oxygen was inserted into inactivated C-H bond of the substrate (hydroxylation), but many other outcomes including halogenations, desulphurization, cyclization, epoxidation and decarboxylation are known. Enzymes, such as Cytochrome P450 (cyt P450) family have evolved into what are in effect nature's fenton reagents, with additional levels of sophistication leading to impressive regio and chemo-selectivity. But enzymatic oxidation catalysis was different from fenton chemistry. The main point of difference between fenton chemistry and enzymatic oxidation catalysis was: In enzymatic oxidation catalysis it was shown that the utilization of the terrestrial pool of dioxygen while fenton chemistry deals with the reduced form of the enzyme.[8, 9]

Oxygen-containing mononuclear metal (Fe, Mn, Ni, Co) species like metal(III)–peroxo, metal(III)–hydroperoxo, metal(III/II)-superoxo and metal(IV)–oxo are key intermediates in the catalytic activation of dioxygen by metalloenzymes.[10-26] Many non-heme Fe/Mn containing enzymes act by catalyzing the activation of dioxygen (O_2) in many metabolically important functions.[27-32] Oxygen-coordinating metal intermediates, such as metal superoxo, peroxo, hydroperoxo and oxo species, play central roles in many biological and catalytic processes. In all the iron and manganese catalyzed biochemical reactions the suspected intermediates are described below in Figure 1.3.[32, 33]

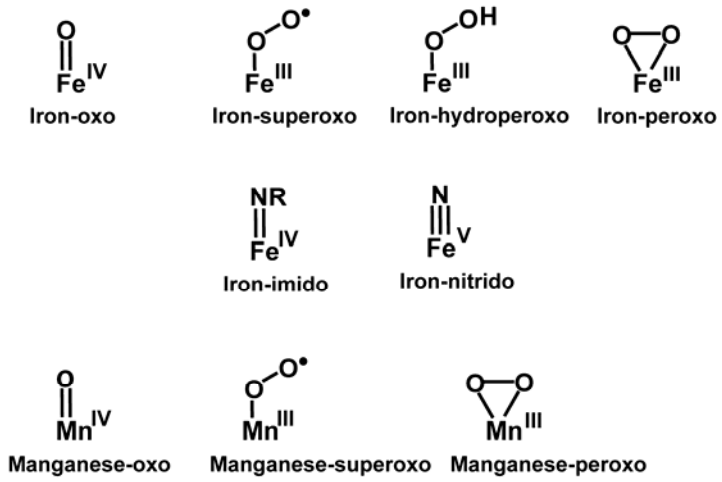

Figure 1.3. Plausible high-valent Iron and Manganese intermediates with Oxygen and Nitrogen.

Understanding the catalytic reaction of enzymes, especially the nature of active oxidizing species has improved recently with intensive mechanistic studies of the enzymes and their model compounds, such as catalytic cycle of dioxygen activation and oxygen atom transfer by α-KG-dependent oxygenases (TauD) .[34, 35] High-valent non-heme iron(IV)-oxo reactive intermediate species have been proposed for decades as the key intermediates in numerous biological oxidation reactions. It was only that, the first direct characterization of such intermediates has been provided by studies of several α-ketoglutarate-dependent (α-KG) oxygenases (TauD) that catalyze either hydroxylation or halogenation of their substrates (Figure 1.4).[36]

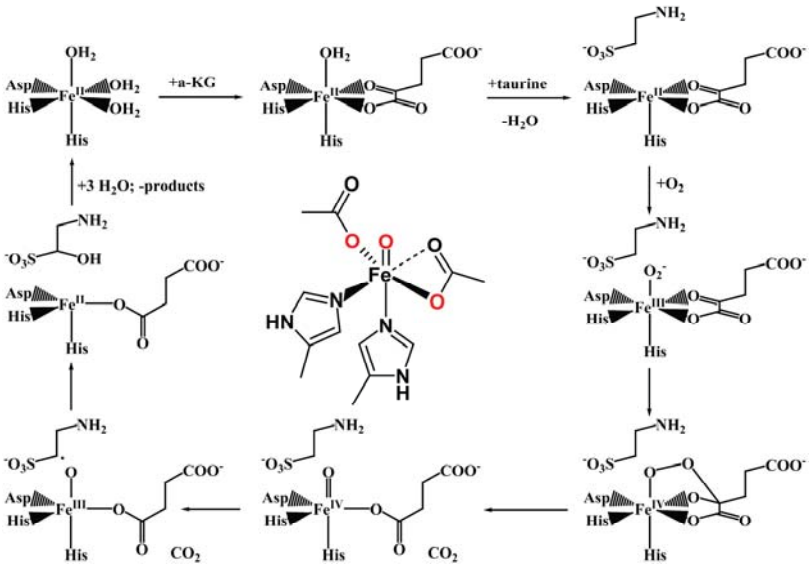

Figure 1.4. Proposed mechanism of TauD

1.2.1 Synthetic non-heme manganese(IV)-oxo systems (Mimics)

In one major aspect of bioinorganic chemistry, researchers study spectroscopic, redox and chemical properties of metal complexes to better understand and finally to mimic the active sites structure of metalloenzymes.[37] There are several high-valent non-heme manganese(IV)-oxo model complexes that were reported in the past decades. Nam and co-workers have shown the generation of a mononuclear non-heme $[Mn^{IV}(O)(BQCN)]^{2+}$ complex (BQCN = N,N'-dimethyl-N,N'-bis(8-quinolyl) cyclohexanediamine) in a reaction of $[Mn^{II}(BQCN)]^{2+}$ with cerium(IV) ammonium nitrate (CAN) in CH_3CN/H_2O (9:1) or acetone/H_2O (9:1) at 0 ^oC ($t_{1/2}$ ≈10 h). The intermediate was characterized by using various spectroscopic methods like UV/Vis, X-band EPR, the electrospray ionization mass spectrum (ESI MS), resonance raman spectrum.[38]

$[Mn^{IV}(O)(N4Py)]^{2+}$ and $[Mn^{IV}(O)(Bn\text{-}TPEN)]^{2+}$ (N4Py = N,N-bis(2-pyridylmethyl)-N-bis(2-pyridyl)-methylamine; Bn-TPEN = N-benzyl-N,N′,N′-tris(2-pyridylmethyl)-1,2-diaminoethane) intermediates were prepared by reacting with 4 equiv. iodosylbenzene (PhIO) in CF_3CH_2OH at 25 °C ($t_{1/2} \approx 2$ h at 25 °C for N4Py and $t_{1/2} \approx 40$ min at 25 °C for Bn-TPEN).[39, 40] Borovik group reported the formation of managanese-oxo complex with $[Mn^{III}H_3buea(O)]^{2-}$ ($[H_3buea]^{3-}$, tris[(*N′-tert*-butylureaylato)-Nethylene]aminato) ligand and $[Cp_2Fe]BF_4$ at -45 °C in DMF. [41] Fujii and co-worker reported the $[Mn^{IV}(O)(salen)]^{2+}$ with Mn^{III} salen type ligand and m-chloroperoxybenzoic acid.[42] Busch group reported the manganese-oxo intermediate with cross bridged, cyclam ligand, 4,11-dimethyl-1,4,8,11-tetraazabicyclo-[6.6.2]hexadecane (abbreviated as Me_2EBC).[43] Costas and co-worker reported $[Mn^{IV}(O)(OH)(^{H,Me}Pytacn)]^{+}$ (^{H,Me}Pytacn = 1-[(6-methyl-2-pyridyl)methyl]-4,7-dimethyl-1,4,7-triazacyclono nane) , was generated in situ in an acetonitile/water mixture (5:1) by treating with 1 equivalent of *t*BuOK.[44] All the above complexes shows manganese in +4 oxidation state, but Nam et al. reported manganese(V)oxo species, generated by treatment of $[Mn^{III}(TAML)]^{-}$ (H_4TAML = tetraamido marcrocyclic ligand, 3,4,8,9-tetrahydro 3,3,6,6,9,9-hexamethyl-1H-1,4,8,11-benzotetraazocyclotrideca ne-2,5,7,10 (6H,11 H) tetrone), by activating O_2 in the presence of a hydrogen atom donor .[45] Sun reported the photocatalytic generation of a mononuclear non-heme $[Mn^{IV}(O)(BQCN)]^{2+}$ complex from the starting complex $[Mn^{II}(BQCN)(CF_3SO_3)]^{2+}$ using $[Ru^{II}(bpy)_3]^{2+}$ as a photosensitizer, $[Co^{III}(NH_3)_5Cl]^{2+}$ as a sacrificial electron acceptor, and water as an oxygen source.[46]

Synthetic non-heme manganese(IV)-oxo complexes have shown various reactivity patterns whereas sulphoxidation, epoxidation, hydride transfer, C-H activation, electron transfer, N-dealkylation, reactions, etc.

1.2.2 Synthetic non-heme manganese(III)-peroxo systems (Mimics)

Till date variety of synthetic manganese(III)-peroxo complexes have been reported, and these complex have been typically generated by Mn(II) precursor either H_2O_2 in presence of a base or KO_2.[47-53] There are only one case where dioxygen(O_2) has been used as oxidant.[49] Due to lack of thermal stabilities and high reactivities, these intermediates often requires low temperature. X-ray crystal structure of the peroxo complex have reveled O-O bond length ranging from 1.40-1.43 Å, firmly establishing the peroxo moiety.[48, 50, 52] The Mn-O bond lengths vary from 1.841 to 1.901 Å, which is similar to Mn^{III}-OH distance observed in synthetic complexes as well as manganese enzyme.[54] Nam and co-workers have shown the generation of a mononuclear peroxidomanganese(III) complex bearing a tetradentate N4 macrocyclic ligand, $[Mn^{III}(tmc)(O_2)]^+$ (tmc = 1,4,8,11-tetramethyl-1,4,8,11-tetraazacyclotetradecane) with the reaction of 5 equivalents of H_2O_2 to a solution containing $[Mn(tmc)(CF_3SO_3)_2]$ and triethylamine (TEA; 2.5 equiv) in CH_3CN at 25 °C.[50] Borovik group reported the formation of managanese-peroxo complex with $[Mn^{II}H_2bupa]^-$ ($[H_2bupa]^{3-}$, bis[(N'-t-butylurealy)-N-ethyl](6-pivalamido-. 2-pyridylmethyl)-aminato) ligand and O_2 at room temperature.[49] Jackson group reported formation of a series of peroxomanganese(III) complexes supported by aminopyridyl ligands with either H_2O_2 and Et_3N or KO_2 in CH_3CN at -40 °C.[53] Recently, a non-heme manganese(III)-peroxo complex with cyclam-type ligand was spectroscopically characterized with electronic absorption, EPR and X-ray absorption techniques.

Moreover, the complex was shown to react with manganese(II)-chloride to form manganese(IV)-oxo and manganese(III)-hydroxo complexes.[55] Jackson, Dorlet and Anxolabéhére–Mallart group have shown that electrochemical generation of Mn^{III}-peroxo complexes by pentadentate amino pyridine and imidazole ligands.[56] Reactivity studies of Mn^{III}-peroxo complex have shown that the peroxo ligand is nucleophilic in nature. A characteristic reaction is the deformylation of aldehydes to ketone, as validated for the $[Mn^{III}(O_2)(TMC)]^+$ and $[Mn^{III}(O_2)(H_3bupa)]^-$ complexes.[49, 50]

1.2.3 Synthetic non-heme iron(IV)-oxo systems (Mimics)

In the year of 2000 first high-valent non-heme iron(IV)-oxo model complex was reported by Karl Weighardt and co-workers, this species has been generated by ozonolysis at -40°C or -80°C of $[Fe^{III}(cyclam\text{-}acetate)(CF_3SO_3)]^+$ in the water and acetone mixture to give rise to a green complex (λ_{max} = 676 nm), but persisted for less than an hour. Mössbauer data revealed that δ = 0.01 mm/s and ΔE_Q = 1.37 mm/s, parameters which are consistent with heme iron(IV)-oxo model systems. This initial iron(IV)-oxo was generated in lower yields (< 25%), obstructing for further characterization.[57]

Que and Nam groups reported high yield route for a non-heme iron(IV)-oxo $[Fe^{IV}(O)(TMC)(CH_3CN)]^{2+}$ species using the macrocyclic N4 ligand (TMC) by treating iron(II) precursor with either PhIO or H_2O_2 at -40 °C in CH_3CN solvent, which resulted in a green solution with absorption maxima at 820 nm (ε = 400 M^{-1} cm^{-1}). Mössbauer parameters of δ = 0.17 mm/s and ΔE_Q = 1.24 mm/s indicates that iron(IV) species with S = 1.[58] ESI-MS also supports its formulation as $[Fe^{IV}(O)(TMC)(CH_3CN)]^{2+}$ and IR spectrum was consistent that it possesses a terminal Fe-O double bond. X-ray crystals structure provided the first example of

a crystallographically characterized mononuclear iron(IV)-oxo unit.[58] Perhaps the most important feature of this structure was the short Fe-O bond length of 1.646(3) Å, this bond length that reveals an appropriate shortening from the 1.813(3) Å distance from an earlier reported iron(III)-oxo species.[59]

$[Fe^{IV}(O)(TPA)(CH_3CN)]^{2+}$ was reported by Que and co-workers, using the TPA ligand at -40 °C in CH_3CN. It shows a low intensity near-IR absorption band at 724 nm (ε = 300 M^{-1} cm^{-1}) which is also supported by Mössbauer and ESI-MS analysis.[60]

There are number of other non-heme mononuclear iron(IV)-oxo complexes that have been generated and characterized using the synthetic and spectroscopic methods.[61-67] Most of the iron-oxo complexes were in non-aqueous solvents and low-spin state *S*=1, but only one exceptional example is there, reported by Bakac and co-workers, which is a high spin *S*=2 non-heme iron(IV)-oxo complex $[Fe^{IV}(O)(H_2O)_5]^{2+}$, generated in aqueous solvent.[64,68-69] Recently Que et al. reported another high-spin *S* = 2 iron(IV) complex with TMG_3tren ligand. $[Fe^{IV}(O)(TMG_3tren)](CF_3SO_3)_2$, half-life period is $t_{1/2}$ = 4.3 h at -30 °C; $t_{1/2} \approx$ 30 sec at 25 °C. This complex shows absorption features at λ_{max} (ε_{max}) 400 (9800), 825 (260) and 866 (250) nm and ESI-MS patterns at *m/z* = 661.3 and *m/z* = 256.2, which were assigned as $\{[Fe^{IV}(O)(TMG_3tren)](OTf)\}^{+}$ and $[Fe^{IV}(O)(TMG_3tren)]^{2+}$.[70] All the above mentioned complexes shows +4 oxidation state of iron, but Collins et al. reported iron(V)-oxo species, generated by $[Fe^{III}(TAML)]^{-}$ (TAML = tetra amido macro cyclic ligand) with *m*-CPBA, r(Fe-O) of 1.58 Å and an *S* = 1/2 ground state.[71]

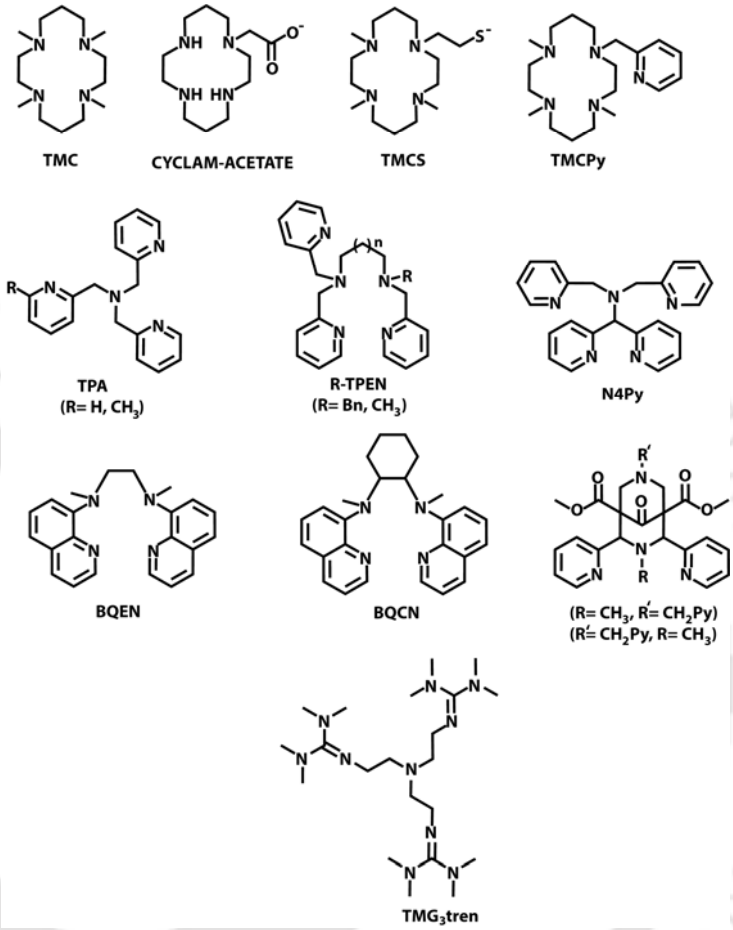

Figure 1.5. Ligands capable of supporting high-valent iron-oxo intermediate.

1.2.2 Oxidants

Non-heme iron(IV)-oxo complexes were generated using various oxidants. First report of iron(IV)-oxo species was generated by ozonolysis of iron cyclam-acetate.[57] $[Fe^{IV}(O)(TMC)(CH_3CN)]^{2+}$ was generated by treating with

PhIO or H_2O_2. $[Fe^{IV}(O)(TPA)(CH_3CN)]^{2+}$ was generated using peracid.[59,60] Collins et al. used *m*-CPBA to generate iron(V)-oxo species.[71] Nam et al. used oxone and CAN as oxidant to generate iron(IV)-oxo species in aqueous solvent.[68,72] Also, the same group has generated the iron(IV)-oxo using the molecular oxygen as an oxidant.[73,74] Que et al. generated iron(IV)-oxo by homolytic cleavage of $Fe^{(III)}$-OOR complex with pyridine N-oxide. However iron(IV)-oxo can be generated by electrochemical method in H_2O and also by treating iron(III)-peroxo complexes with Sc^{+3} like salts.[75-77]

1.2.3 Reactions of non-heme iron(IV)-oxo

Synthetic non-heme iron(IV)-oxo complexes have shown various reactivity patterns like sulfoxidation, phosphorous oxidation, epoxidation, alcohol oxidation, hydroxylation, hydride transfer, C-H activation, electron transfer, halide oxidation, N-dealkylation, ligand exchange and water exchange reactions, etc., (Figure 1.6).

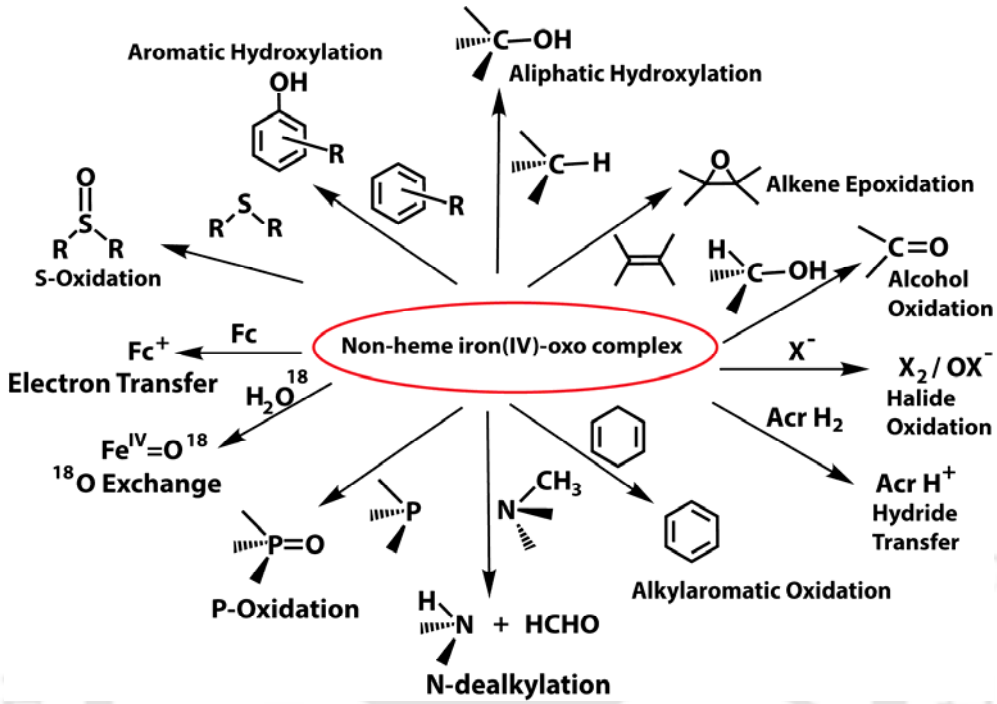

Figure 1.6. Reactions carried out by synthetic non-heme iron(IV)-oxo complexes.

1.3 Non-heme iron(III)-peroxo history

The first high-valent non-heme iron(III)-peroxo complex was generated using iron complex of EDTA by reacting with H_2O_2 as oxidant and triethylamine. It shows a low intensity band at 500-600 nm region ($\varepsilon \sim 500\ M^{-1}\ cm^{-1}$) in the visible region for $[Fe^{III}(O_2)(EDTA)]$.[78,79] Peroxo complexes of iron aminopyridine complexes has been well studied in detail by Neese and Solomon groups. Mössbauer, EPR and ESI-MS analysis revealed that it possesses iron(III) center. EPR of these iron(III)-peroxo complexes explained that the iron present in the rhombic high-spin nature.[80,81]

Tetradentate and pentadentate ligands based iron complexes were used to generate iron(III)-peroxo intermediates.[82] Recently Nam et al. reported the first crystal structure of iron(III)-peroxo bearing a tetradentate TMC ligand.[83]

Iron(III)-peroxo complexes shows reactivity towards nucleophilic aldehyde deformylation reactions. Oxygen atom transfer from iron(III)-peroxo to substrates were also evaluated and it was confirmed by ^{18}O labeled experiments.[84]

1.4 Non-heme iron(III)-hydroperoxo history

Iron(III)-hydroperoxo species (Fe^{III}-OOH) has been proposed as a "second electrophilic oxidant" in a variety of oxygenation reactions.[85-93] Low-spin Fe^{III}-OOH species has been characterized for "activated bleomycin" which was the last detectable intermediate in the reaction cycle of bleomycin (BLM) and a plausible oxidant responsible for DNA cleavage reaction and the oxygenation of hydrocarbons.[94-96]

Non-heme high-valent iron(III)-hydroperoxo complexes are supported by tetra-, pentadentate ligand architechtures.[97-104] Iron(III)-hydroperoxo complexes were generated by using H_2O_2 in methanolic solution at lower temperatures. These complexes were unstable at higher temperature. Iron(III)-hydroperoxo shows a high intensity LMCT band at 500-600 nm region ($\varepsilon \sim 1000\ M^{-1}\ cm^{-1}$). Mössbauer, EPR and ESI-MS analysis confirmed the iron(III) center.[105] EPR analysis suggests that iron is present in low-spin (S =1/2) state. EPR analysis in every case signals existence of a low-spin iron center, spectra was closer to their iron(III) precursors like iron(III)-BLM (g = 2.45, 2.18, 1.89) and iron(III)-BLM hydroperoxo (g = 2.27, 2.17, 1.94).[106]

Iron(III)-hydroperoxo complexes shows electrophilic as well as neocleophilic nature.[83, 107, 108]

1.5 Non-heme iron isolobal intermediates

Non-heme high-valent iron(V)-nitrido complex was first reported by Weighart in the year of 2000, from photolysis of a ferric-azide cyclam-acetate precursor. Spectroscopic analysis revealed the spin state $S = 1/2$ ground state and a short r(Fe-N) of 1.61 Å.[57,109] Laser irradiation of the electrochemically generated iron(IV)-azide again led to photo-oxidation to give iron(VI)-nitrido species, it shows bond length of r(Fe-N) of 1.57(2) Å and Mössbauer analysis shows very negative δ value of -0.29 mm/s revealing the iron(VI) compound and applied field Mössbauer studies indicated an $S = 0$ d^2 ground state.[110]

Non-heme iron(IV)-nitrido complexes bearing tris-(phosphino)borate ligands were generated in two steps, first step iron(I) precursor treated with a nitrene transfer reagent Li(dbabh) to form iron(III)-imide intermediate and in second step, iron(IV)-nitride species was formed by warming of iron(III)-imide and loss of anthracene.[111,112] The spin state $S = 0$ ground state was confirmed in each complex. XAS studies revealed very short Fe-N bond distances of 1.51-1.55 Å, which were short bond lengths, consistent with a formal iron-nitrogen triple bond previously described in iron-nitrides.[112]

First report of iron(IV)-imido complex $[Fe_4(\mu_3\text{-}N^tBu)_4]$ in 2000 is a cubane like structure. Iron(IV) center as one corner in cubane, in which three of the bridged iron centers were bound to a terminal chloride anion and the fourth iron center was ligated by a terminal *t*-butyl imide, it was synthesized by a self-assembly reaction and yielded 1-2 % only. Mössbauer and single crystal analysis also confirmed the oxidation state of the iron(IV)-imido center, bond distances between iron-nitrogen were r(Fe-N) of 1.635(4) Å and a nearly linear Fe-N-C and angle of 178.6(3)°.[113]

High yield of iron(IV)-imido complex was generated using iron pyrazolyl/bis(phosphino)borate complex, it was synthesized in two steps. First

step iron(III)-imide was synthesized from iron(I) complex and two equivalents of adamantly azide, second step desired iron(IV)-imido compound was synthesized by chemical reaction of ferrocenium and iron(III)-imide. X-ray diffraction revealed a terminal r(Fe-N) of 1.634(4) Å and an Fe-N-C angle about the terminal imide of 176.2(3)°. Both of these iron(IV)-imido species were in linear binding mode with the imide group.[113,114]

These high-valent metal-nitrido/imido complexes should have strong oxidative power and capable to catalyse isoloble amination reactions. During the past decade, the chemistry of metal catalysed aziridination of alkenes and aminidation of aliphatic C–H bonds using iminoiodane reagents have been studied by several groups.[110, 115-121]

1.6 Chlorine oxyanion chemistry

Oxido anions of chlorine (ClO_x^-) play an important role in modern chemistry and health not least in their use in bleaching and disinfection. The high solubility of chlorine oxido anions in water, however, means that they create a major contamination of ecological and drinking water, which present challenges with regard to environmental contamination and retention in drinking water. This directly affects the environment and biosphere as well as human health.[122-124] Hence, processes for environmental friendly remediation of oxido chlorine contamination in drinking water are seeing an increase in demand. The oxidation state of chlorine in ClO_x^- can vary from I to VII, which has major consequences with regard to their chemical properties and reactivity. For example, perchlorate (ClO_4^-) is commonly used as an oxidant in rocket fuel, missiles, and fireworks.[125] Although perchlorate is a strong oxidant, it is relatively inert in aqueous media, and hence accumulates readily in the environment.[126] Bioremediation of perchlorate has focused on the use of microbes as well as specific chemicals.[4]

Chlorate (ClO_3^-), by contrast, is used as a herbicide and acts as a source of oxygen, whereas chlorite (ClO_2^-) is mainly used as a source of chlorine dioxide in the pulp bleaching industry.[127, 128] From an environmental perspective the bioremediation of ClO_x^- from water supplies is performed efficiently by perchlorate respiring bacteria. These classes of microorganisms achieve this reactivity using two enzymes, namely perchlorate reductase, which catalyzes the conversion of perchlorate to chlorate and subsequently to chlorite, and chlorite dismutase that converts chlorite to chloride (Cl^-) and molecular oxygen (O_2).[129-133]

The catalytic conversion of chlorite to either chlorine dioxide or a mixture of O_2 and Cl^- has been investigated by several groups over the past few decades,[134–140] including the study of the reactivity of chlorine with chlorite, chlorous acid and Cl^{III} complexes.[134] Collman, Braumann and their co-workers investigated the electrochemical reduction of chlorite by metalloporphyrins in addition to the alkane oxidation using chlorite as terminal oxidant,[135, 136] whereas Groves et al. have shown that chlorine dioxide is generated from chlorite by a water soluble manganese porphyrin.[137] Abu-Omar et al. used an analogous manganese porphyrin to generate chlorine dioxide from ClO_2^-, and have achieved the conversion of chlorite to O_2 and Cl_2 with a water soluble iron catalyst.[138,139] The majority of studies have focused on porphyrinoid-based catalysts, with comparatively few examples of reactivity with nonheme iron complexes, such as the report by Nam, Abu-Omar and their co-workers of two nonheme manganese(IV)-oxo complexes. They achieved efficient generation of chlorine dioxide from chlorite under ambient temperature and at physiological pH.[140]

1.7 Background on Ligand Topology

Nature takes the advantage of the ligand topology to carry out reaction. Upon careful observation of the active site structure of the His64Ser myoglobin (Mb) and horseradish peroxidase (HRP), one can find that metal center in the enzyme is in the surface in case of Mb but in HRP metal center inside the cavity (Figure 1.7). For this structural changes can make drastic effect in reaction mechanism. Due to open structure substrate can directly approach to metal center in Mb, so Mb do reaction via directly atom transfer pathway but in HRP, substrate cannot reach up to the metal center due to steric factor so it do reaction via electron transfer pathway.[141]

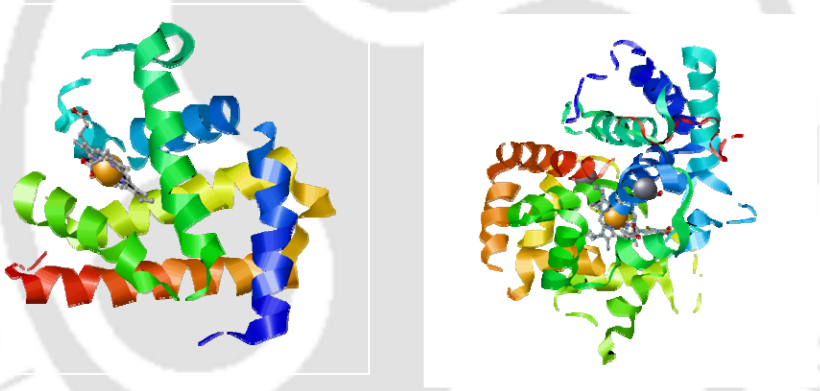

Figure 1.7. Enzyme structure of His64Ser myoglobin (Mb; PDB code: 5HLQ) (left) and horseradish peroxidase (HRP; PDB code: 2YLJ) (right).

There are few literature reports on how ligand topology can influence in the reaction mechanism in synthetic non-heme chemistry. These reports are described below.

$[Fe^{II}(BPMCN)(OTf)_2]$ (OTf- trifluoromethanesulfonate) complexes in both *cis*-α and *cis*-β ligand topologies can be synthesized by independent routes. The N-

methyl groups of the ligand have distinct configurations in the two topologies, *anti*-relative to each other in the *cis*-α isomer and *syn* in the *cis*-β isomer.

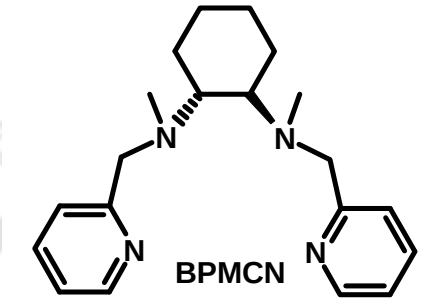

Figure 1.8. Structure of BPMCN ligand.

The effect of ligand topology has been demonstrated in the catalytic oxidation of olefins and alkanes by non-heme iron(II) complexes and H_2O_2. It was seen that the *cis*-α topology was more efficient than its *cis*-β in catalytic oxidation of hydrocarbon. The reactivity difference arises due to change in spin state.[142]

Since non-heme iron(IV)-oxo complexes have been considered as active oxidants in the oxidation of organic substrates but the topology effect on their reactivity has never been explored previously, so they synthesized non-heme iron(II) complexes with two different topologies, *cis*-α and *cis*-β-$[Fe^{II}(BQCN)(CH_3CN)_2]_2$.

The reaction of BQCN ligand with iron(II) salts, $Fe^{II}(ClO_4)_2.4CH_3CN$ and $Fe^{II}(CF_3SO_3)_2.2CH_3CN$, afforded iron(II) complexes with different topologies, *cis*-α-$[Fe^{II}(BQCN)(CH_3CN)_2](ClO_4)_2$ and *cis*-β- $[Fe^{II}(BQCN)(CH_3CN)_2](CF_3SO_3)_2$ in CH_3CN. The N-methyl groups of the BQCN ligand have different configuration in the two topologies: *anti* relative to each other in the *cis*-α isomer and *syn* in the *cis*-β isomer.

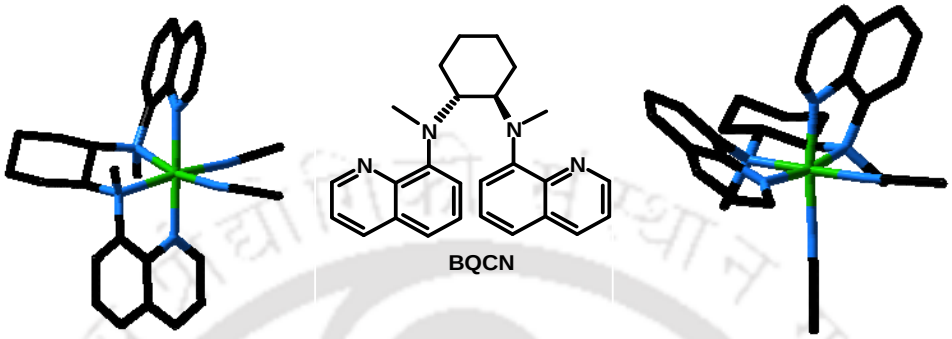

Figure 1.9. Structure of BQCN ligand. Left side shows *cis-α* form and right side *cis-β*.

The high-valent Fe^{IV}=O was prepared by addition of peracetic acid (PAA, 3 equiv) to reaction solutions containing Fe(II) complex of corresponding BQCN ligands gave a pale green intermediate with an absorption band at 758 nm (ε ≈ $120M^{-1}$ cm^{-1}) of *cis-α* form and a yellowish green intermediate with an absorption band at 770 nm (ε ≈ 180 M^{-1} cm^{-1}) of *cis-β*, respectively, in CH_3CN at 0 °C.

The reactivity study was carried out of both the complex in C-H bond activation and oxygen atom transfer reaction. In case of C-H bond activation reaction the *cis-α* form was 20 times faster than its corresponding *cis-β* form. In oxygen atom transfer reactions (OAT) were also investigated in the oxidation of thioanisole. In this case the *cis-α* was 100 times faster over its *cis-β* form.

The *cis-α*-$[Fe^{IV}(O)(BQCN)]^{2+}$ complex is more reactive than the *cis-β*-$[Fe^{IV}$-$(O)(BQCN)]^{2+}$ complex in C-H bond activation and sulfur oxidation reactions. The reactivity difference of the *cis-α* and *cis-β* isomers of $[Fe^{IV}(O)(BQCN)]^{2+}$ is rationalized with their Fe $^{IV/III}$ redox potentials: the redox potential of *cis-α* isomer is 0.11 V higher than that of *cis-β* isomer.[143]

Fe(II) complexes of the following bipidine ligands have been reported by Comba *et. al*. Iron(IV)-oxo complexes were made by the treatment of the iron(II) precursors with excess solid PhIO in CH_3CN at 25 °C.

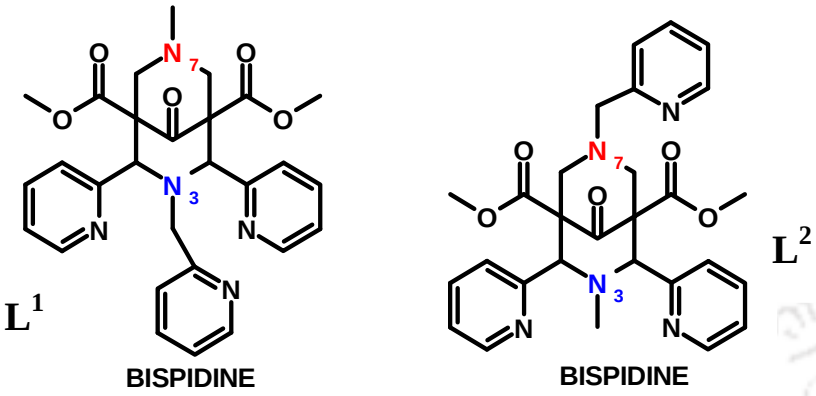

Figure 1.10. Structures of two isomeric Bispidine ligands.

These complexes exhibit pale green intermediate with an absorption band at 730 nm ($\varepsilon \approx 400$ M^{-1} cm^{-1}) of Fe(II) complex of L^1 and L^2 with an absorption band at 730 nm ($\varepsilon \approx 380$ M^{-1} cm^{-1}) respectively, in CH_3CN at 25 °C.

Reactivity was carried out in C-H bond activation as well as oxygen atom transfer reaction. In case of C-H bond activation reaction Fe(IV)-oxo of L^2 was 25 times faster than its L^1 analog, the same trend also follows in oxygen atom transfer reaction. In oxidation of thioanisole Fe(IV)-oxo of L^2 was almost 100 times more than L^1. The reactivity difference arises due to Fe $^{III/II}$ redox potentials: the redox potential of L^2 isomer is 0.05 V higher than that of L^1 isomer.[144]

1.8 Scope and aim of the thesis

Over the recent decade, kinetics and reactivity studies of high-valent intermediates towards substrates oxidations were given more important role in

bio-inorganic chemistry. The review of literature as delineated above clearly reveals that current topic is of significance from the point of view of understanding non-heme enzymatic mechanism. The proposed study will not only introduce research on non-heme high-valent metal intermediates in the national perspective but will also lead to better understanding how the tuning of ligand topology will play a key role in reactivity. Recent burst in reports on generation and characterization of metal-oxo intermediates has thrown a new challenge on the role of regulating the reactivity of such high-valent metal intermediates. A modular approach on the metal ion function mainly depends on regulating the properties within the primary coordination sphere. An approach toward studying the structure–function relationships within the primary coordination sphere is to construct a series of synthetic complexes having structurally tunable primary spheres.

Chapter-I is introduction, which describes about history, reactions and importance of high-valent metal complexes. Chapter-II discusses the synthesis and characterization of ligands and metal intermediates. Chapter-III is a thorough discussion of the reactivity of Mn(IV)-oxo complexes towards oxidation reaction (S-oxidation and hydrogen atom abstraction), this chapter concludes that Mn(IV)-oxo complexes shows opposite reactivity than iron(IV)-oxo. Chapter-IV includes detailed analysis of deformylation reaction by Mn(III)-peroxo and that invokes a novel reaction mechanism between manganese(III)-peroxo complexes with aldehydes starting from an α-hydrogen atom abstraction step. Chapter-V explores the generation of chlorine dioxide from water with water soluble iron complexes. Finally, Chapter-VI explores the reactivity and comparative study of high-valent iron(IV)-oxo and iron(IV)-imido complexes towards alcohol oxidation reaction.

1.7 References.

1. I. Schlichting, J. Berendzen, K. Chu, A. M. Stock, S. A. Maves, D. E. Benson, B. M. Sweet, D. Ringe, G. A. Petsko and S. G. Sligar, Science **2000**, *287*, 1615–1622.
2. S. Shaik, Y. Wang, H. Chen, J. Song, Rinat Meir, *Faraday Discuss.* **2010**, *145*, 49–70.
3. *Cytochrome P450: Structure, Mechanism, and Biochemistry*, 3rd ed. (Ed.: P. R. Ortiz de Montellano), Kluwer Academic/Plenum Publishers, New York, **2005**.
4. I. G. Denisov, T. M. Makris, S. G. Siligar, I.Schlichting, *Chem. Rev.* **2005,** *105*, 2253–2277.
5. B. Meunier, S. P. de Visser, S. Shaik, *Chem. Rev.* **2004,** *104*, 3947–3980.
6. M. M. Abu–Omar, A. Loaiza, N. Hontzeas, *Chem. Rev.* **2005***, 105*, 2227–2252.
7. M. Costas, M. P. Mehn, M. P. Jensen, L. Que Jr., *Chem. Rev.* **2004,** *104,* 939–986.
8. T. K. Matthew, G. R. Charle, *Acc. Chem. Res.* **2007,** *40*, 618–625.
9. P. Hlavica, *Eur. J. Bio–chem.* **2004,** *271*, 4335–4360.
10. E. I. Solomon, *Chem. Rev*. **2000**, *100*, 235–350.
11. E. G. Kovaleva, J. D. Lipscomb, *Nature Chem. Biol.* **2008**, *4*, 186–193.
12. L. C. Blasiak, F. H. Vaillancourt, C. T. Walsh, C. L. Drennan, *Nature* **2006**, *440*,368–371.
13. J. Rittle, M. T. Green, *Science* **2010**, *330*, 933–937.
14. E. G. Kovaleva, J. D. Lipscomb, *Science* **2007**, *316*, 453–457.
15. A. Karlsson, *Science* **2003**, *299*, 1039–1042.
16. R. M.Cicchillo, *Nature* **2009**, *459*, 871–874.

17. M. J. Park, J. Lee, Y. Suh, J. Kim, W. Nam, *J. Am. Chem. Soc.* **2006**, *128*, 2630–2634.
18. Y. M. Kim, K.−B. Cho, J. Cho, B. Wang, C. Li, S. Shaik, W. Nam, *J. Am. Chem. Soc.* **2013***, 135,* 8838−8841.
19. L. V. Liu, S. Hong, J. Cho, W. Nam, E. I. Solomon, *J. Am. Chem. Soc.* **2013,** *135*, 3286−3299.
20. H. So, Y. J. Park, K.−B. Cho, Y.−M. Lee, M. S. Seo, J. Cho, R. Sarangi, W. Nam, *J. Am. Chem. Soc.* **2014**, *136*, 12229−12232.
21. J. Annaraj, Y. Suh, M. S. Seo, S. O. Kim, W. Nam, *Chem. Commun*. **2005**, 4529–4531.
22. J. Annaraj, J. Cho, Y.–M. Lee, S. Y. Kim, R. Latifi, S. P. de Visser, W. Nam, *Angew. Chem. Int. Ed*. **2009**, *48*, 4150–4153.
23. M. S. Seo, J. Y. Kim, J. Annaraj, Y. Kim, Y.–M. Lee, S.–J. Kim, J. Kim, W. Nam, *Angew. Chem. Int. Ed.* **2007**, *46*, 377–380.
24. R. A. Geiger, S. Chattopadhyay, V. W. Day, T. A. Jackson, *Dalton Trans.* **2011**, *40*, 1707–1715.
25. Y. Goto, S. Wada, I. Morishima, Y. Watanabe, *J. Inorg. Biochem.* **1998**, *69*, 241–247.
26. J. Cho, R. Sarangi, J. Annaraj, S. Y. Kim, M. Kubo, T. Ogura, E. I. Solomon, W. Nam, *Nat. Chem*. **2009**, *1*, 568–572.
27. E. I. Solomon, T. C. Brunold, M. I. Davis, J. N. Kemsley, S.–K. Lee, N. Lehnert, F. Neese, A. J. Skulan, Y.–S. Yang, J. Zhou, *Chem. Rev.* **2000**, *100*, 235–349.
28. M. Costas, M. P. Mehn, M. P.Jensen, L. Que Jr., *Chem. Rev.*2004**, 104***,*** 939–986.
29. R. P. Hausinger, *Crit. Rev. Biochem. Mol. Biol*. **2004**, *39*, 21–68.

30. E. G. Kovaleva, J. D. Lipscomb, *Nat. Chem. Biol*. **2008**, *4*, 186–193.
31. C. Loenarz, C. J. Schofield, *Nat. Chem. Biol*. **2008**, *4*, 152–156.
32. W. Nam, *Acc. Chem. Res*. **2007**, *40*, 522–531, and review articles in the special issue.
33. M. J. Park, J. Lee, Y. Suh, J. Kim and W. Nam, *J. Am. Chem. Soc.* **2006,** *128,* 2630–2634.
34. J. M. Bollinger Jr., J. C. Price, L. M. Hoffart, E. W. Barr, C. Krebs, *Eur. J. Inorg. Chem.* **2005**, 4245–4254.
35. C. Krebs, J. C. Price, J. Baldwin, L. Saleh, M. T. Green, J. M. Bollinger Jr., *Inorg. Chem.* **2005**, *44*, 742–757.
36. J. C. Price, E. W. Barr, B. Tirupati, J. M. Bollinger Jr., C. Krebs, *Biochemistry* **2003**, *42*, 7497–7508.
37. S. J. Lippard, J. M. Berg, *Principles of Bioinorganic Chemistry*; University Science Books, **1994**.
38. S. C. Sawant, X. Wu, J. Cho, K.–B. Cho, S. H. Kim, M. S. Seo, Y.–M. Lee, M. Kubo, T. Ogura, S. Shaik, W. Nam, *Angew. Chem. Int. Ed.* **2010**, *49*, 8190–8194.
39. J. Chen, Y.–M. Lee, K. M. Davis, X. Wu, M. S. Seo, K.–B. Cho, H. Yoon, Y. J. Park, S. Fukuzumi, Y. N. Pushkar, W. Nam, *J. Am. Chem. Soc.* **2013**, *135*, 6388−6391.
40. X. Wu, M. S. Seo, K. M. Davis, Y.−M. Lee, J. Chen, K.−B. Cho, Y. N. Pushkar, W. Nam, *J. Am. Chem. Soc.* **2011,** *133*, 20088–20091.
41. T. H. Parsell, R. K. Behan, M. T. Green, M. P. Hendrich, A. S. Borovik, *J. Am. Chem. Soc.* **2006,** *128*, 8728–8729.
42. T. Kurahashi, A. Kikuchi, Y. Shiro, M. Hada, H. Fujii, *Inorg. Chem.* **2010**, *49*, 6664–6672.

43. G. Yin, A. M. Danby, D. Kitko, J. D. Carter, W. M. Scheper, D. H. Busch, *J. Am. Chem. Soc.* **2007**, *129*, 1512–1513.
44. I. Garcia–Bosch, A. Company, C. W. Cady, S. Styring, W. R. Browne, X. Ribas, M. Costas, *Angew. Chem., Int. Ed.* **2011**, *50*, 5648–5653.
45. S. Hong, Y.–M. Lee, M. Sankaralingam, A. K. Vardhaman, Y. J. Park, K.–B. Cho, T. Ogura, R. Sarangi, S. Fukuzumi, W. Nam, *J. Am. Chem. Soc.* **2016**, *138*, 8523–8532.
46. X. Wu, X. Yang, Y.–M. Lee, W. Nam, L. Sun, *Chem. Commun.* **2015**, *51*, 4013–4016.
47. S. Groni, G. Blain, R. Guillot, C. Policar, E. Anxolabéhére–Mallart, *Inorg. Chem.* **2007**, *46*, 1951−1953.
48. N. Kitajima, H. Komatsuzaki, S. Hikichi, M. Osawa, Y. Moro–oka, *J. Am. Chem. Soc.* **1994**, *116*, 11596−11597.
49. R. L. Shook, W. A. Gunderson, J. Greaves, J. W. Ziller, M. P. Hendrich, A. S. Borovik, *J. Am. Chem. Soc.* **2008**, *130*, 8888–8889.
50. M. S. Seo, J. Y. Kim, J. Annaraj, Y. Kim, Y.–M. Lee, S.–J. Kim, J. Kim, W. Nam, *Angew. Chem. Int. Ed.* **2007**, *46*, 377–380.
51. R. A. Geiger, S. Chattopadhyay, V. W. Day, T. A. Jackson, *Dalton Trans.* **2011**, *40*, 1707–1715.
52. R. B. VanAtta, C. E. Strouse, L. K. Hanson, J. S. Valentine, *J. Am. Chem. Soc.* **1987**, **109**, 1425–1434.
53. R. A. Geiger, S. Chattopadhyay, V. W. Day, T. A. Jackson, *J. Am. Chem. Soc.* **2010**, *132*, 2821–2831.
54. T. A. Jackson, T. C. Brunold, *Acc. Chem. Res.* **2004**, *37*, 461–470.
55. H. E. Colmer, A. W. Howcroft, T. A. Jackson, *Inorg. Chem*. **2016**, *55*, 2055–2069.

56. S. E. Ghachtouli, H. Y. V. Ching, B. Lassalle-Kaiser, R. Guillot, D. F. Leto, S. Chattopadhyay, T. A. Jackson, P. Dorlet, E. Anxolabéhére–Mallart, *Chem. Commun.* **2013**, *49*, 5696–5698.

57. C. A. Grapperhaus, B. Mienert, E. Bill, T. Weyhermüller, K. Wieghardt, *Inorg. Chem.* **2000**, *39*, 5306–5317.

58. J.–U. Rohde, J.–H. In, M.–H. Lim,W. W. Brennessel, M. R. Bukowski, A. Stubna, E. Münck, W. Nam, L. Que Jr., *Science* **2003**, *229*, 1037–1039.

59. C. E. MacBeth, A. P. Golombek, V. G. Young Jr., C. Yang, K. Kuczera, M. P. Hendrich, A. S. Borovik, *Science* **2000**, *289*, 938–941.

60. M. H. Lim, J.–U. Rohde, A. Stubna, M. R. Bukowski, M. Costas, R. Y. N. Ho, E. Münck, W. Nam, L. Que Jr., *Proc. Natl. Acad. Sci. U. S. A.,* **2003**, *100*, 3665–3670.

61. M. R. Bukowski, K. D. Koehntop, A. Stubna, E. L. Bominaar, J. A. Halfen, E. Münck, W. Nam, L. Que Jr., *Science* **2005**, *310*,1000–1002.

62. J. Kaizer, M. Costas and L. Que Jr., *Angew. Chem. Int. Ed.* **2003**, *42*, 3671–3673.

63. J. Kaizer, E. J. Klinker, N. Y. Oh, J.–U. Rohde, W. J. Song, A. Stubna, J. Kim, E. Münck, W. Nam and L. Que Jr., *J. Am. Chem. Soc.* **2004**, *126*, 472–473.

64. O. Pestovsky, S. Stoian, E. Bominaar, X. Shan, E. Munck, L. Que Jr., A. Bakac, *Angew. Chem. Int. Ed.* **2005**, *44*, 6871–6874.

65. V. Balland, M.–F. Charlot, F. Banse, J.–J. Girerd, T. A. Mattioli, E. Bill, J.–F. Bartoli, P. Battioni, D. Mansuy, *Eur. J. Inorg. Chem.* **2004**, 301–308.

66. M. Martinho, F. Banse, J.–F. Bartoli, T. A. Mattioli, P. Battioni, O. Horner, S. Bourcier and J.–J. Girerd, *Inorg. Chem.* **2005**, *44*, 9592–9596.

67. T. K. Paine, M. Costas, J. Kaizer, L. Que Jr., *J. Biol. Inorg. Chem.* **2006**, *11*, 272–276.
68. C. V. Sastri, M. S. Seo, M. J. Park, K. M. Kim, W. Nam, *Chem. Commun.* **2005**, 1405–1407.
69. J. Bautz, M. R. Bukowski, M. Kerscher, A. Stubna, P. Comba, A. Lienke, E. Münck and L. Que Jr., *Angew. Chem. Int. Ed.* **2006**, *45*, 5681–5684.
70. J. England, Y. Guo, E. R. Farquhar, V. G. Young Jr., E. Munck, L. Que Jr., *J. Am. Chem. Soc.* **2010**, *132*, 8635–8644.
71. F. Tiago de Oliveira, A. Chanda, D. Banerjee, X. Shan, S. Mondal, L. Que Jr., E. Bominaar, E. Münck, T. J. Collins, *Science* **2007**, *315*, 835–838.
72. Y. M. Lee, S. N. Dhuri, S. C. Sawant, J. Cho, M. Kubo, T. Ogura, S. Fukuzumi, W. Nam, *Angew. Chem. Int. Ed.* **2009**, *48*, 1803–1806.
73. S. O. Kim, C. V. Sastri, M. S. Seo, J. Kim, W. Nam, *J. Am. Chem. Soc.* **2005**, *127*, 4178–4179.
74. Y.–M. Lee, S. Hong, Y. Morimoto, W. Shin, S. Fukuzumi, W. Nam, *J. Am. Chem. Soc.***2010**, *132*, 10668–10670.
75. J. Kaizer, M. Costas, L. Que Jr., *Angew. Chem. Int. Ed.* **2003**, *42*, 3671–3673.
76. M. J. Collins, K. Ray, L. Que Jr., *J. Am. Chem. Soc.* **2006**, *45*, 8009–8011.
77. F. Li, K. M. V. Heuvelen, K. K. Meier, E. Munck, L. Que Jr., *J. Am. Chem. Soc.* **2013**, *135*, 10198–10201.
78. C. Walling, M. Kurz, H. J. Schugar, *Inorg. Chem.* **1970**, *9*, 931–937.
79. S. Ahmad, J. D. McCallum , A. K. Shiemke , E. H. Appelman, T. M. Loehrand J. S.–Loehr, *Inorg. Chem.* **1988**, *27*, 2230–2233.
80. F. Neese, E. I. Solomon, *J. Am. Chem. Soc.* **1998**, *120*, 12829–12848.

81. A. J. Simaan, F. Banse, P. Mialane, A. Boussac, S. Un, T. K.–Grisel, G. Bouchoux, J.–J. Girerd, *Eur. J. Inorg. Chem.* **1999**, 993–996.
82. K. B. Jensen, C. J. McKenzie, L. P. Nielsen, J. Z. Pedersen, H. M. Svendsen, *Chem. Commun.* **1999**, 1313–1314.
83. J. Cho, S. Jeon, S. A. Wilson, L. V. Liu, E. A. Kang, J. J. Braymer, M. H. Lim, B. Hedman, K. O. Hodgson, J. S. Valentine, E, I. Solomon, W. Nam, *Nature* **2011**, *478*, 502–505.
84. J. Annaraj, Y. Suh, M. –S. Seo, S. O. Kim and W. Nam, *Chem. Commun.* **2005**, 4529–4531.
85. P. Hlavica, *Eur. J. Biochem*. **2004**, *271*, 4335–4360.
86. S. Jin, T. A. Bryson, J. H. Dawson, *J. Biol. Inorg. Chem*. **2004**, *9*, 644–653.
87. W. Nam, Y. O. Ryu, W. J. Song, *J. Biol. Inorg. Chem*. **2004**, *9*, 654–660.
88. S. Shaik, S. P. de Visser, D. Kumar, *J. Biol. Inorg. Chem*. **2004**, *9*, 661–668.
89. M. Newcomb, P. F. Hollenberg, M. J. Coon, *Biochem. Biophys*. **2003**, *409*, 72–79.
90. W. J. Song, Y. O. Ryu, R. Song, W. Nam, *J. Biol. Inorg. Chem*. **2005**, *10*, 294–304.
91. M. Newcomb, R. Shen, S.–Y. Choi, P. H. Toy, P. F. Hollenberg, A. D. N. Vaz, M. J. Coon, *J.Am. Chem. Soc*. **2000**, *122*, 2677–2686.
92. P. H. Toy, M. Newcomb, M. J. Coon, A. D. N. Vaz, *J. Am. Chem. Soc*. **1998**, *120*, 9718–9719.
93. A. D. N. Vaz, D. F. Mc Ginnity, M. J. Coon, *Proc. Natl. Acad. Sci. U.S.A*. **1998**, *95*, 3555–3560.
94. N. Lehnert, F. Neese, R. Y. N. Ho, L. Que Jr., E. I. Solomon, *J.Am. Chem. Soc.* **2002**, *124*, 10810–10822.

95. J. W. Sam, X.–J. Tang, J. Peisach, *J. Am. Chem. Soc.* **1994**, *116*, 5250–5256.
96. N. Murugesan and S. M. Hecht, *J. Am. Chem. Soc.* **1985**, *107*, 493–500.
97. A. J. Simaan, S. Dopner, F. Banse, S. Bourcier, G. Bouchoux, A. Boussac, P. Hildebrandt, J.–J. Girerd, *Eur. J. Inorg. Chem.* **2000**, *7*, 1627–1633.
98. I. Bernal, I. M. Jensen, K. B. Jensen, C. J. McKenzie, H. Toftlund, J.–P. Tuchagues, *J. Chem. Soc. Dalton Trans.***1995**, 3667–3675.
99. P. Mialane , A. Nivorojkine , G. Pratviel , L. Azéma , M. Slany , F. Godde, A. Simaan , F. Banse , T. K.–Grisel , G. Bouchoux , J. Sainton , O. Horner , J. Guilhem , L. Tchertanova , B. Meunier, J.–J. G. Laborat, *Inorg. Chem.* **1999**, *38*, 1085–1092.
100. K. B. Jensen, C. J. McKenzie, L. P. Nielsen, J. Z. Pedersen, H. M. Svendsen. *Chem.Commun.* **1999**, 1313–1314.
101. M. Lubben, A. Meetsma, E. C. Wilkinson, B. Feringa, L. Que Jr., *Angew. Chem. Int. Ed.* **1995**, *34*, 1512–15146.
102. R. Y. N. Ho , G. Roelfes , B. L. Feringa, L. Que Jr., *J. Am. Chem. Soc.***1999**, *121*, 264–265.
103. G. Roelfes, M. Lubben, K. Chen, R. Y. N. Ho, A. Meetsma, S. Genseberger, R. M. Hermant, R. Hage, S. K. Mandal, V. G. Young Jr., Y. Zang, H. Kooijman, A. L. Spek, L. Que Jr., B. L. Feringa, *Inorg. Chem.* **1999**, *38*, 1929–1936.
104. M. E. de Vries, R. M. La Crois, G. Roelfes, H. Kooijman, A. L. Spek, R. Hage and B. L. Feringa, *Chem. Commun.***1997**, 1549–1550.
105. J. W. Sam, X.–J. Tang, J. Peisach. *J. Am. Chem. Soc.* **1994**, *116*, 5250–5256.

106. R. M. Burger, S. B. Horwitz, J. Peisach, J. B. Wittenberg. *J. Biol. Chem.* **1979**, *254*, 12299–12302.
107. A. K. Vardhaman, C. V. Sastri, D. Kumar, S. P. de Visser, *Chem. Commun*. **2011**, *47*, 11044–11046.
108. A. K. Vardhaman, P. Barman, S. Kumar, C. V. Sastri, D. Kumar, S. P. de Visser, *Chem. Commun.* **2013**, *49*, 10926–10928.
109. N. Aliaga–Alcalde, S. D. George, B. Mienert, E. Bill, K. Wieghardt, F. Neese, *Angew. Chem. Int. Ed.* **2005**, *44*, 2908–2912.
110. J. F. Berry, E. Bill, E. Bothe, S. D. George, B. Mienert, F. Neese, K. Wieghardt, *Science* **2006**, *312*, 1937–1941.
111. T. A. Betley, J. C. Peters. *J. Am. Chem. Soc.* **2004**, *126*, 6252–6254.
112. J.–U. Rohde, T. A. Betley, T. A. Jackson, C. T. Saouma, J. C. Peters, L. Que Jr., *Inorg. Chem.* **1999**, *38*, 1929–1936.
113. A. K. Verma, T. N. Nazif, C. Achim, S. C. Lee,*J. Am. Chem. Soc.***2000**, *122*, 11013–11014.
114. C. M. Thomas, N. P. Mankad, J. C. Peters, *J. Am. Chem. Soc.***2006**, *128*, 4956–4957.
115. P. Comba, C. Lang, C. Lopez de Laorden, A. Muruganatham, G. Rajaraman, H. Wadepohl, M. Zajaczkowski, *Chem. Eur. J.* **2008**, *14*, 5313–5328.
116. K. L. Klotz, L. M. Slominski, M. E. Riemer, J. A. Phillips, J. A. Halfen, *Inorg. Chem*. **2009**, *48*, 801–803.
117. J. J. Scepaniak, J. A. Young, R. P. Bontchev, J. M. Smith, *Angew. Chem. Int. Ed*. **2009**, *48*, 3158–3160.
118. P. Leeladee, G. N. L. Jameson, M. A. Siegler, D. Kumar, S. P. de Visser, D. P. Goldberg, *Inorg. Chem*. **2013**, *52*, 4668–4682.

119. M. J. Zdilla, M. M. Abu–Omar, *J. Am. Chem. Soc*. **2006**, *128*, 16971-16979.
120. S. Kundu, E. Miceli, E. Farquhar, F. F. Pfaff, U. Kuhlmann, P. Hildebrandt, B. Braun, C. Greco, K. Ray, *J. Am. Chem. Soc.* **2012**, *134,*14710−14713.
121. J. W. W. Chang, P. W. H. Chan, *Angew. Chem. Int. Ed.* **2008**, *47*, 1138–1140.
122. *Drinking Water and Health* (Ed.: J. Boraks), National Research Council, National Academy Press, Washington DC, **1987**, pp. 99–111.
123. A. Rosemarin, K.-J. Lehtinen, M. Notini, J. Mattsson, *Environ. Pollut.* **1994**, *85*, 3–13.
124. K.–J. Lehtinen, M. Notini, J. Mattsson, L. Landner, *Ambio.* **1988**, *17***,** 387–393.
125. W. E. Motzer, *Environ. Forensics* **2001**, *2*, 301−311.
126. *Perchlorate, Environmental Occurrence, Interactions and Treatment* (Ed.: B. Gu, J. D. Coates), Springer, New York, **2006**, pp. 411.
127. J. D. Coates, L. A. Achenbach in *Perchlorate, Environmental Occurrence, Interactions and Treatment* (Ed.: B. Gu, J. D. Coates), Springer, New York, **2006**, pp. 279–291.
128. K. D. Hurley, Y. X. Zhang, J. R. Shapley, *J. Am. Chem. Soc*. **2009**, *131*, 14172–14173.
129. S.W. M. Kengen, G. B. Rikken, W. R. Hagen, C. G. van Ginkel, A.J .M. Stams, *J. Bacteriol*. **1999**, *181*, 6706–6711.
130. Bender, C. Shang, R. Cakraborty, S. M. Belckik, J. D. Coates, J. A. Achenback, *J. Bacteriol*. **2005**, *187*, 5090–5096.
131. B. C. Okeke, B. W. T. Frankenberger Jr, *Microbiol. Res*. **2003**, *158*, 337–344.

132. K. Stenklo , H. D. Thorell, H. Bergius, R. Aasa, T. Nilsson, *J. Biol. Inorg. Chem*. **2001**, *6*, 601–607.
133. A. Q. Lee, B. R. Streit, M. J. Zdilla, M. M. Abu-Omar, J. L. DuBois, *Proc. Natl. Acad. Sci. U.S.A* **2008,** *105,* 15654–15659.
134. I. Fábián, *Coord. Chem. Rev*. **2001**, *216*, 449–472.
135. P. Collman, R. Boulatov, C. J. Sunderland, I. M. Shiryaeva, E. K. Berg, *J. Am. Chem. Soc*. **2002**, *124*, 10670−10671.
136. L. M. Slaughter, J. P. Collman, T. A. Eberspacher, J. I. Brauman, *Inorg. Chem*. **2004**, *43*, 5198−5204.
137. T. P. Umile, J. T. Groves, *Angew. Chem. Int. Ed.* **2011**, *50*, 695–698.
138. S. D. Hicks, J. L. Petersen, C. J. Bougher, M. M. Abu-Omar, *Angew. Chem. Int. Ed.* **2011**, *50*, 699–702.
139. M. J. Zdilla, A. Q. Lee, M. M. Abu-Omar, *Angew. Chem. Int. Ed.* **2008**, *47*, 7697–7700.
140. S. D. Hicks, D. Kim, S. Xiong, G. A. Medvedev, J. Caruthers, S. Hong, W. Nam, M. M. Abu-Omar, *J. Am. Chem. Soc.* **2014**, *136*, 3680−3686.
141. Y. Goto, T. Matsui, S. Ozaki, Y. Watanabe, S. Fukuzumi, *J. Am. Chem. Soc.* **1999**, *121*, 9497–9502.
142. M. Costas, L. Que, Jr, *Angew. Chem. Int. Ed*. ***2002***, *41*, 2179–2181.
143. S. Hong, Y.M. Lee, K.B. Cho, K. Sundaravel, J. Cho, M. J. Kim, W. Shin, W. Nam, *J. Am. Chem. Soc*. ***2011***, *133*, 11876–11879.
144. D. Wang, K. Ray, M. J. Collins, E. R. Farquhar, J. R. Frish, L. Gomez, T. A. Jackson, M. Kerscher, A. Waleska, P. Comba, M. Costas, Que, L., Jr. *Chem. Sci.* ***2013****, 4,* 282-291.

CHAPTER-II

Materials and Methods

2.1 Introduction

Oxygen-containing mononuclear species like metal(III)–peroxo, metal(III)–hydroperoxo, metal(III)–superoxo and metal(IV)–oxo are key intermediates in the catalytic activation of dioxygen in the metalloenzymes.[1-7] Many of the non-heme iron enzymes act by catalyzing the activation of dioxygen (O_2) in many metabolic important functions.[8-12] Oxygen/nitrogen coordinating metal intermediates, such as metal super-oxo, peroxo, hydroperoxo, oxo and imido species play central roles in many biological and catalytic processes.[13]

This chapter aims to present synthetic procedures, characterization of ligands and intermediates. It also discusses about solvents and substrates used in various reactions. Spectroscopic methods, kinetics, reactivity studies, synthetic procedures and data interpretation methods were discussed.

2.2 Experimental section

2.2.1 Solvents

Solvents were dried according to published procedures and distilled under argon prior to use.[14] CH_3CN was dried over CaH_2 powder over period of 48 hours in steelhead fixed to the condensers using heating mantle and collected by cannula using vacuum pump into dried glassware which were extensively dried in vacuum oven. Tetrahydrofuran was dried over sodium using benzophenone.

2.2.2 Substrates

All chemicals obtained from Aldrich Chemical Co. were the best available purity and were used without further purification unless otherwise noted. Thioanisole, *para*-X-substituted thioanisoles (X= $–OCH_3$, $–CH_3$, –H, –Cl), *para* substituted 2,6-di-*tert*-butylephenol (X = –OMe, –Me, –H, –CN), 2,4-di-*tert*–butylphenol, 2–phenylpropionaldehyde (2–PPA), Sodium chlorite ($NaClO_2$),

Sodium chlorate ($NaClO_3$), o–Tolidine, Benzyl alcohol were purchased from Aldrich Chemical Co. Benzyl alcohol-d_7 ($C_6D_5CD_2OH$) was purchased from C/D/N Isotopes Inc. (Pointe-Claire, Quebec, Canada). α–[D_1]–2–phenylpropionaldehyde (~ 90 %, D enriched) was purchased from RVL Scientific & Engineering Pvt. Ltd. (Lucknow, India).

Preparation of 2–Methyl–2–phenylpropionaldehyde[15]

NaH (3.2 g, 0.080 mol) was dissolved in dry THF (70 mL). The suspension was stirred in an ice bath during 10 minutes and 2–phenylpropionaldehyde (10 mL, 0.073 mol) was added slowly. The solution became slightly yellow and some effervescence was observed. After effervescence finished a solution of iodomethane (5 mL, 1.1 eq.) in THF (10 mL) was slowly added. Then the solution was allowed to stir overnight at room temperature. Next morning water was added to the white turbid solution which was then extracted 3 times with Et_2O, dried over Na_2SO_4, filtered and the solvents removed under vacuum to yield yellow oil. This oil was distilled at 70 ºC to give 2–Methyl–2–phenylpropionaldehyde with some small impurities. The crude was again washed with water and brine and extracted with ethyl ether. The solvent was dried and removed under vacuum and the remaining oil was distilled again at 40 ºC to give 5.7g of pure 2–Methyl–2–phenylpropionaldehyde (Yield ~ 48 %).

2.2.3 Oxidants

Iodosylbenzene was prepared by a literature method.[16] 32.2 g (0.10 mole) finely ground iodosobenzene diacetate was placed in 250 mL beaker, then slowly 150 mL of 3 N NaOH solution was added over a 5-minutes time with vigorous stirring. Then the lumps which were formed in the reaction mixture were mixed for 15 minutes with glass rod and spatula and the reaction mixture was stirred for another 45 minutes to complete the reaction. Then 100 mL water was added to the reaction mixture, stirred vigorously and crude solid iodosobenzene was collected on Buchner funnel. The wet solid was returned to the beaker and triturated in 200 mL water. The solid was again collected by Buchner funnel, washed with 200 mL of water and dried over vacuum and finally washed with 75 mL chloroform, filtered, dried and stored in a cold and dark place.

PhINTs was prepared by a literature method.[17] 3.20 g (10 mmol) (Diacetoxyiodo) benzene was added to the stirred mixture of para-toluenesulonamide and potassium hydroxide in methanol at below 10 ºC. The resulting yellow colored solution was stirred for 3 hours at room temperature. Then the reaction mixture was poured into water to get yellow colored solid, which was recrystallized from methanol to give crystalline N-tosyliminophenyliodinane.

50 % H_2O_2 was purchased from Merck-India.

2.3.1 Synthesis of ligand N,N-bis(2-pyridylmethyl)-N-bis(2-pyridyl) methylamine (N4Py):

(a) 5 g (0.027 mol) of Dipyridylketone, 4.17g (0.06 mol) of Hydroxyl amine hydrochloride and 10 mL ethanol were taken in a 100 mL round bottom flask which contained 4 g of NaOH and 20 mL of water and refluxed for 2 hours. Then

excess ethanol was evaporated and the solution was diluted to one litre, next the solution was neutralized with HCl properly up to pH =7, pinkish white precipitate dipyridyl ketoxime appeared, and then the precipitate was filtered off and dried for one day.

(b) The whole amount of dipyridyl ketoxime was taken in a three necked round bottom flask with 90 mL of ethanol and fitted with a reflux condenser, 60 mL of Hydrazine hydrate and Zn powder were added in conjugative steps over a six hours period. Then the solution was kept refluxing overnight. The product obtained was taken in a 100 mL round bottom flask and dissolved with 40 mL 5N sodium hydroxide solution.

(c) 2-Picolyl chloride hydrochloride was added to the solution and kept in reflux condition for two days. A brownish black colored solution appeared which was neutralized by $HClO_4$ and finally the solid product was obtained. (Yield: 3 g) (Scheme 2.1).[18]

2.3.2 Preparation of $[Fe^{II}(N4Py)(CH_3CN)](CF_3SO_3)_2$

N4Py (0.237 mmol, 100 mg) was dissolved in 3 mL of anhydrous ethyl acetate. To this, iron(II) triflate (0.284 mmol, 124 mg) in 1mL of acetonitrile was added in a dropwise manner. Orange-red precipitate was formed within 15 minutes. The reaction was allowed to stir further for 45 minutes. Excess of solvent was removed and washed thoroughly with ethyl acetate and dried. Pure complex was obtained by recrystallization from acetonitrile-diethyl ether mixture (1:4). (Yield: 0.125 g) (Scheme 2.1).[18, 19]

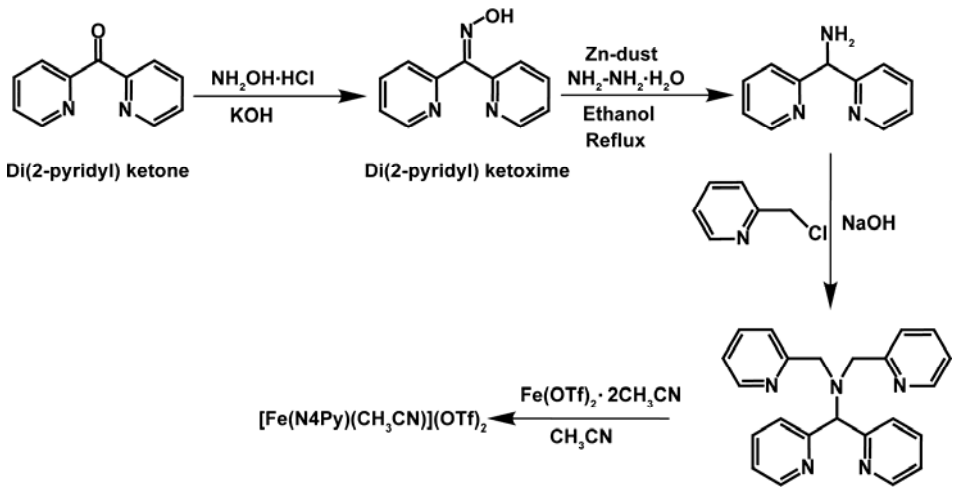

Scheme 2.1. Preparation of N4Py ligand and $[Fe^{II}(N4Py)(CH_3CN)](CF_3SO_3)_2$ complex.

2.3.3 General procedure for the synthesis of piperidones (pL^1 and pL^2):[20, 21]

Dimethyl acetonedicarboxylate (4.80 mL, 33.33 mmol) was taken in 20 mL of CH_3OH and was pre-cooled to -10 °C. A solution of pyridine-2-carboxyaldehyde (6.37 mL, 66.66 mmol) and corresponding amine (for pL^1: 2-picolylamine and pL^2: benzyl amine) (33.33 mmol) were added to it drop wise. After complete addition of amines, the solution was allowed to stir at room temperature overnight. The white precipitate thus obtained was filtered and washed with cold ethanol and dried in vacuum. The product obtained sufficient purity and was used as such for the synthesis of bispidines. Yield ~ 84 % (pL^1) (Scheme 2.2) and ~ 80 % (pL^2) (Scheme 2.3).

2.3.4 General procedure for the synthesis of bispidines (L^1 and L^2):[20, 21]

To a suspension of piperidone (12.70 g, 33.10 mmol) in 200 mL ethanol were added aqueous formaldehyde (37 %, 6.50 mL , 79.40 mmol) and corresponding amine (for L^1: benzyl amine and L^2: 2-Picolylamine) (39.70 mmol) dropwise. The reaction was allowed to reflux for 4 hours. Clear brown solution obtained after the end of the reaction, was concentrated to half and kept at -20 ºC. White crystals were obtained after several days (Scheme 2.2 and 2.3).

2.3.4 General procedure for the preparation of manganese(II) complexes:[22]

Bispidine ligand (0.10 g, 0.17 mmol) was dissolved in CH_3CN and $Mn^{II}(ClO_4)_2$ salt (0.089 g, 0.22 mmol) in CH_3CN was added dropwise under inert conditions. The pale yellow solution was allowed to reflux overnight. After the end of the reaction, the solution was syringe filtered and layered with ether to obtain colorless crystals which were suitable for X-ray diffraction (Scheme 2.2 and 2.3). The cif file of both the complexes has been deposited at the Cambridge Crystallographic Data Centre (CCDC) with the following deposition numbers. CCDC 1022749 and 1022750.

Caution! While we have had no problems with this compound, perchlorate salts are potentially explosive and should be handled with great care.

Spectral data for L^1: *Elemental analysis*: measured C 68.84, H 5.43, and N 12.07; calculated for $C_{34}H_{33}N_5O_5$: C 69.02, H 5.62 N 11.84. MW: 591.67. ^{1}H NMR (400 MHz, $CDCl_3$): 8.48 (d, J=4.5 2H,Py-H), 8.01 (d, J=4.2, 1H, Py-H), 7.85 (d, J=4.6, 1H, Py-H), 7.72-7.80 (m, 2H, Py-H), 7.64-7.52 (m, 2H, Py-H), 7.43-7.37 (m, 2H, Py-H), 7.10-7.00 (m, 5H, Ph-H), 6.37 (m, 2H, Py-H), 5.38 (s, 2H, -CH-Py), 3.75

(s, 6H, -OCH_3), 3.68 (s, 2H, -CH_2-Ph), 3.39(s, 2H, -CH_2-Py), 3.17(d, J=9.6Hz, 2H, -CH_2-), 2.63(d, J=11.6Hz, 2H, -CH_2-). Melting point 164 ^oC Yield: 26 %.

Spectral data for L^2: measured C 68.57, H 5.18, and N 12.07; calculated for $C_{34}H_{33}N_5O_5$: C 69.02, H 5.62 N 11.84. MW: 591.67. ^1H NMR (400 MHz, $CDCl_3$): 8.73(d, J=4.8Hz, 2H, Py-H), 8.52(d, J=4.4Hz, 1H, Py-H), 8.09(d, J=7.6Hz, 1H, Py-H), 7.73-7.69(m, 2H, Py-H), 7.54-7.50(m, 2H, Py-H), 7.36-7.30(m, 2H, Py-H), 7.20-7.13(m, 5H, Ph-H), 6.86(m, 2H, Py-H), 5.12(s, 2H, -CH-Py), 3.73 (s, 6H, -OCH_3), 3.61 (s, 2H, -CH_2-Ph), 3.52 (s, 2H, -CH_2-Py), 3.19 (d, J=12Hz, 2H, -CH_2-), 2.67 (d, J=12Hz, 2H, -CH_2-). Melting point 171 ^oC, Yield: 24 %.

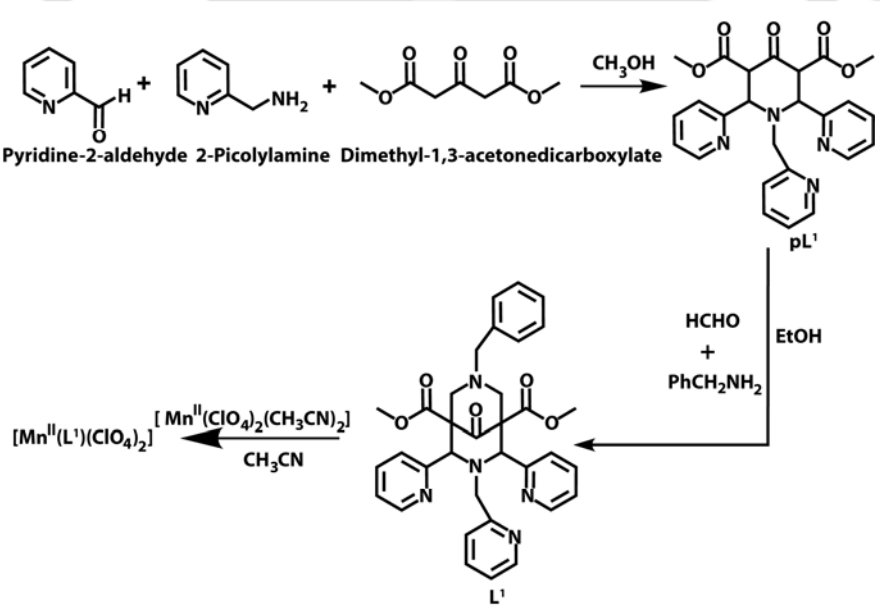

Scheme 2.2. Preparation of L^1 ligand and $[Mn^{II}(L^1)(ClO_4)_2]$ complex.

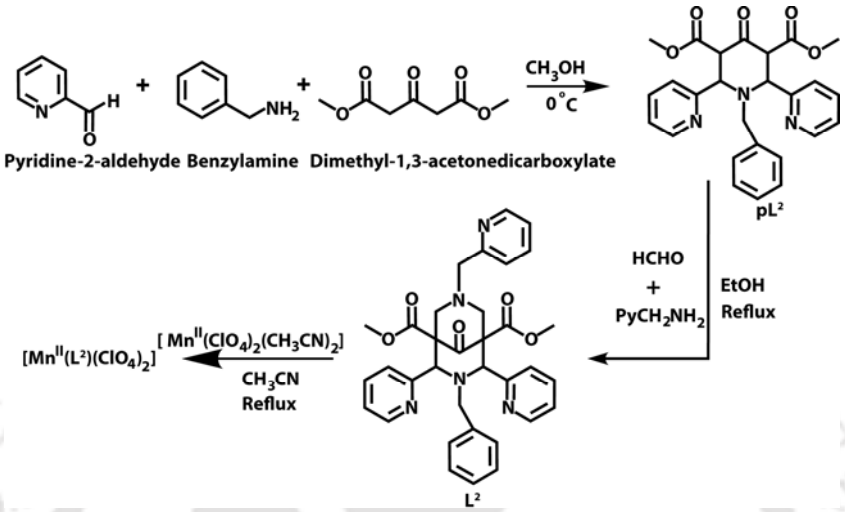

Scheme 2.3. Preparation of L^2 ligand and $[Mn^{II}(L^2)(ClO_4)_2]$ complex.

2.4 Characterization of metal (Fe/Mn) (II) complexes

Tetradentate nature of TPA and TMC ligands provides a labile site accounting for the instability of the corresponding complexes and so synthesis of stable high-valent metal complexes supported by pentadentate ligands were sought. A pentadentate system supporting high-valent iron and manganese unit should provide higher thermal stability and eliminates the possibility of exogenous ligand binding to metal. The pentadentate ligands N4Py and bispidines were selected as target ligands to support potential high-valent metal systems.

2.4.1 ESI-MS

Electrospray ionization mass spectra in CH_3CN at 25 °C of complex $[Mn^{II}(L^1)(ClO_4)]^+$ shows peak assigned for *m/z* = 322.97 and 744.93 corresponds to $[Mn(L^1)]^{2+}$ and $[Mn(L^1)(ClO_4)]^+$ and for $[Mn^{II}(L^2)(ClO_4)]^+$ peak distribution at *m/z* = 323.06, 343.59, 745.14 whose mass and isotope distribution patterns corresponds to $[Mn(L^2)]^{2+}$, $[Mn(L^2)(CH_3CN)]^{2+}$ and $[Mn(L^2)(ClO_4)]^+$ respectively(Figure 2.1).

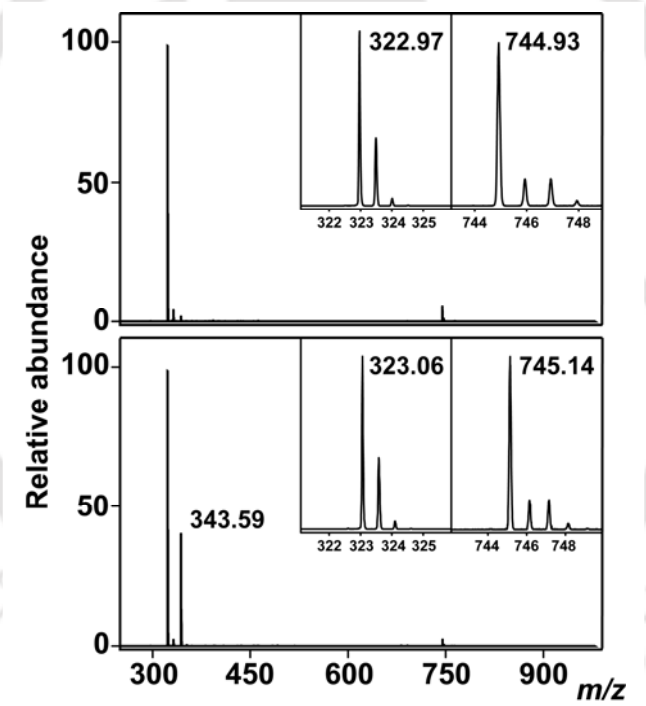

Figure 2.1. Electrospray ionization mass spectra in CH_3CN at 25 °C of $[Mn^{II}(L^1)(ClO_4)]^+$, peak assigned for *m/z* = 322.97 and 744.93 corresponds to $[Mn(L^1)]^{2+}$ and $[Mn(L^1)(ClO_4)]^+$ (top). $[Mn^{II}(L^2)(ClO_4)]^+$, peak distribution at *m/z* = 323.06, 343.59, 745.14 whose mass and isotope distribution patterns corresponds to $[Mn(L^2)]^{2+}$, $[Mn(L^2)(CH_3CN)]^{2+}$ and $[Mn(L^2)(ClO_4)]^+$ respectively (bottom).

Electrospray ionization mass spectra of $[(L^1)Fe^{II}(CH_3CN)](BF_4)_2$ shows a peak at *m/z* = 294.64 corresponding to $[Fe^{II}(L^1)]^{2+}$ in CH_3CN at 25 °C (Figure 2.2). Complex $[Fe^{II}(CH_3CN)(L^2)](BF_4)_2$ gives a peak at *m/z* = 294.63 which corresponds to $[Fe^{II}(L^2)]^{2+}$ in CH_3CN at 25 °C (Figure 2.3). Analysis of complexes $[Fe^{II}(N4Py)CH_3CN](CF_3SO_3)_2$ by high-resolution ESI-MS gave convincing initial evidence for their formulation as iron(II)complexes. Complexes shows ESI-MS peak at *m/z* = 572.03 which corresponding to $[Fe^{II}(N4Py)CF_3SO_3]^+$ with an isotope pattern that matches the theoretically expected distribution, Figure 2.4.

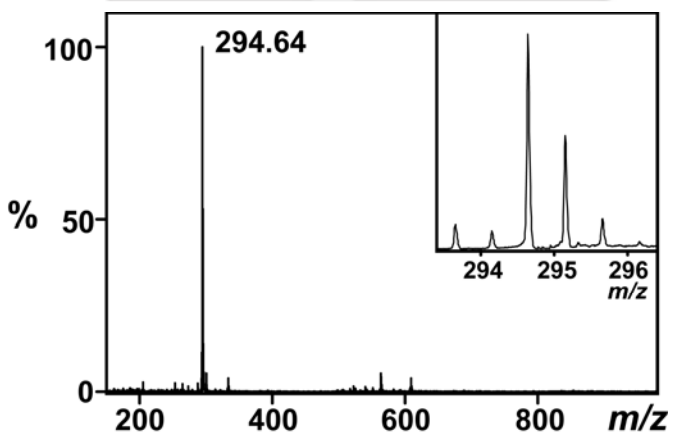

Figure 2.2. Electrospray ionization mass spectra of $[(L^1)Fe^{II}(CH_3CN)](BF_4)_2$, peak assigned for *m/z* = 294.64 correspond to $[(L^1)Fe^{II}]^{2+}$ in CH_3CN at 25 °C.

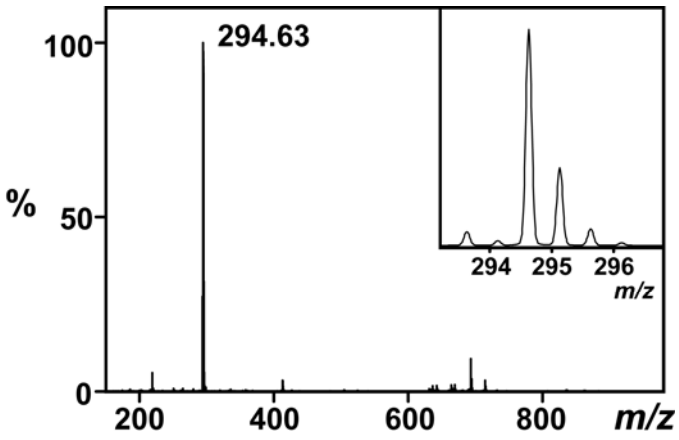

Figure 2.3. Electrospray ionization mass spectra of $[(L^2)Fe^{II}(CH_3CN)](BF_4)_2$, peak assigned for m/z = 294.63 correspond to $[(L^2)Fe^{II}]^{2+}$ in CH_3CN at 25 °C.

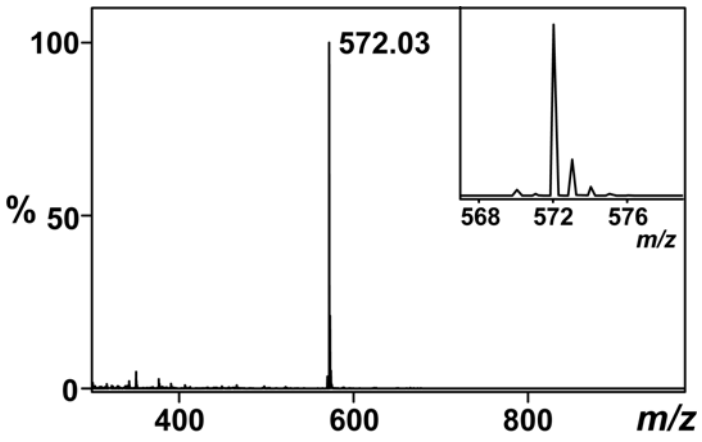

Figure 2.4. Electrospray ionization mass spectra of $[Fe^{II}(CH_3CN)(N4Py)](CF_3SO_3)_2$. The peak assigned for m/z = 572.03 corresponds to $[Fe^{II}(CF_3SO_3)(N4Py)]^+$ in CH_3CN at 25 °C.

2.4.2 Elemental analysis:

$[Mn^{II}(L^1)(CH_3CN)](ClO_4)_2.CH_3CN$: Elemental analysis: measured C 48.74, H 3.92, N 11.02; calculated for $C_{38}H_{39}N_7O_{13}Cl_2$ Mn, C 49.20, H 4.24, N 10.57 MW 927.60; ESI-MS *m/z* = 322.97 $[Mn(L^1)]^{2+}$, 744.93 $[Mn(L^1)(ClO4)]^+$.

$[Mn^{II}(L^2)(CH_3CN)](ClO_4)_2$: Elemental analysis: measured C 47.91, H 3.75, N 10.05; calculated for $C_{36}H_{36}N_6O_{13}Cl_2Mn$, C 48.77, H 4.09, N 9.48 MW 886.55; ESI-MS *m/z* = 323.06 $[Mn(L^2)]^{2+}$, 343.59 $[Mn(L^2)(CH_3CN)]^{2+}$, 745.14 $[Mn(L^2)(ClO4)]^+$.

2.4.3 X-ray structural studies:

The X-ray crystallographic data were collected at 23 °C with Mo Kα radiation (λ = 0.71073 Å) using a Bruker Nonius SMART CCD diffractometer equipped with graphite monochromator. The SMART software was used for data collection and also for indexing the reflections and determining the unit cell parameters; the collected data were integrated using SAINT software.[23] The structures were solved by direct methods and refined by full-matrix least-squares calculations using SHELXTL software[23] All the non-H atoms were refined in the anisotropic approximation against F^2 of all reflections. The H-atoms attached to water molecules were located in the difference Fourier synthesis maps, and refined with isotropic displacement coefficients. The crystals of compound MnL^2 were of poor quality and had microscopic cracks in it. As a result, the obtained reflections were slightly weak in intensity. In spite of this, the structure of the molecule was solved with firmly established connectivity and good thermal ellipsoids for all the atoms.

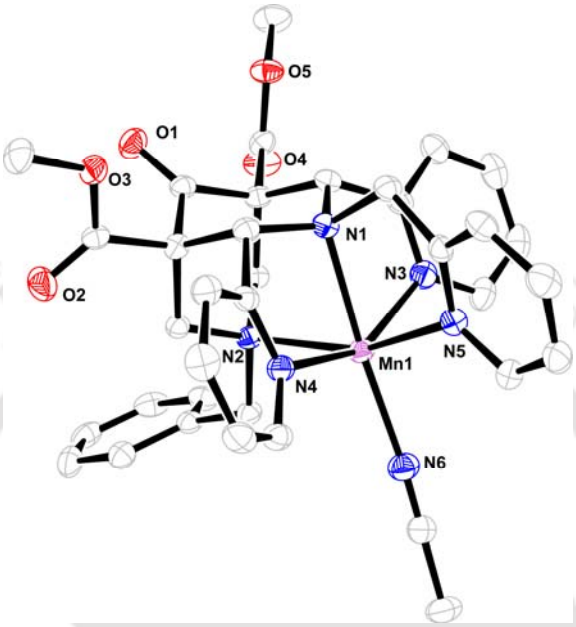

Figure 2.5. ORTEP plot of $[Mn^{II}(L^1)(CH_3CN)_2]^{2+}$ with thermal ellipsoids drawn at the 50 % probability level. Hydrogen atoms and counter ions are omitted for clarity.

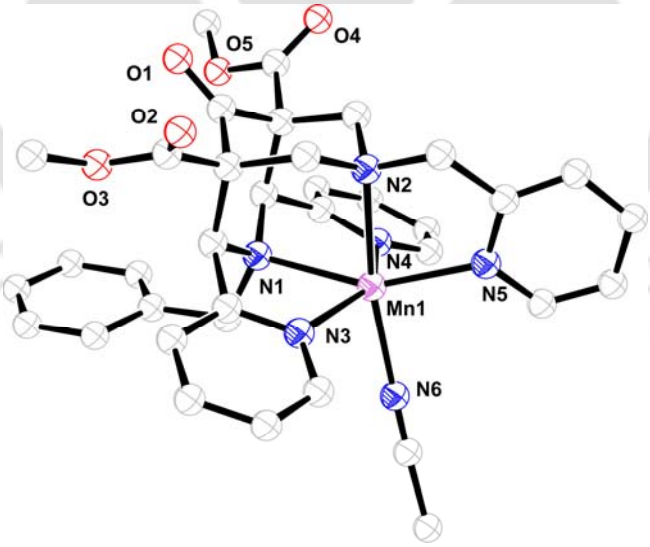

Figure 2.6. ORTEP plot of $[Mn^{II}(L^2)(CH_3CN)_2]^{2+}$ with thermal ellipsoids drawn at the 50 % probability level. Hydrogen atoms and counter ions are omitted for clarity.

Table 2.1. Crystal data and structure refinement for **L^1 & L^2**

	L^1	**L^2**
Formula	C_{38} H_{39} Cl_2 Mn N_7 O_{13}	C_{36} H_{36} Cl_2 Mn N_6 O_{13}
Formula weight	927.60	886.55
Temperature (K)	296	296
Wavelength (Å)	0.71073	0.71073
Crystal system	Monoclinic	Triclinic
Space group	P21/n	P-1
a (Å)	11.3329(2)	10.873(3)
b (Å)	19.7985(3)	12.490(4)
c (Å)	18.3664(3)	15.605(7)
α (deg)	90.00	100.47(2)
β (deg)	99.2850(10)	98.73(2)
γ (deg)	90.00	109.895(15)
V (Å^3)	4066.96(12)	1906.5(12)
Z	4	2
$\rho_{calc.}$ (g ·cm^{-3})	1.541	1.544
μ (mm^{-1})	0.534	0.561
F(000)	1948.0	914
reflections collected	7166	6623

reflns unique	6267	3155
θ range (deg)	1.52–25.00	1.79–25.00
Δ_r (max, min), e· Å^{-3}	0.717, –1.164	0.884, –1.063
R_{int}	0.0464	0.1082
$R_1[I \geq 2\sigma(I)]$	0.0475	0.0822
wR_2 $[I \geq 2\sigma(I)]$	0.1721	0.2189
R_1 (all data)	0.0532	0.1202
wR_2 (all data)	0.1764	0.2490

Table 2.2. Selected bond lengths (Å) and angels (°) for $[Mn^{II}(L^1)(CH_3CN)_2](ClO_4)_2$

	Distances (Å)		
Mn1-N1	2.265(2)	Mn1-N4	2.263(2)
Mn1-N2	2.347(2)	Mn1-N5	2.253(2)
Mn1-N3	2.252(2)	Mn1-N6	2.129(2)
	Angels (°)		
N1-Mn1-N2	80.05(8)	N5-Mn1-N3	90.75(8)
N1-Mn1-N3	75.06(8)	N5-Mn1-N4	81.07(8)
N1-Mn1-N4	76.14(8)	N5-Mn1-N6	93.88(9)
N2-Mn1-N3	89.58(8)	N6-Mn1-N1	172.24(9)
N4-Mn1-N2	88.02(8)	N6-Mn1-N2	107.15(8)
N4-Mn1-N3	151.08(8)	N6-Mn1-N3	107.37(9)
N5-Mn1-N1	78.64(8)	N6-Mn1-N4	100.86(9)
N5-Mn1-N2	157.84(8)		

Table 2.3. Selected bond lengths (Å) and angels (°) for $[Mn^{II}(L^2)(CH_3CN)_2](ClO_4)_2$

Distances (Å)			
Mn1-N1	2.276(7)	Mn1-N4	2.262(6)
Mn1-N2	2.334(7)	Mn1-N5	2.163(7)
Mn1-N3	2.213(6)	Mn1-N6	2.185(9)
Angels (°)			
N1-Mn1-N4	73.70(2)	N3-Mn1-N5	118.5(3)
N2-Mn1-N1	75.06(8)	N3-Mn1-N6	88.10(3)
N2-Mn1-N4	93.10(2)	N5-Mn1-N1	154.3(3)
N2-Mn1-N5	77.30(3)	N5-Mn1-N4	94.10(3)
N2-Mn1-N6	167.8(3)	N5-Mn1-N6	92.70(3)
N3-Mn1-N1	74.80(2)	N6-Mn1-N1	110.4(3)
N3-Mn1-N2	90.70(2)	N6-Mn1-N4	94.50(3)
N3-Mn1-N4	147.2(2)		

2.5 Generation of high-valent metal complexes

Mn^{IV}=O complexes, *viz.* $[Mn^{IV}(O)(L^1)]^{2+}$ (**3**) and $[Mn^{IV}(O)(L^2)]^{2+}$ (**4**) were prepared by reacting their corresponding Mn^{II} complex with cerium(IV) ammonium nitrate (CAN) in acetonitrile/water (9:1) or acetone/water (9:1) at 5 °C. $[Mn^{III}(L^1)(O_2)]^+$ Intermediate was prepared by reacting their corresponding Mn^{II} complex with 10 equivalents of H_2O_2 and 2.5 equivalents triethylamine (TEA) in CH_3CN (2 mL) in acetonitrile at 15 ºC. Iron(IV)-oxo complexes $[Fe(O)(N4Py)]^{2+}$ (**6**) were generated by vigorous stirring with excess solid PhIO at room temperature and remaining unreacted PhIO was removed by 0.2 μm syringe filters. This **6** was stable at room temperature and has a half-life period of

~60 hours in acetonitrile at 25 °C. Iron(IV)-imido complex **7** was generated in an acetonitrile solution *in-situ* using 1.5 equiv. of PhINTs as tosylimido donor following procedures reported before. Stability of these compounds helped for the various characterizations like ESI-MS, UV/Vis and also structural X-ray crystallographic characterization. These yields and purities were ideal for the reactivity studies.[24-27]

2.6 Characterization of high-valent manganese and iron based complex

2.6.1 ESI-MS analysis

Analysis of complexes **3** and **4** by high-resolution ESI-MS gave convincing initial evidences for their formulation as Mn(IV)-oxo species. The electro-spray ionization mass spectra (ESI-MS) of **3** and **4** exhibit prominent peaks at *m/z* ≅ 332, and the isotope patterns show that these correspond to $[Mn^{IV}(O)L^{1,2}]^{2+}$, an appropriate isotope pattern which matches with the theoretically expected distribution pattern. Upon introduction of $H_2{}^{18}O$ into the solution of **3** and **4**, a mass shift from *m/z* = 331.85 to 332.81 for **3** (Figure 2.7 inset) and *m/z* = 331.76 to 331.78 for **4** were observed (Figure 2.8, inset), indicating that the oxygen atom of the Mn(IV)-oxo species exchanges with labeled water, giving ^{18}O-labeled **3** and **4**. The ESI mass spectra of **5** exhibit a prominent ion peak with *m/z* = 678.31 whose isotopic distribution pattern corresponds to $[Mn^{III}(L^1)(O_2)]^+$ (Figure 2.9). ESI-MS spectra of $[Fe^{IV}(O)(L^1)]^{2+}$ shows a peak at *m/z* = 302.83 (Figure 2.10) and *m/z* = 302.81 for $[Fe^{IV}(O)(L^2)]^{2+}$ (Figure 2.11). Iron(IV)-oxo complexes **6** in ESI-MS (Figure 2.12) shows major peaks at *m/z* =588.01 which corresponds to $\{[Fe^{IV}(O)N4Py](CF_3SO_3)\}^+$ and , an appropriate isotope pattern which matches with theoretically expected distribution. ESI-MS of **7** (Figure 2.13) gave a major peak at *m/z* = 741.07

corresponding to $\{[Fe^{IV}(NTs)N4Py](CF_3SO_3)\}^+$ with an isotope pattern which matches with the theoretically expected distribution.

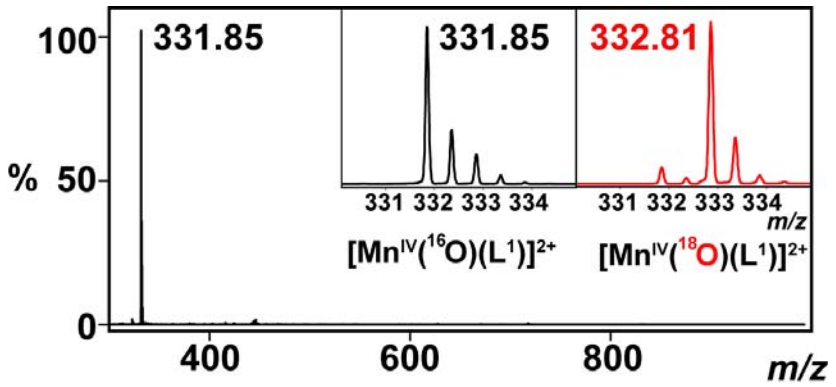

Figure 2.7. The ESI-MS spectra of $[Mn^{IV}(O)(L^1)]^{2+}$ (**3**) formed in the reaction of **1** (2 mM) and CAN (8 mM) in CH_3CN/H_2O (9:1) at 5 °C. Mass peak at *m/z* = 331.85 is assigned for $[Mn^{IV}(O)(L^1)]^{2+}$. Insets show observed isotopic distribution of $[Mn^{IV}(^{16}O)(L^1)]^+$ (left panel) and $[Mn^{IV}(^{18}O)(L^1)]^+$ (right panel).

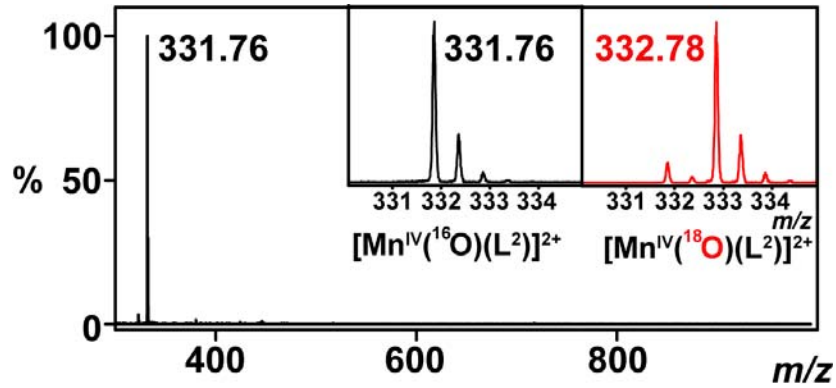

Figure 2.8. The ESI-MS spectra of $[Mn^{IV}(O)(L^2)]^{2+}$ (**4**) formed in the reaction of **2** (2 mM) and CAN (8 mM) in CH_3CN/H_2O (9:1) at 5 °C. Mass peak at *m/z* = 331.76 is assigned for $[Mn^{IV}(O)(L^2)]^{2+}$. Insets show observed isotopic distribution of $[Mn^{IV}(^{16}O)(L^2)]^+$ (left panel) and $[Mn^{IV}(^{18}O)(L^2)]^+$ (right panel).

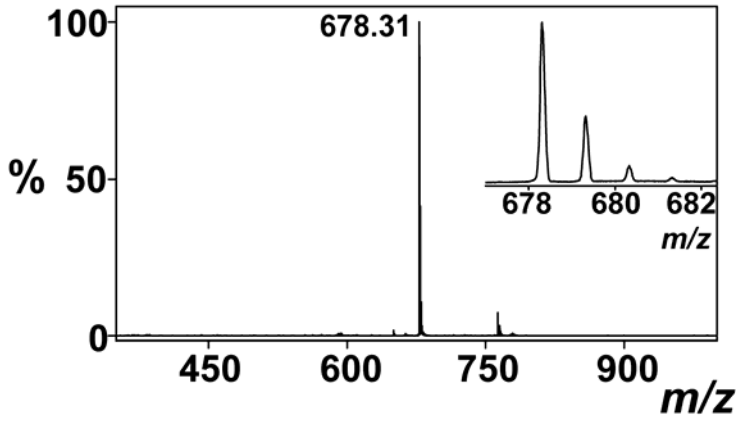

Figure 2.9. ESI-MS spectrum of **5** in CH_3CN at 15 °C. Mass peak at *m/z* = 678.31 is assigned for $[Mn(L^1)(O_2)]^+$. Inset shows the observed isotope distribution patterns for $[Mn(L^1)(O_2)]^+$.

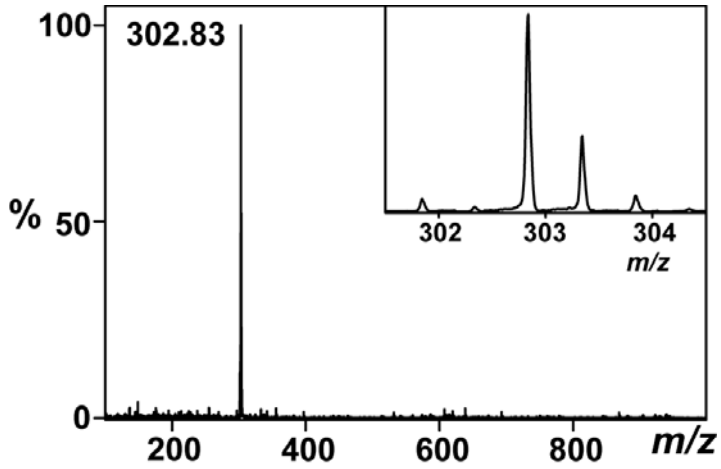

Figure 2.10. ESI-MS spectrum of $[Fe^{IV}(O)(L^1)]^{2+}$ at 25 °C. Mass peak at *m/z* = 302.83 is assigned for $[Fe^{IV}(O)(L^1)]^{2+}$. Inset shows the observed isotope distribution patterns for $[Fe^{IV}(O)(L^1)]^{2+}$.

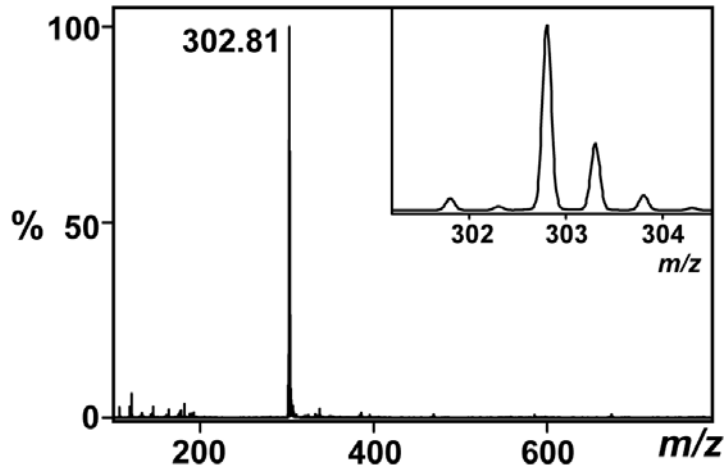

Figure 2.11. ESI-MS spectrum of $[Fe^{IV}(O)(L^2)]^{2+}$ at 25 °C. Mass peak at *m/z* = 302.81 is assigned for $[Fe^{IV}(O)(L^2)]^{2+}$. Inset shows the observed isotope distribution patterns for $Fe^{IV}(O)(L^2)]^{2+}$.

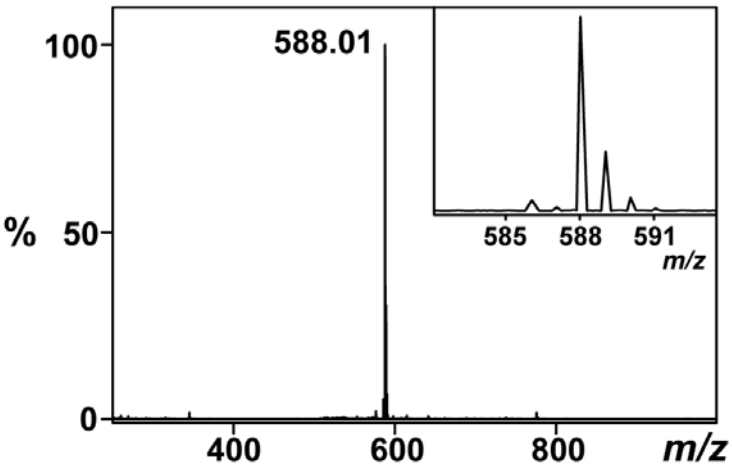

Figure 2.12. ESI-MS spectrum of $[Fe^{IV}(O)(N4Py)]^{2+}$ at 25 °C. Mass peak at *m/z* = 588.01 is assigned for $\{[Fe^{IV}(O)N4Py](CF_3SO_3)\}^+$. Inset shows the observed isotope distribution patterns for $[Fe^{IV}(O)(N4Py)]^{2+}$.

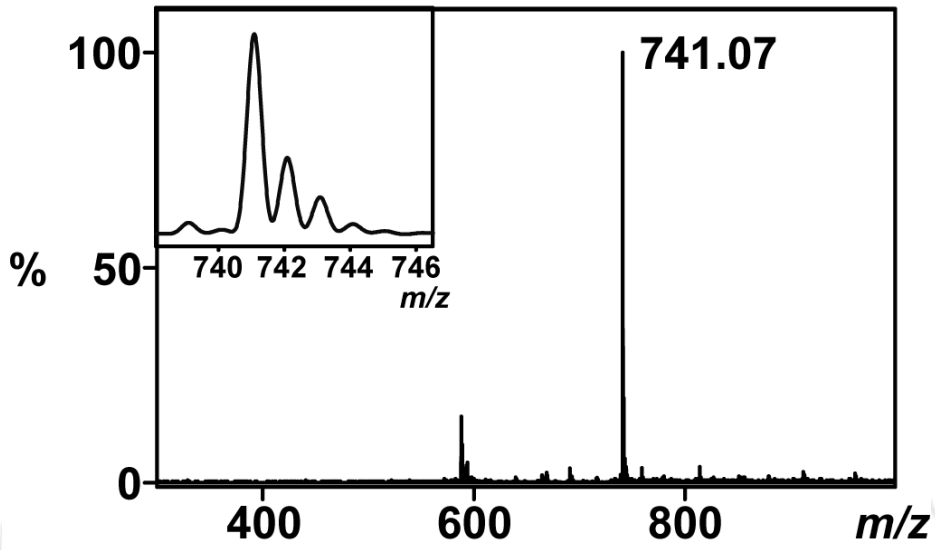

Figure 2.13. ESI-MS spectra of $[[Fe^{IV}(NTs)N4Py](CF_3SO_3)_2$. A mass peak at *m/z* of 741.07 is assigned to $\{[Fe^{IV}(NTs)(N4Py)]CF_3SO_3\}^+$, Inset shows the isotopic distribution for $[Fe^{IV}(NTs)(N4Py)]^{2+}$.

2.6.2 UV/Vis analysis

The initial identifications were made based on visible features as the absorption bands of high-valent complexes. Complex **3** exhibits an absorption spectrum with an intense band at 545 nm (ε = 400 $M^{-1}cm^{-1}$), with a weak absorption in the near IR region at 970 nm (ε = 35 $M^{-1}cm^{-1}$). Similarly, complex **4** has electronic transitions at 570 nm (ε = 400 $M^{-1}cm^{-1}$) and at 975 nm (ε =103 $M^{-1}cm^{-1}$, Figure 2.14). $[Mn^{III}(L^1)(O_2)]^+$ (**5**) afforded a blue intermediate with an absorption band at 605 nm (ε = 270 M^{-1} cm^{-1}; with a half-life ~60 minutes, Figure 2.15). $[Fe^{IV}(O)(L^1)]^{2+}$ shows an absorption band at 730 nm (ε = 400 M^{-1} cm^{-1}) (Figure 2.16) and $[Fe^{IV}(O)(L^2)]^{2+}$ giving a prominent peak at 730 nm (ε = 380 M^{-1} cm^{-1}) (Figure 2.17). Iron(IV)-oxo intermediate **6** was confirmed on the

basis of visible features with low energy 695 nm (ε = 400 M^{-1} cm^{-1}), that arises from the ligand field transitions characteristic for S = 1 iron(IV) complexes , (Figure 2.18). The identity of iron(IV)-imido complex **7** was confirmed on the basis of visible features of an intense LMCT band at 445 nm (ε = 2700 M^{-1} cm^{-1}) and a low energy 660 nm band (ε = 250 M^{-1} cm^{-1}) that arises from ligand field transitions characteristic for S = 1 iron(IV) complexes(Figure 2.18).

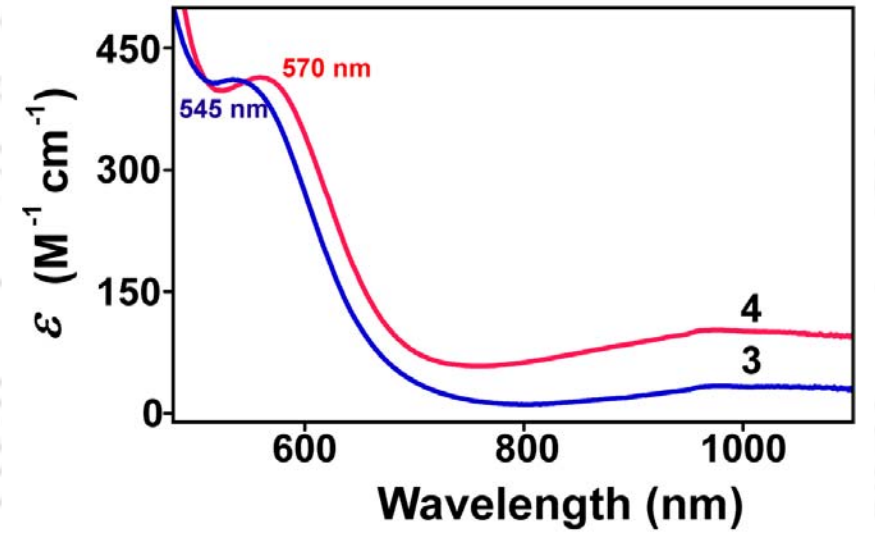

Figure 2.14. UV/Vis spectra of **3** and **4** generated in the reactions of **1** (2 mM) and **2** (2 mM) with CAN (8 mM) in CH_3CN/H_2O (9:1) at 5 ºC.

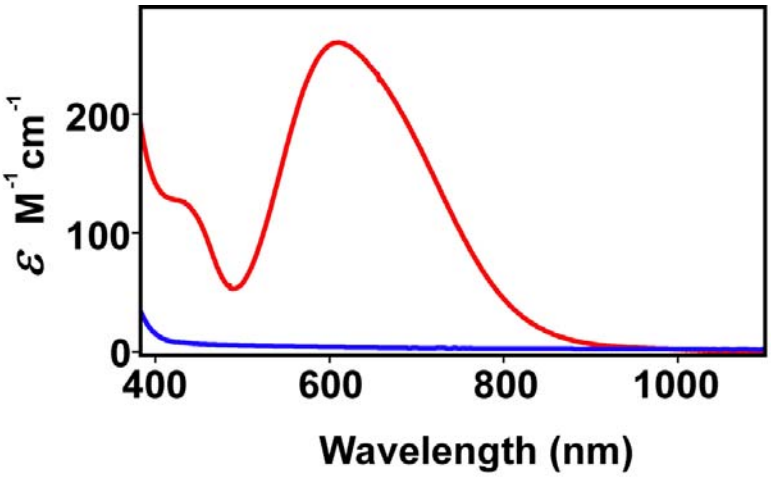

Figure 2.15. UV/Vis spectra of formation of **5** (2 mM) upon addition of $[Mn(L^1)]^{2+}$ (**1**) in the presence of TEA (5 mM) and H_2O_2 (20 mM) in CH_3CN at 15 ºC.

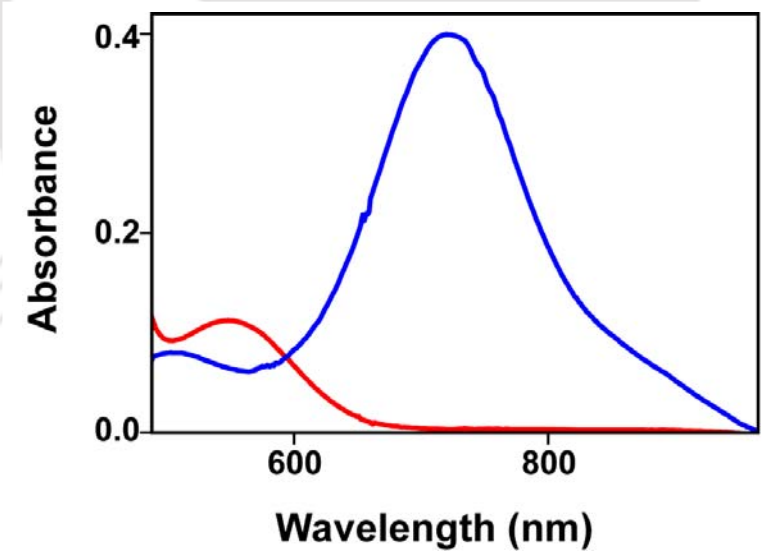

Figure 2.16. UV/Vis absorption spectra of the iron(IV)-oxo intermediate formed during the reaction of 1 mM $[Fe^{II}(L^1)]^{2+}$ with 1.2 equiv. of $NaClO_2$ at 25 ºC in acetate buffer at pH=5.0.

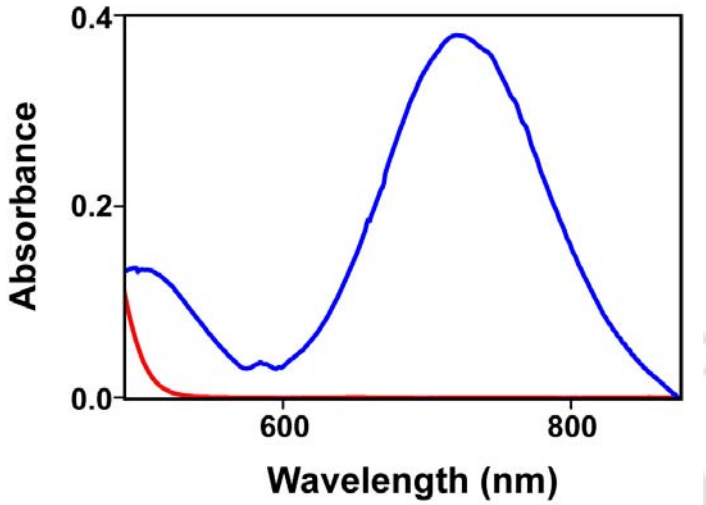

Figure 2.17. UV/Vis absorption spectra of the iron(IV)-oxo intermediate formed during the reaction of 1 mM $[Fe^{II}(L^2)]^{2+}$ with 1.2 equiv. of $NaClO_2$ at 25 ºC in acetate buffer at pH 5.0.

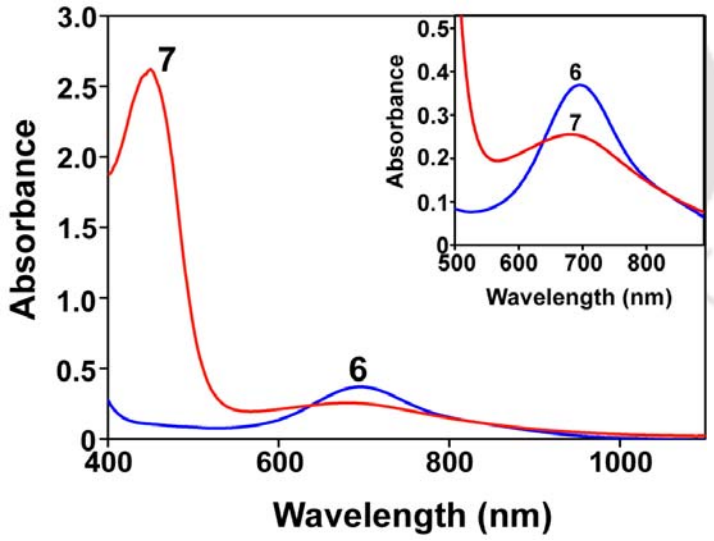

Figure 2.18. UV/Vis spectra of 1mM solution of $[Fe^{IV}(NTs)(N4Py)]^{2+}$ (**7**) and $[Fe^{IV}(O)(N4Py)]^{2+}$ (**6**) in CH_3CN at 0 ºC . Inset shows expanded lower energy region.

2.7 Physical methods

UV/Vis spectra were recorded on a Hewlett Packard 8453 spectrophotometer equipped with either constant temperature circulating water bath or a liquid nitrogen cryostat (Unisoku) with a temperature controller. Electrospray ionization mass spectra (ESI-MS) were recorded on a Waters (Micromass MS Technologies) Q-TOF Premier mass spectrometer by infusing samples directly into the source at 15 μL/min using a syringe pump. The spray voltage was set at 2 kV and the capillary temperature at 80 °C. NMR (^{1}H and ^{13}C) spectra were recorded with either Bruker 600/150 MHz or Varian 400 MHz spectrometer. Elemental analysis (C, H, N) were recorded on Eurovector EA3000.

2.8 Reactivity studies

All reactions were run in a 10 mm path length UV cuvette by monitoring UV/Vis spectral changes of reaction solutions. The rate constants were determined by fitting the changes in absorbance of the intermediates under study. The rate constants were averaged by the three determinations, and standard deviation was less than 10 % of the given values.

2.9 Product analysis

All experiments were done at least in triplicate. Product analysis for thioanisole oxidation was performed on WATERS ACQUITY UPLC equipped with a variable wavelength UV-200 detector. Products were separated on Waters Symmetry C18 reverse phase column (4.6 x 250 mm), and detection was made at 215 and 254 nm and product yields were determined by comparison with standard curves of known authentic samples. In the case of 2,4-di-tert-

butylphenol (2,4-*t*-$Bu_2C_6H_3OH$) as substrate, we observed the formation of 2,2'-dihydroxy-3,3',5,5'-tetra-tertbutylphenol (~100 % based on the intermediates used).

2.10 Confirmation of chlorine dioxide

To determine whether chlorine dioxide is produced in the reaction mixture, the gas was extracted from the aqueous medium using diethyl ether as a solvent. Approximately 500 μL of diethyl ether was added to the reaction mixture, mixed for 30 seconds, allowed the mixture to settle down, and then the resulting yellow colored top layer solution was removed with the pipette. Negative mode electrospray ionization mass spectroscopy (ESI-MS) of the diethyl ether extract confirmed that ClO_2 (*m/z* = 67.14) was formed during the reaction. To confirm the ClO_2 at *m/z* = 67.14 was that of chlorine dioxide, a sample of chlorite was added to diethyl ether and mixed for 40 minutes. A considerable amount of solid chlorite remained insoluble in diethyl ether. ESI-MS of the resulting solution confirmed this by the absence of a peak at *m/z* = 67.14. Therefore, the peak at 67.14 *m/z* is that of ClO_2 and not ClO_2^- (Figure 2.19).

2.11 *o*-Tolidine product analysis

Chlorate content was determined using 3,3'-dimethyl-4,4'-diaminobiphenyl (*o*-tolidine) as described previously.[28] A typical reaction was carried out with 10 μM Fe^{II} solution with 4.0 mM $NaClO_2$ and 1 mM *o*-tolidine in acetate buffer at ambient temperature. The *o*-tolidine product was extracted from the aqueous medium into ethyl acetate and analyzed by ESI-MS.

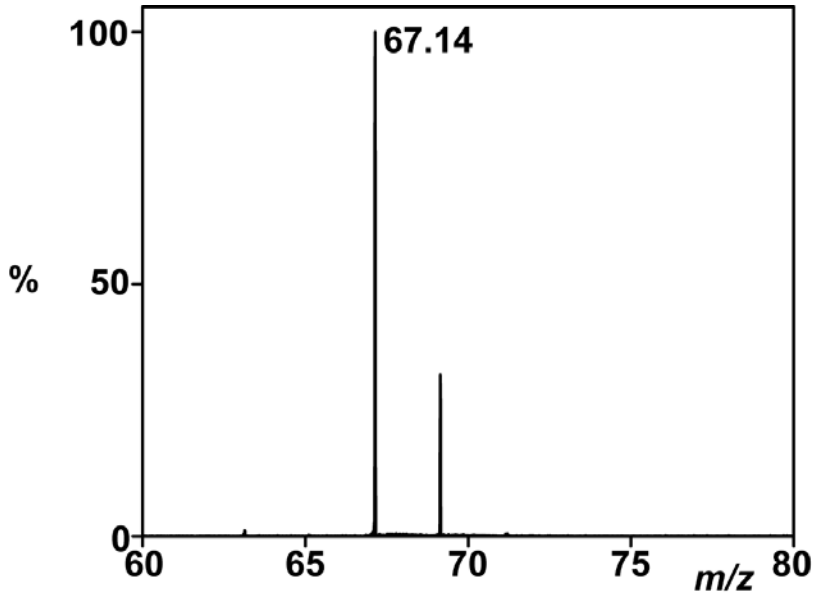

Figure 2.19. ESI-MS of extracted ClO_2 from the reaction of 10 μM $[Fe^{II}(N4Py)]^{2+}$ and 4.00 mM $NaClO_2$ in diethyl ether at 25 ºC.

2.12 Kinetic studies

At 5 ºC kinetic experiments were performed by using the following procedures, 2 mM Mn^{IV}=O complexes including $[Mn^{IV}(O)(L^1)]^{2+}$ (**3**) and $[Mn^{IV}(O)(L^2)]^{2+}$ (**4**) were prepared from 2 mM solutions of either $[Mn^{II}(L^1)(ClO_4)_2]$ (**1**) or $[Mn^{II}(L^2)(ClO_4)_2]$ (**2**) by reacting with cerium(IV) ammonium nitrate (CAN) in acetonitrile/water (9:1) or acetone/water (9:1) at 5 ºC. Each time 2.5 mL portion of Mn(II) solution was taken in a 4 mL glass vial, from this 2 mL was transferred into cuvette and deoxygenated with argon gas sealed with rubber septum and kept in UV/Vis spectrophotometer cuvette holder which is attached with low temperature cryostat and equilibrated at 1 ºC, then

slowly 50 µL diluted 4 equivalents of CAN was added through the 250 µL hamiltonian syringe, immediately mixed with another 1 ml syringe until characteristic peaks of intermediates in visible regions were monitored in the UV/Vis spectrophotometer. As it reaches maximum formation of Mn^{IV}=O intermediate, a few minutes were given to equilibrate the solution temperature. Then substrates were slowly added through a 250 µL hamiltonian syringe to the solutions, mixed with another 1 mL syringe and the time course of the decay of the Mn^{IV}=O chromophore was monitored. Concentrations of the substrates were used ranging from 0.005 M to 0.5 M and were adjusted to achieve convenient reaction times.

At 15 ºC kinetic experiments were performed by using the following procedure: 2 mM solution of $[Mn^{III}(L^1)(O_2)]^+$ (**5**) was prepared from 2 mM solution of $[Mn^{II}(L^1)(ClO_4)_2]$ (**1**) by reacting with H_2O_2 (20 mM) in the presence of triethylamine (TEA, 5 mM) in CH_3CN at 15 ºC. Each time 2.5 mL of Mn(II) solution in 4 mL glass vial was taken, from this 2 mL was transferred into cuvette and deoxygenated with argon gas sealed with rubber septum and kept in UV/Vis spectrophotometer cuvette holder which was attached with low temperature cryostat and waited till equilibrated at 1 ºC, then slowly 50 µL of 10 equivalents of H_2O_2 was added in the presence of 2.5 equivalents triethylamine through the 250 µL hamiltonian syringe, immediately mixed with another 1 ml syringe until characteristic peaks of intermediates in visible region was monitored in the UV/Vis spectrophotometer. After it reaches maximum formation of Mn(III)-peroxo intermediate a few minutes were given to equilibrate the solution temperature. Then substrates were slowly added through a 250 µL hamiltonian syringe to the solutions, mixed with another 1 mL syringe and the time course of the decay of the Mn(III)-peroxo chromophore was monitored. Concentrations of

the substrates were used ranging from 0.005 M to 0.5 M and were adjusted to achieve convenient reaction times.

Formation of ClO_2 were monitored by the addition of the iron(II) complexes to solutions of sodium chlorite ($NaClO_2$), there was an increase in absorbance at 360 nm, characteristic for the formation of chlorine dioxide in acetate buffer (50 mM) at pH=5.0 at 25 °C. This reaction was also carried out with above mentioned procedure.

Iron(IV)-oxo and iron(IV)-imido complexes, **6** and **7,** was prepared at 25 ºC, from1 mM solution of $[Fe^{II}(N4Py)(CH_3CN)](CF_3SO_3)_2$ in CH_3CN. Every time 2.5 mL portion of iron(II) solution in 4 mL glass vial was taken and excess solid PhIO/PhINTs was added and thoroughly mixed by vortex for 5 minutes affording oxo/imido complex. The solution was filtered through 0.2 μM syringe-filter into another clean dried 4 mL glass vial and deoxygenated with argon gas. 2 mL of it was transferred into a cuvette and sealed with rubber septum and kept in UV/Vis spectrophotometer cuvette holder and equilibrated at 25 ºC, then substrates were slowly added using the 250 μL hamiltonian syringe to the solutions and mixed with another 1 mL syringe and the time course of the decay of the iron(IV)-oxo/ iron(IV)-imido chromophore were monitored. Concentrations of the substrates were used ranging from 0.005 M to 0.5 M and were adjusted to achieve convenient reaction times.

Concentrations of substrates were used ranging from 0.005 M to 0.5 M, achieving pseudo first-order conditions. Reactions were monitored through a minimum of 5 half-lives and k_{obs} were determined by fitting the decay curve of the intermediates' visible bands to the Eq 2.1.

$$[A] = [A_0] + b*(e^{-kt}) \qquad \text{----- (Eq 2.1)}$$

Plots of k_{obs} against substrate concentration yielded second-order rate constants for each system.

Reaction mixtures were removed from the cuvette, oxidation products and metal salts were separated and passed through the silica gel and washed subsequently with CH_3CN. Product yields were determined by peak area ratios relative to the standard samples by different (like GC, NMR and ESI-MS) spectroscopic techniques.

2.14 References

1. E. I. Solomon, *Chem. Rev*. **2000**, *100*, 235–350.
2. E. G. Kovaleva J. D. Lipscomb, *Nature Chem. Biol.* **2008**, *4*, 186–193.
3. L. C. Blasiak, F. H. Vaillancourt, C. T. Walsh, C. L. Drennan, *Nature* **2006**, *440*, 368–371.
4. J. Rittle, M. T. Green, *Science* **2010**, *330*, 933–937.
5. E. G. Kovaleva, J. D. Lipscomb, *Science* **2007**, *316*, 453–457.
6. A. Karlsson, *Science* **2003**, *299*, 1039–1042.
7. R. M. Cicchillo, *Nature* **2009**, *459*, 871–874.
8. E. I. Solomon, T. C. Brunold, M. I. Davis, J. N. Kemsley, S.–K. Lee, N. Lehnert, F. Neese, A. J. Skulan, Y.–S. Yang, J. Zhou, *Chem. Rev.* **2000**, *100*, 235–349.
9. M. Costas, M. P. Mehn, M. P. Jensen, L. Que Jr., *Chem. Rev.* **2004,** *104,* 939–986.
10. R. P. Hausinger, *Crit. Rev. Biochem. Mol. Biol*. **2004**, *39*, 21–68.
11. E. G. Kovaleva, J. D. Lipscomb, *Nat. Chem. Biol*. **2008**, *4*, 186–193.
12. C. Loenarz, C. J. Schofield, *Nat. Chem. Biol*. **2008**, *4*, 152–156.
13. W. Nam, *Acc. Chem. Res*. **2007**, *40*, 522–531, and review articles in the special issue.
14. W. L. F. Armarego, in *Purification of Laboratory Chemicals*, (Ed: D. D. Perrin), Pergamon Press, Oxford, **1997**.
15. Y. Goto, S. Wada, I. Morishima, Y. Watanabe, *J. Inorg. Biochem.* **1998**, *69*, 241–247.
16. H. Saltzman, in *Organic Syntheses*, Vol. V (Ed: J. G. Sharefkin), Wiley, New York, **1973**, pp. 658.

17. S. Taylor , J. Gullick , P. McMorn , D. Bethell , P. C. Bulman Page , F. E. Hancock , F. King, G. J. Hutchings, *J. Chem. Soc. Perkin Trans*. **2001**, *2*, 1714–1723.
18. M. Lubben, A. Meetsma, E. C. Wilkinson, B. Feringa, L. Que Jr., *Angew. Chem. Int. Ed. Engl.***1995**, *34*, 1512–1514.
19. A. K. Vardhaman, C. V. Sastri, D. Kumar, S. P. de Visser, *Chem. Commun*. **2011**, *47*, 11044–11046.
20. H. Börzel, P. Comba, K. S. Hagen, Y. D. Lampeka, A. Lienke, G. Linti, M. Merz, H. Pritzkow, L. V. Tsymbal, *Inorg. Chim. Acta*. **2002**, *337*, 407–419.
21. P. Comba, S. Kuwata, G. Linti, H. Pritzkow, M. Tarnai, H. Wadepohl, *Chem. Commun.* **2006**, 2074–2076.
22. P. Comba, B. Kanellakopulos, C. Katsichtis, A. Lienke, H. Pritzkow, F. Rominger, *J. Chem. Soc. Dalton Trans.* **1998**, 3997–4001.
23. G.M. Sheldrick, *Acta Crystallogr. Sect. A* **2008**, *64*, 112–122.
24. A. Hazell, C. J. McKenzie, L. P. Nielsen, S. Schindler, M. Weitzer, *J. Chem. Soc. Dalton Trans.* **2002**, 310–314.
25. K. D. Koehntop, J.–U. Rohde, M. Costas, L. Que Jr., *Dalton Trans.* **2004**, 3191–3198.
26. H. S. Soo, M. T. Sougrati, F. Grandjean, G. J. Long, C. J. Chang, *Inorg. Chim. Acta.* **2011**, *369*, 82–96.
27. E. J. Klinker, T. A. Jackson, M. P. Jensen, A. Stubna, G. Juhász, E. L. Bominaar, E. Münck, L. Que Jr., *Angew. Chem. Int. Ed*. **2006**, *45*, 7394–7397.
28. P. Urone, E. Bonde, *Anal. Chem*. **1960**, *32*, 1666–1668.

CHAPTER-III

Influence of Ligand Architecture on Oxidation Reactions by High-Valent Non-Heme Manganese-Oxo Complexes Using Water as a Source of Oxygen

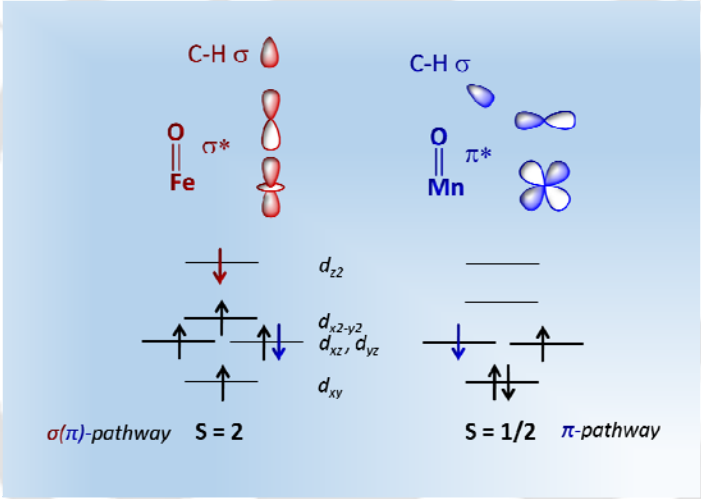

Angew. Chem. Int. Ed. **2015,** *54*, 2095-2099.

3.1 Introduction

High-valent manganese-oxo complexes with heme and non-heme ligands have attracted much interest in the fields of bioinorganic and oxidation chemistry in the past decades. This is due to their importance as intermediates in the oxidation of organic substrates as well as in water oxidation by the oxygen-evolving complex (OEC) in photosystem II (PS II).[1,2] In order to reveal the chemical and physical properties of high-valent manganese-oxo intermediates, a number of non-heme Mn^{IV}=O and Mn^{V}=O complexes have been reported.[3-9]

The ability to control the reactivity of metal-oxo complexes has important consequences in a variety of chemical processes. The selective oxidation of hydrocarbon compounds and the oxidation of organic substrates by oxygen atom transfer are fundamental transformations. One of the challenges associated with improving these processes is the choice of the ligand architecture, which helps to stabilize high-valent metal-based intermediates and optimize their reactivity.[10-12]

In PS II, the high-valent Mn species of the OEC uses water as a source of oxygen. In biomimetic studies, the formation of high-valent ruthenium oxo complexes has been achieved with the strong oxidants Ce^{IV} or $[Ru(bpy)_3]^{3+}$ (bpy = 2,2'-bipyridine).[13-17] Similarily, Fe^{IV}=O and Mn^{IV}=O complexes have also been generated using water as a source of oxygen and Ce^{IV} as a one electron oxidant.[3,18] Herein, we report the generation of mononuclear non-heme Mn^{IV}=O complexes with water as an oxygenation source and Ce^{IV} as one electron oxidant. Detailed spectroscopic and preliminary DFT studies were employed to evaluate the reactivity of the Mn^{IV}=O and the corresponding Fe^{IV}=O intermediates.

3.2 Experimental Section

High-valent manganese intermediates, Mn^{IV}=O complexes, including $[Mn^{IV}(O)(L^1)]^{2+}$ and $[Mn^{IV}(O)(L^2)]^{2+}$ were prepared by reacting their

corresponding Mn^{II} complex with cerium(IV) ammonium nitrate (CAN) in acetonitrile/water (9:1) or acetone/water (9:1) at 5 ºC. Oxidation reactions of S-oxidation as well as phenol O-H bond activation were followed by monitoring the change in the absorption spectrum of the intermediates using UV/Vis spectroscopy. Second order rate constants were determined by varying the concentration of substrates.

3.3 Results and discussions

The inherently rigid adamantane-derived bispidine moiety has been used extensively as a widely variable ligand platform for transition metal complexes, in particular also for ferryl-based oxidation catalysts,[19, 20] and derivatives of the two isomeric pentadentate ligands L^1 (X = N, Y = C, i.e., methylpyridine at N^3) and L^2 (X = C, Y = N, i.e., methylpyridine at N^7) have been of particular interest.[20] These ligands enforce square pyramidal geometries, and the open coordination site, occupied by the oxo-group in high-valent M^{n+}=O complexes, is *trans* to N^3 or N^7 for L^1 and L^2, respectively. This geometric variation is known to lead to striking differences in structural and electronic properties, stabilities and reactivities, because N^7 is part of a rather flexible six-membered chelate ring, while N^3 is part of a very rigid five-membered chelate.[19, 22-24]

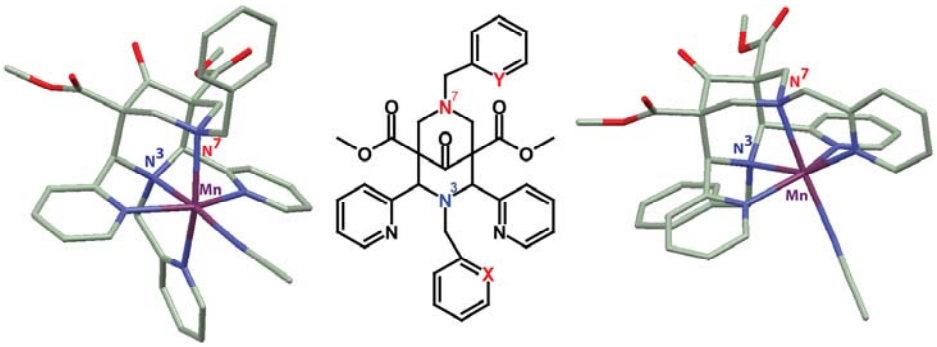

Figure 3.1. Plots of the X-ray structures of $[Mn^{II}(MeCN)(L^1)]$ (left, X = N, Y = C), and $[Mn^{II}(MeCN)(L^2)]$ (right, X = C, Y = N).

$[Mn^{II}(L^1)(ClO_4)_2]$ (**1**) and $[Mn^{II}(L^2)(ClO_4)_2]$ (**2**) were prepared in analogy to earlier reports and were structurally characterized (Figure 2.1).[23] The high-valent Mn^{IV}=O intermediates, $[Mn^{IV}(O)L^1]^{2+}$ (**3**; 2 mM) and $[Mn^{IV}(O)L^2]^{2+}$ (**4**; 2 mM) were generated from their Mn^{II} precursors, using CAN (8 mM) as an one electron oxidant in acetonitrile/water (9:1) or acetone/water (9:1) at 5 ºC. The addition of CAN to the colorless solution of the Mn^{II} complexes produced pale green solutions. Complex **3** exhibits an absorption spectrum with an intense band at 545 nm ($\varepsilon \approx 400\ M^{-1}cm^{-1}$), with a weak absorption in the near IR region at 970 nm ($\varepsilon \approx 35\ M^{-1}cm^{-1}$). Similarly the complex **4** has electronic transitions at 570 nm ($\varepsilon \approx 400\ M^{-1}cm^{-1}$) and at 975 nm ($\varepsilon \approx 103\ M^{-1}cm^{-1}$, Figure 3.2). The electro-spray ionization mass spectra (ESI-MS) of **3** and **4** exhibit prominent peaks at *m/z* ≅ 332, and the isotope patterns show that these correspond to $[Mn^{IV}(O)L^{1,2}]^{2+}$ (Figures 3.3 and Figure 3.4).

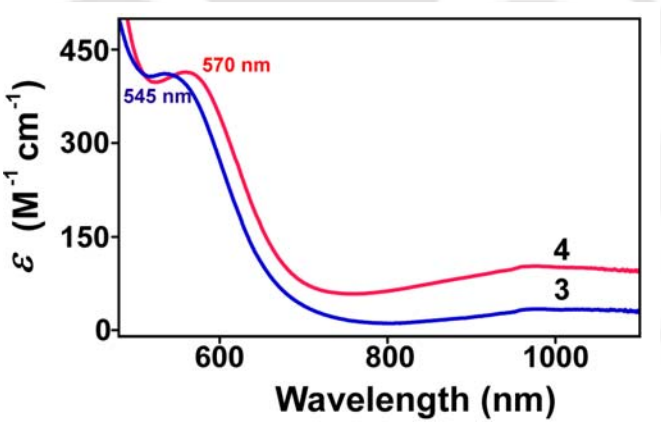

Figure 3.2. UV/Vis spectra of **3** and **4** generated in the reactions of **1** (2 mM) and **2** (2 mM) with CAN (8 mM) in CH_3CN/H_2O (9:1) at 5 ºC.

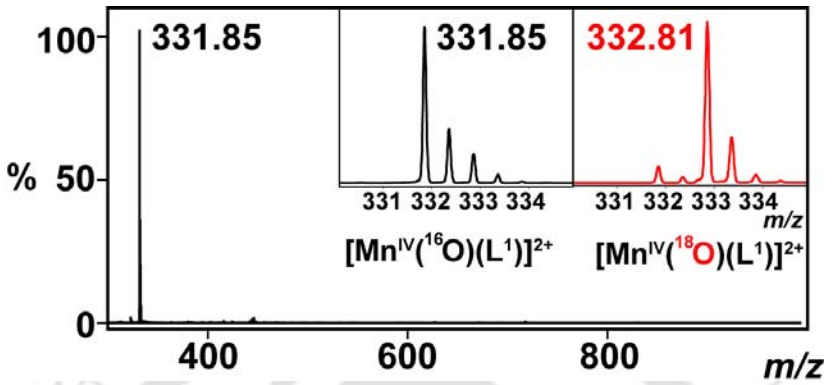

Figure 3.3. The ESI-MS spectra of $[Mn^{IV}(O)(L^1)]^{2+}$ (**3**) formed in the reaction of **1** (2 mM) and CAN (8 mM) in CH_3CN/H_2O (9:1) at 5 ºC. Mass peak at *m/z* = 331.85 is assigned for $[Mn^{IV}(O)(L^1)]^{2+}$. Insets shows observed isotopic distribution of $[Mn^{IV}(^{16}O)(L^1)]^{+}$ (left panel) and $[Mn^{IV}(^{18}O)(L^1)]^{+}$ (right panel).

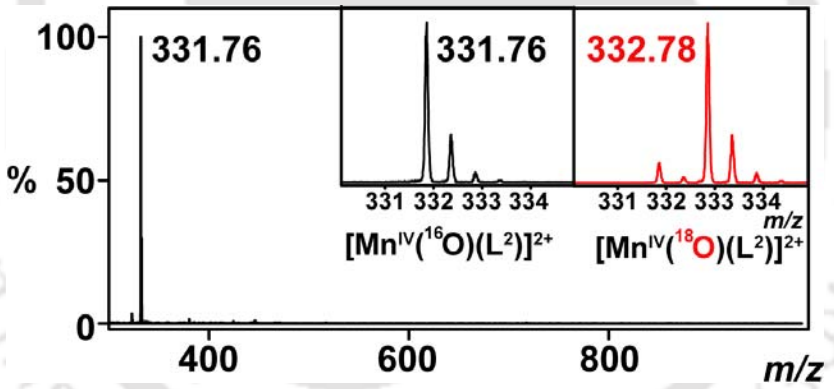

Figure 3.4. The ESI-MS spectra of $[Mn^{IV}(O)(L^2)]^{2+}$ (**4**) was formed in the reaction of **2** (2 mM) and CAN (8 mM) in CH_3CN/H_2O (9:1) at 5 ºC. Mass peak at *m/z* = 331.76 is assigned for $[Mn^{IV}(O)(L^2)]^{2+}$. Insets shows observed isotopic distribution of $[Mn^{IV}(^{16}O)(L^2)]^{+}$ (left panel) and $[Mn^{IV}(^{18}O)(L^2)]^{+}$ (right panel).

The reactivity of **3** and **4** were investigated with 2-electron oxidation reactions such as the oxidation of the sulphur atom of thioethers. Upon addition of thioanisole to the corresponding Mn^{IV}=O species at 5 ºC, the intermediates

decayed immediately and gave methyl phenyl sulfoxide as major product (Figure 3.5a).The pseudo-first-order rate constants of the decay of **3** and **4** increased linearly with increasing thioanisole concentration, giving second-order rate constants of the sulfoxidation reactions with **3** and **4** of 1.20 x 10^{-1} M^{-1} s^{-1} and 1.20 x 10^{-2} M^{-1} s^{-1}, respectively (Figure 3.5b).

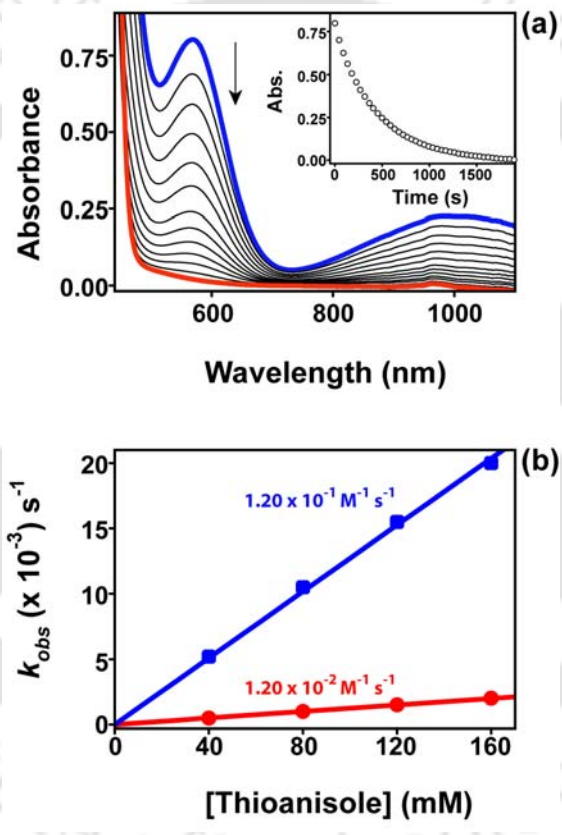

Figure 3.5. a) UV/Vis spectral changes of **4** (2 mM) upon addition of thioanisole (160 mM) in CH_3CN / H_2O (9:1) at 5 ºC (the Inset shows the time trace at 570 nm for the decay of Mn^{IV}=O). b) Second order rate constants determined in the reaction of 2 mM of **3** (■) and **4** (•) in CH_3CN / H_2O (9:1) against various concentrations of thioanisole at 5 ºC.

Therefore, it appears that **3** *react with thioanisole about ten times faster than the isomeric oxidant* **4.** In order to further elucidate the reaction pathway, second-order rate constants (k_X) for the oxidation of various *para* substituted thioanisole substrates (k_H is the second order rate constant for thioanisole) with the oxidant **4** were also determined (Table 3.1, Figure 3.6).

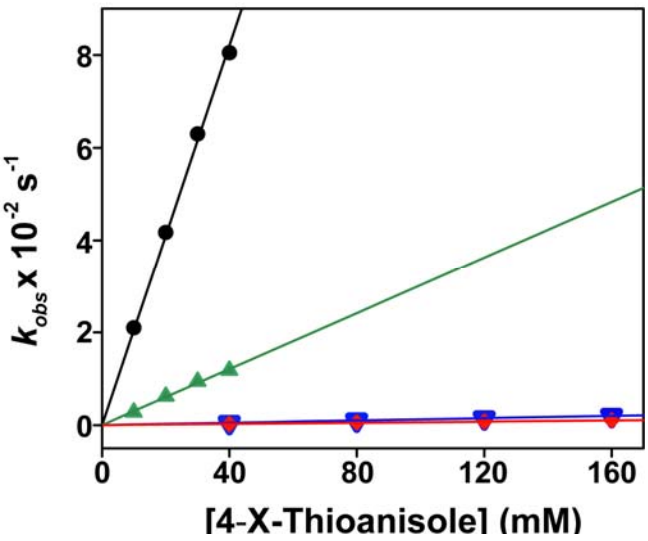

Figure 3.6. Plot of k_{obs} against substrate concentration to determine second-order rate constants in the reactions of $[Mn^{IV}(O)(L^2)]^{2+}$ **4** (2 mM) with 4-methoxythioanisole (●), 4-methylthioanisole (◀), thioanisole (▼) and 4-chlorothioanisole (◆) in CH_3CN/H_2O (9:1) at 5 ºC.

Then created Hammett plots, for a quantitative examination of the substituent effect on the reaction rates. For **4**, a linear correlation with σ was found with a ρ = –5.12 (Figure 3.7), which is likely as a result of additional stabilization of positive charge in the transition state by electron donating groups in the para position of thioanisole and thus enhanced the overall rate of oxidation. To accommodate the additional stabilization of the positive charge in transition

state, new Hammett plots were now made using σ^+ values leading to ρ values of –2.91 (Figure 3.8).

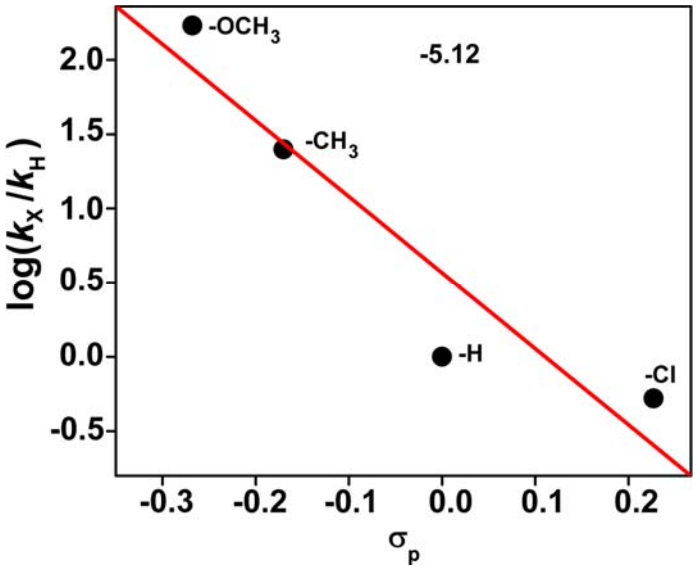

Figure 3.7. Plot of log (k_X/ k_H) against σ_p of *para*-X-thioanisole of $[Mn^{IV}(O)(L^2)]^{2+}$ **4** (●) at 5 ºC. The k_X and k_H are the second order rate constants of *p*-X-Ph-S-Me and Ph-S-Me respectively at 5 ºC.

A plot of the logarithm of the rate constant ratio [log(k_X/k_H)] against the one-electron oxidation potentials (E^0_{OX}) of the sulfides gave a linear correlation with a slope of -10.8 (Figure 3.9). Similar large slope values were also obtained in Hammett correlations (Figure 3.7 Figure 3.8 and Figure 3.9). Such a large negative slope implies that the electron transfer from the sulfides to **4** rather than a group transfer are the rate-determining step.[25-28]

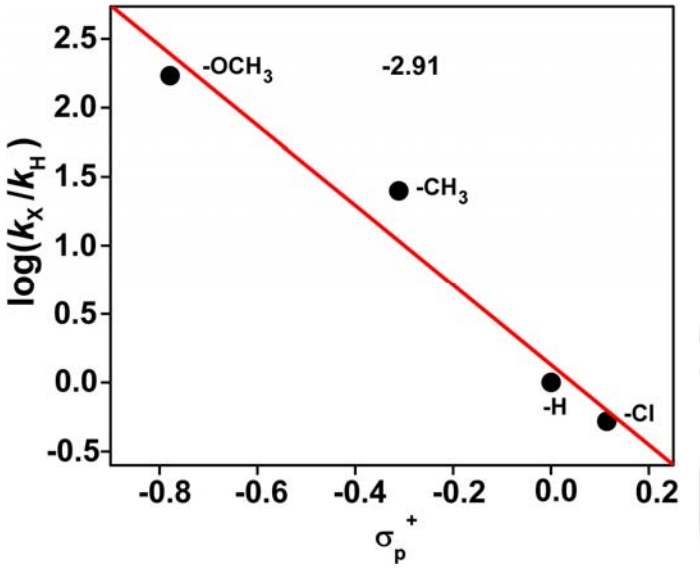

Figure 3.8. Plot of log (k_X/ k_H) against σ_p^+ of *para*-X-thioanisole of $[Mn^{IV}(O)(L^2)]^{2+}$ **4** (●) at 5 ºC. The k_X and k_H are the second order rate constants of *p*-X-Ph-S-Me and Ph-S-Me respectively at 5 ºC.

Table 3.1. Pseudo first order rate constants determined reactions of $[Mn^{IV}(O)L^2]^{2+}$ (**4**; 2 mM solution) in the presence of various *para* substituted thioanisoles at 5 ºC in CH_3CN/H_2O (9:1).

Substituent of *para*-X-Thioanisole	E^0_{ox} **vs. SCE (V)**	σ_p	σ_p^+	$[Mn^{IV}(O)L^2]^{2+}$	
				k_2 ($M^{-1} s^{-1}$)	$\log(k_X/k_H)$
CH_3O–	1.13	-0.268	-0.778	2.051(1)	2.233
CH_3–	1.24	-0.170	-0.311	$3.02(2) \times 10^{-1}$	1.398
H–	1.34	0.0	0.0	$1.2(1) \times 10^{-2}$	0
Cl–	1.37	0.227	0.114	$6.3(3) \times 10^{-3}$	-0.279

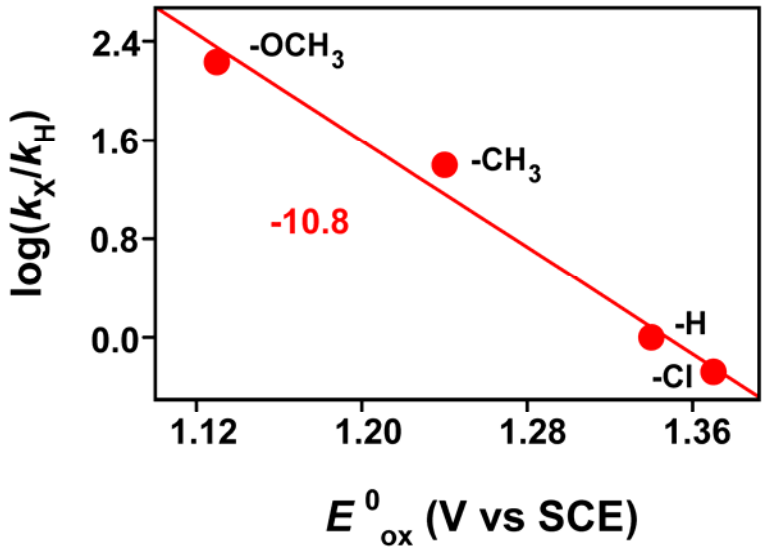

Figure 3.9. Plot of log (k_X/k_H) against E^0_{ox} of *para*-X-thioanisole of $[Mn^{IV}(O)(L^2)]^{2+}$ **4** (●) at 5 ºC. The k_X and k_H are the second order rate constants of *p*-X-Ph-S-Me and Ph-S-Me respectively at 5 ºC.

To further evaluate the reactivity of the two isomeric Mn^{IV}=O oxidants, H-atom abstraction reactions were also studied. The oxidation of 2,4-di-*tert*–butylphenol (2,4-*t*-$Bu_2C_6H_3OH$) with **3** and **4** yielded 2,2'-dihydroxy-3,3',5,5'-tetra-*tert*-butylphenol. The second order rate constants reveal that the reactivity of **3** is again larger (~ 40 times) than that of **4 (**Figure 3.10 and Table 3.2).

Table 3.2. Second order rate constants of sulfoxidation of thioanisole and hydrogen atom abstraction of 2, 4-di-*tert* -butylphenol (2,4-di-*tert*-$Bu_2C_6H_3OH$) by **3** and **4**.

Catalyst	**k_2 (thioanisole)** **5 ºC**	**k_2 (2,4-di-*tert* –butylphenol)** **-40 ºC**
3	1.20(2) x 10^{-1} M^{-1} s^{-1}	2.30(3) M^{-1} s^{-1}
4	1.20(1) x 10^{-2} M^{-1} s^{-1}	6.50(1) x 10^{-2} M^{-1} s^{-1}

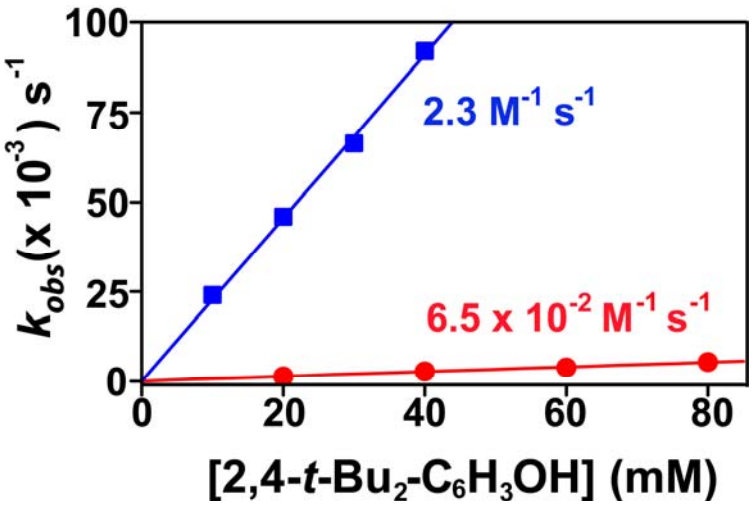

Figure 3.10. Second order rate constants determined in the reaction of 2 mM of **3** (■) and **4** (●) in CH_3CN / H_2O (9:1) against various concentrations of 2,4-di-*tert*–butylphenol at -40 ºC.

The O-H bond cleavage in phenols can be achieved via a H atom abstraction or by a proton-coupled electron transfer (PCET) mechanism.[29,30] PCET can be discarded, when two substrates with similar O-H bond strengths and pK_a values but substituents with different steric demand, such as 2,6-di-*tert*-$Bu_2C_6H_3OH$ [BDE(O-H) = 81.65 kcal/mol; pK_a = 11.70, aqueous solution] and 2,4-di-*tert*-$Bu_2C_6H_3OH$ [BDE(O-H) = 81.65 kcal/mol; pK_a = 11.64, aqueous solution] show different reactivities.[31,32] The observed approximately 50-fold rate enhancement in the reaction of **4** with 2,4-di-*tert*-$Bu_2C_6H_3OH$ [9.5(1) x 10^{-1} M^{-1} s^{-1}] as compared to 2,6-di-*tert*-$Bu_2C_6H_3OH$, [1.7(2) x 10^{-2} $M^{-1}s^{-1}$] (Figure 3.11) suggests a H-atom abstraction pathway.[29,30,32,33] To further substantiate the H-atom abstraction reaction with phenol, we evaluated the corresponding second-order rate constants with series of *para* substituted 2,6-di-*tert*-butylephenol substrates (X = –OMe, –Me, –H, –CN) (Table 3.3 and Figure 3.12).

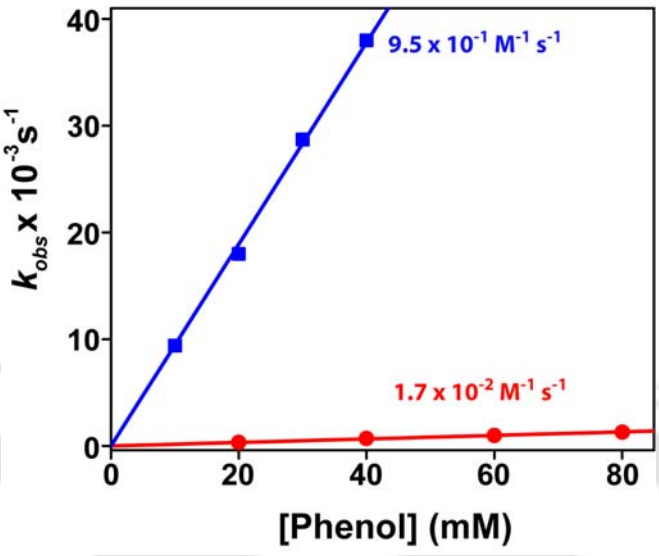

Figure 3.11. Second-order rate constants determined in the reactions of 2 mM $[Mn^{IV}(O)(L^2)]^{2+}$ of **4** in CH_3CN/H_2O (9:1) solution against various concentrations of 2,4-di-*tert*-butylphenol (2,4-di-*tert*-$Bu_2C_6H_3OH$; ■) and 2,6-di-*tert*-butylphenol (2,6-di-*tert*-$Bu_2C_6H_3OH$; ●) at 0 ºC.

Table 3.3. Data for the reaction of $[Mn^{IV}(O)(L^2)]^{2+}$ (**4**; 2 mM solution) in the presence of *para* substituted 2,6-di-*tert*-$Bu_2C_6H_2OH$ in CH_3CN/H_2O (9:1) at 0 ºC.

Substituent of *para*-X-2,6-di-*tert*-$Bu_2C_6H_2OH$	**BDE (kcal/mol)**	$[Mn^{IV}(O)(L^2)]^{2+}$	
		k_2 ($M^{-1}s^{-1}$)	**log(k_X/k_H)**
CH_3O–	78.31	1.37(3)	1.9063
CH_3–	81.02	1.14(2) x 10^{-1}	0.8265
H–	82.8	1.70(2) x 10^{-2}	0
CN–	84.24	6.0(1) x 10^{-3}	-0.4523

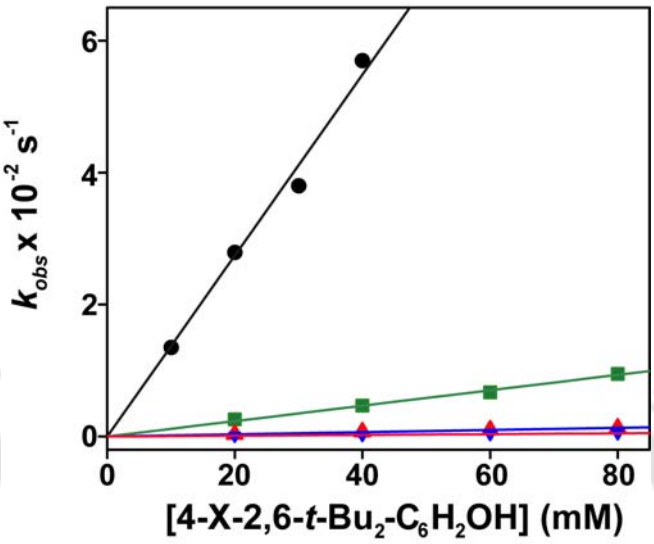

Figure 3.12. Plot of k_{obs} against substrate concentration to determine second order rate constants in the reactions of $[Mn^{IV}(O)(L^2)]^{2+}$ **4** (2 mM) with various *para*-X-2,6-di-*tert*-butylphenol. X = –OMe (●),–Me (■),–H (▼) and –CN (▲) in CH_3CN/H_2O (9:1) at 0 ºC.

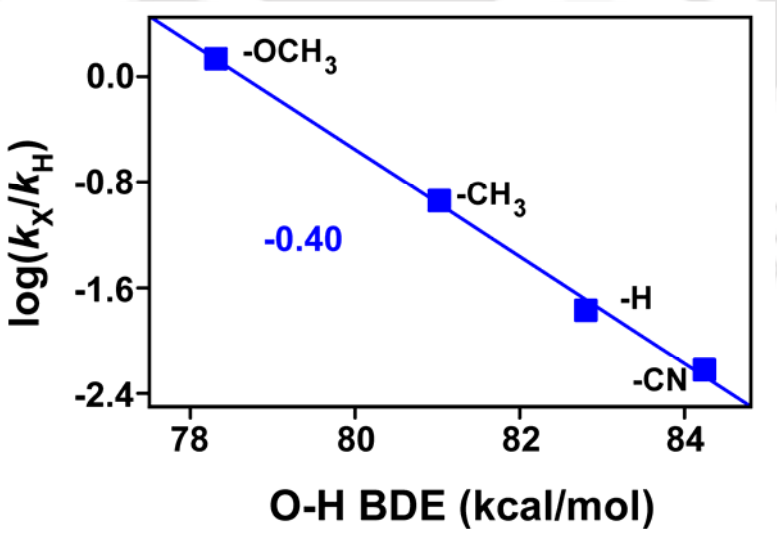

Figure 3.13. Correlations of second order rate constants, log (k_X/k_H) of **4** against BDE_{O-H} of *p*-X-2,6-di-*tert*-$Bu_2C_6H_2OH$ in CH_3CN/H_2O (9:1) at 0 ºC.

A plot of the logarithm of the rate constant ratio [$\log(k_X/k_H)$] as a function of σ_p^+ shows an excellent Hammett correlation with a ρ value of -1.6. Such a linear relationship has been used as evidence for a H-atom abstraction pathway in the oxidation of phenol O-H bonds by $[Mn^V(O)(Cz)]$ (where Cz is corrolazine), $[(L)Ru^{VI}(O)_2]^{2+}$ and $[Fe^{IV}(O)(TMC)]^{2+}$ (where TMC is tetramethyl cyclam).[29,31,33] As further support, we have also plotted log (k_X/k_H) values against the phenol O-H bond dissociation energy (BDE), which afforded a good correlation with a slope of -0.40 (Figure 3.13), matching well with earlier reports.[30, 32,34,35]

3.4 Conclusion

Mn(II) complexes of ligand L^1 and L^2 has been successfully synthesized and well characterized by spectroscopic techniques. Generation of high-valent Mn^{IV}=O complexes using water as an oxygen source by reacting Mn(II) complexes with Ce(IV) in CH_3CN / H_2O (9:1) at 5 ºC. The reactivity and mechanistic pathway of oxygen atom transfer reactions with thioanisole and various *para* substituted thioanisole and proved that Mn^{IV}=O complex of L^1 shows 10 times faster reactivity than L^2 and reaction proceed by an electron transfer pathway. Where as in hydrogen atom abstraction reaction Mn^{IV}=O of L^1 complex shows 40 times more reactive than L^2. Interestingly Mn^{IV}=O complexes were showing an opposite reactivity pattern with recently reported corresponding Fe^{IV}=O complexes. This inversion of reactivity is discussed on the basis of DFT and molecular mechanics (MM) model calculations, which indicate that the order of reactivities are primarily due to a switch of reaction channels (σ vs.π) and concomitant steric effects.[36]

3.5 References

1. S. Tanase, E. Bouwman, *Advances in Inorganic Chemistry Vol. 58* (Ed.: R. van Eldik, J. Reedijk), Elsevier, San Diego, **2006**, pp. 29–75.
2. I. Garcia–Bosch, A. Company, C. W. Cady, S. Styring, W. R. Browne, X. Ribas, M. Costas, *Angew. Chem. Int. Ed*. **2011**, *50*, 5648–5653.
3. S. C. Sawant, X. Wu, J. Cho, K.–B. Cho, S. H. Kim, M. S. Seo, Y.–M. Lee, M. Kubo, T. Ogura, S. Shaik, W. Nam, *Angew. Chem. Int. Ed.* **2010**, *49*, 8190–8194.
4. W. Liu, X. Huang, M.–J. Cheng, R. J. Nielsen, W. A. Goddard III, J. T. Groves, *Science* **2012**, *337*, 1322–1325.
5. T. Taguchi, R. Gupta, B. Lassalle–Kaiser, D. W. Boyce, V. K. Yachandra, W. B. Tolman, J. Yano, M. Hendrich, A. S. Borovik, *J. Am. Chem. Soc.* **2012**, *134*, 1996–1999.
6. D. F. Leto, R. Ingram, V. W. Day, T. A. Jackson, *Chem. Commun*. **2013**, *49*, 5378-5380.
7. H. M. Neu, T. Yang, R. A. Baglia, T. H. Yosca, M. T. Green, M. G. Quesne, S. P. de Visser, D. P. Goldberg, *J. Am. Chem. Soc*. **2014**, *136*, 13845–13852.
8. J. Chen, Y.–Min Lee, K. M. Davis, X. Wu, M. S. Seo, K.–B. Cho, H. Yoon, Y. J. Park, S. Fukuzumi, Y. N. Pushkar, W. Nam, *J. Am. Chem. Soc.* **2013**, *135*, 6388–6391.
9. S. D. Hicks, D. Kim, S. Xiong, G. A. Medvedev, J. Caruthers, S. Hong, W. Nam, M. M. Abu-Omar, *J. Am. Chem. Soc.* **2014**, *136*, 3680–3686.
10. M. Costas, L. Que Jr., *Angew. Chem. Int. Ed.* **2002**, *114*, 2283–2285.
11. S. Hong, Y.–M. Lee, K.–B. Cho, K. Sundaravel, J. Cho, M. J. Kim, W. Shin, W. Nam, *J. Am. Chem. Soc.* **2011**, *133*, 11876–11879.

12. D. Wang, K. Ray, M. J. Collins, E. R. Farquhar, J. R. Frisch, L. Gömez, T. A. Jackson, M. Kerscher, A. Waleska, P. Comba, M. Costas, L. Que Jr., *Chem. Sci.* **2013**, *4*, 282–291.
13. S. Romain, L. Vigara, A. Llobet, *Acc. Chem. Res.* **2009**, *42*, 1944–1953.
14. C.–M. Che, V. W.–W. Yam, T. C. W. Mak, *J. Am. Chem. Soc.* **1990**, *112*, 2284–2291.
15. Y. Hirai, T. Kojima, Y. Mizutani, Y. Shiota, K. Yoshizawa, S. Fukuzumi, *Angew. Chem. Int. Ed.* **2008**, 47, 5772–5776.
16. A. Sartorel, M. Carraro, G. Scorrano, R. De Zorzi, S. Geremia, N. D. McDaniel, S. Bernhard, M. Bonchio, *J. Am. Chem. Soc.* **2008**, *130*, 5006–5007.
17. Y. V. Geletii, B. Botar, P. Kgerler, D. A. Hillesheim, D. G. Musaev, C. L. Hill, *Angew. Chem. Int. Ed.* **2008**, 47, 3896–3899.
18. Y.–M. Lee, S. N. Dhuri, S. C. Sawant, J. Cho, M. Kubo, T. Ogura, S. Fukuzumi, W. Nam, *Angew. Chem. Int. Ed*. **2009**, *48*, 1803–1806.
19. P. Comba, M. Kerscher, W. Schiek, *Progr. Inorg. Chem.* **2007**, *55*, 613–704.
20. P. Comba, in *Molecular Catalysis,* (Ed.: L. H. Gade, P. Hofmann), Wiley–VCH, **2014**, pp. 123–145.
21. M. Bukowski, P. Comba, C. Limberg, M. Merz, L. Que Jr., T. Wistuba, *Angew. Chem. Int. Ed.* **2004**, *43*, 1283–1287.
22. P. Comba, A. Lienke, *Inorg. Chem.* **2001**, *40*, 5206–5209.
23. A. E. Anastasi, P. Comba, J. McGrady, A. Lienke, H. Rohwer, *Inorg. Chem.* **2007**, *46*, 6420–6426.
24. P. Comba, B. Kanellakopulos, C. Katsichtis, A. Lienke, H. Pritzkow, F. Rominger, *J. Chem. Soc. Dalton Trans*. **1998**, 3997–4001.

25. Y. Goto, T. Matsui, S.–I. Ozaki, Y. Watanabe, S. Fukuzumi, *J. Am. Chem. Soc.* **1999**, *121*, 9497–9502.
26. J. Park, Y. Morimoto, Y.–M. Lee, W. Nam, S. Fukuzumi, *J. Am. Chem. Soc.* **2011**, *133*, 5236–5239.
27. P. Comba, S. Fukuzumi, H. Kotani, S. Wunderlich, *Angew. Chem. Int. Ed.* **2010**, *49*, 2622–2625.
28. A. K. Vardhaman, P. Barman, S. Kumar, C. V. Sastri, D. Kumar, S. P. de Visser, *Angew. Chem. Int. Ed.* **2013**, *52*, 12288–12292.
29. I. J. Rhile, J. M. Mayer, *J. Am. Chem. Soc.* **2004**, *126*, 12718–12719.
30. D. T. Y. Yiu, M. F. W. Lee, W. W. Y. Lam, T.–C. Lau, *Inorg. Chem.* **2003**, *42*, 1225–1232.
31. A. H.–Yangjeh, M. D.–Jenagharad, M. Nooshyar, *J. Mol. Model.* **2006**, *12*, 338–347.
32. D. E. Lansky, D. P. Goldberg, *Inorg. Chem.* **2006**, *45*, 5119–5125.
33. M. Lucarini, P. Pedrielli, G. F. Pedulli, S. Cabiddu, C. Fattuoni, J. *Org. Chem.* **1996**, *61*, 9259–9263.
34. C. V. Sastri, L. Lee, K. Oh, Y. J. Lee, J. Lee, T. A. Jackson, K. Ray, H. Hirao, W. Shin, J. A. Halfen, J. Kim, L. Que Jr., S. Shaik, W. Nam, *Proc. Natl. Acad. Sci. USA* **2007**, *104*, 19181–19186.
35. P. Mulder, O. W. Saastad, D. Griller, *J. Am. Chem. Soc.* **1988**, *110*, 4090–4092.
36. P. Barman, A. K. Vardhaman, B. Martin, S. J. Wörner, C. V. Sastri, P. Comba, *Angew. Chem. Int. Ed.* **2015**, *54*, 2095–2099.

CHAPTER-IV

Deformylation Reaction by a Non-Heme Manganese(III)-Peroxo Complex via Initial Hydrogen Atom Abstraction

Angew. Chem. Int. Ed. **2016**, *55*, 11091–11095.

4.1 Introduction

The chemistry of metal–dioxygen intermediates has attracted interest in the field of biological as well as bioinorganic chemistry communities for many decades. These complexes are key intermediates in the catalytic cycles of metalloenzymes that activate and utilize molecular oxygen for vital biological processes in the human body, including the metabolism of drugs and the biosynthesis of hormones.[1,2] Although many metalloenzymes use iron as the central cofactor, several actually use manganese instead. Biologically active manganese ions are included, for instance, in the oxygen-evolving complex of Photosystem II,[3-6] but also in superoxide dismutase that catalyzes the detoxification of superoxide and hydrogen peroxide to water.[7-9] The manganese-peroxo intermediate has been postulated as an important intermediate in these catalytic cycles; however, as it is short-lived, there currently is no experimental evidence available.

Therefore, synthetic, biomimetic, models have been developed that have a ligand architecture suitable for studies in solution but have a coordination sphere that resembles enzyme analogues and consequently may give insight into the chemical and spectroscopic properties of enzymatic intermediates and their reactivity patterns.[10-13]

In the past few years several biomimetic metal-peroxo adducts of iron and manganese have been prepared and characterized with UV/Vis, electronic absorption, electron paramagnetic resonance (EPR) and X-ray absorption spectroscopic techniques.[14-22] In addition, reactivity patterns with model substrates were studied and showed these metal-peroxo species to mainly react through nucleophilic addition reactions.[23-25] Recently, a non-heme manganese(III)-peroxo complex with cyclam-type ligand was spectroscopically characterized with electronic absorption, EPR and X-ray absorption techniques.

Moreover, the complex was shown to react with manganese(II)-chloride to form manganese(IV)-oxo and manganese(III)-hydroxo complexes.[26]

4.2 Experimental Section

Manganese (II) complexes such as $[Mn^{II}(L^1)](ClO_4)_2$ was prepared by reacting with ligand L^1 and $[Mn^{II}(ClO_4)_2]$ salt. $[Mn^{III}(L^1)(O_2)]^+$complex was prepared by reacting their corresponding Mn^{II} complex with 10 equivalents of H_2O_2 and 2.5 equiv triethylamine (TEA) in CH_3CN (2 mL) in acetonitrile at 15 ºC. 2–Methyl–2–phenylpropionaldehyde was prepared according to literature methods.[27] Deformylation reaction of aldehyde was followed by monitoring the change in absorption spectrum of the intermediates using UV/Vis spectroscopy. Second order rate constants were determined by varying the concentration of substrates.

4.3 Results and discussions

Synthetic metal-peroxo complexes are known to react with aldehydes efficiently in a proposed nucleophilic reaction mechanism. However, an alternative mechanism, not considered previously, concerns a rate determining hydrogen atom abstraction from the α-position prior to oxygen atom transfer. Recent work of metal-bispidine ligand systems showed these complexes to react efficiently with substrates through hydrogen atom abstraction, due to their rigid ligand framework, and reaction rates could be monitored effectively over a broad temperature and concentration range.[28,29] Therefore, decided to investigate the relative reactivity of the $[Mn^{III}(L^1)(O_2)]^+$ complex, with aldehydes and study the possible nucleophilic addition versus hydrogen atom abstraction mechanisms. In particular, we report the synthesis and characterization of a novel side-on manganese(III)-peroxo complex with a pentadentate bispidine N^5 ligand,

$[Mn^{III}(L^1)(O_2)]^+$ (**1**),[30] Figure 4.1, and study its reactivity patterns with 2-phenylpropionaldehyde (2-PPA) and its α-deuterated form.

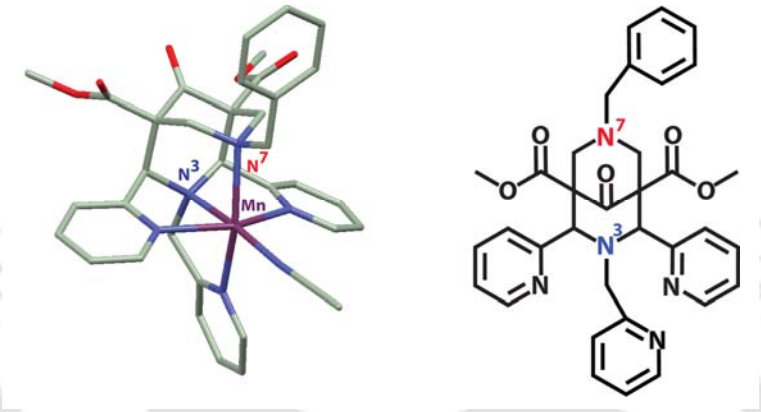

Figure 4.1. Plots of the X-ray structures of $[Mn^{II}(MeCN)(L^1)]$.

The starting manganese(II) complex, $[Mn^{II}(L^1)(ClO_4)_2]^{2+}$ (**1**), was synthesized by reacting $Mn^{II}(ClO_4)_2 \cdot 2CH_3CN$ with the pentadentate bispidine ligand (L^1) in CH_3CN under an argon atmosphere in analogy to previously reported procedures.[31] Addition of 10 equivalents of H_2O_2 to a colorless solution containing $[Mn^{II}(L^1)(ClO_4)_2]^{2+}$ (**5**; 2 mM) and triethylamine (TEA; 2.5 equivalents) in an acetonitrile solution at 15 ºC afforded a blue intermediate (**5**) with an absorption band at 605 nm (ε = 270 M^{-1} cm^{-1}; with a half-life ~60 minutes, Figure 4.2a). The blue intermediate is characterized with various spectroscopic techniques including UV/Vis and ESI-MS. The ESI mass spectra of **5** exhibit a prominent ion peak at *m/z* = 678.31 whose isotopic distribution pattern corresponds to $[Mn^{III}(L^1)(O_2)]^+$ (Figure 4.2b). These spectra are similar to those found by Jackson et al. on an analogous manganese(III)-peroxo complex.[26]

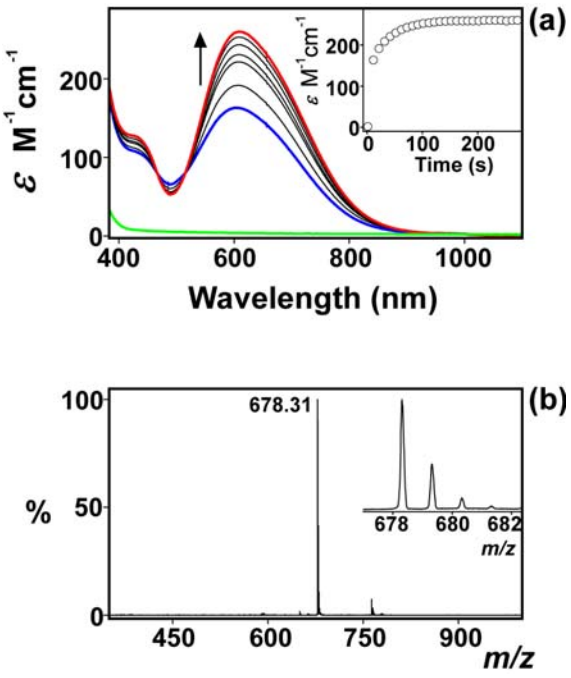

Figure 4.2. a) UV/Vis spectra of formation of **5** (2 mM) upon addition of $[Mn(L^1)]^{2+}$ (**1**; green line) in the presence of TEA (5 mM) and H_2O_2 (20 mM) in CH_3CN at 15 ºC. The inset shows the time trace for the formation the **5**. b) ESI-MS spectrum of **5**. Inset shows the observed isotope distribution patterns for $[Mn(L^1)(O_2)]^+$.

The nucleophilic and electrophilic character of **5** was then investigated in a reaction with 2-PPA as a substrate. Earlier reports showed that manganese(III)-peroxo complexes react with aldehydes to give the corresponding deformylated products by attacking the carbonyl group in a nucleophilic reaction (Scheme 4.1).[21,22] Upon addition of 2-PPA to **5** in CH_3CN at 15 ºC, the intermediate decayed immediately and led to acetophenone as a product. (Figure 4.3a). The pseudo-first-order rate constant of the decay of **5** increased linearly with

increasing 2-PPA concentration, thus giving a second-order rate constant of 2.74 x 10^{-2} M^{-1} s^{-1} (Figure 4.3b).

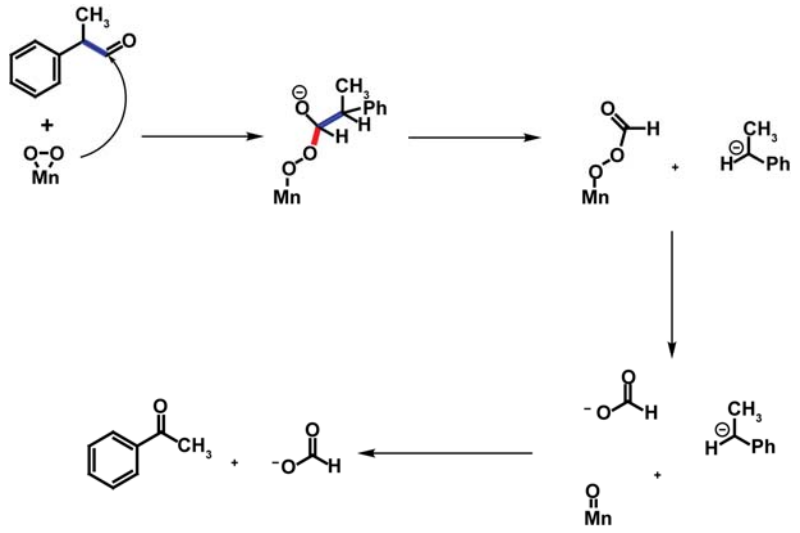

Scheme 4.1. Established mechanism for the deformylation of 2-PPA by Manganese(III)-peroxo complex.

To establish whether the mechanism proceeds through a nucleophilic attack on the carbonyl group, 2-methyl-2-phenylpropionaldehyde (2-Me-2-PPA) used as a mechanistic probe. Upon addition of 2-Me-2-PPA to **5** at 15 ºC, the intermediate decays at the rate of its natural decay. However, when the reaction solutions were analyzed with ESI-MS no deformylated products were observed. These results demonstrate that the manganese(III)-peroxo does not react with 2-PPA through a nucleophilic attack on the carbonyl group. As such, the work contradicts previous studies on the reactivity of non-heme and heme metal-peroxo complexes with aldehydes, that all reported a nucleophilic mechanism.[15, 19, 22, 32-39]

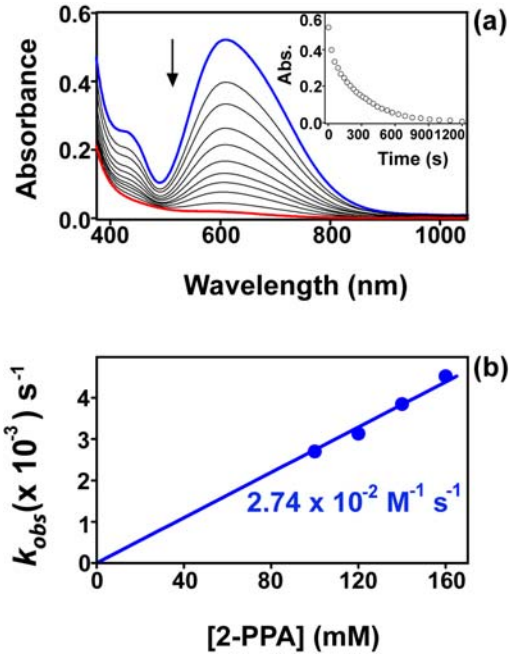

Figure 4.3. Kinetics of the reaction of **5** with 2-PPA: a) UV/Vis spectral changes of **5** (2 mM) upon addition of 2-PPA (160 mM) in the presence of TEA (5 mM) and hydrogen peroxide (20 mM) in CH_3CN at 15 ºC. Inset shows the time course of the absorbance at 605 nm. b) Plot of k_{obs} against the concentration of 2-PPA and the derived second-order rate constant for the reaction of 2 mM **5** with substrate at various concentrations in CH_3CN at 15ºC for 2-PPA (•).

In order to find out, whether an alternative pathway was possible starting with an initial hydrogen atom abstraction, decided to investigate the reaction with α-[D_1]-PPA. Thus, upon addition of α-[D_1]-PPA (~90 %, D enriched) to **5** in CH_3CN at 15 ºC determined a second-order rate constant of 5.05 x 10^{-3} M^{-1} s^{-1} (Figure 4.4b). Therefore, kinetics studies establish the manganese(III)-peroxo complex to react with 2-PPA via a rate determining hydrogen atom abstraction reaction from the α-position with a kinetic isotope effect (KIE) of 5.4.

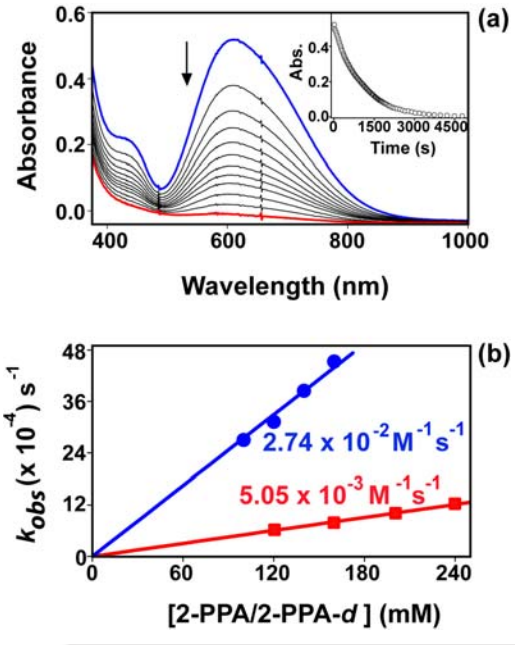

Figure 4.4. a) UV/Vis spectral changes of **5** (2 mM) upon addition of α-[D_1]-2-phenylpropionaldehyde (160 mM) in the presence of TEA (5 mM) and hydrogen peroxide (20 mM) in CH_3CN at 15 ºC. Inset shows the time trace during the course of the reaction. b) Plot of k_{obs} against the concentration of 2-PPA and α-[D_1]-PPA (~90 %, D enriched) and the derived second-order rate constant for the reaction of 2 mM **5** with substrate at various concentrations in CH_3CN at 15 ºC for 2-PPA (•) and α-[D_1]-PPA (■).

To find further evidence of this novel reaction mechanism, performed a radical trapping experiment with bromotrichloro-methane using procedures reported previously.[40, 41] Addition of 2-PPA to intermediate **5** in the presence of excess CCl_3Br (or CBr_4) in CH_3CN at 15 ºC, leads to the formation of α-brominated product of the 2-PPA exclusively, which was confirmed by NMR analysis (Scheme 4.2 and Figure 4.5). Consequently, our kinetics and reactivity studies clearly reveal a novel reaction mechanism between manganese(III)-

peroxo complexes with aldehydes starting from an α-hydrogen atom abstraction step.

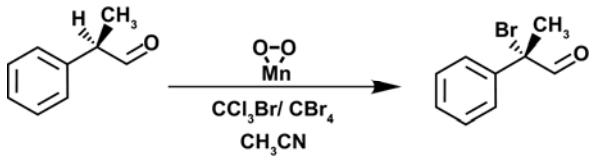

Scheme 4.2. Radical trapping experiment: addition of 2-PPA to intermediate **5** in the presence of excess CCl_3Br (or CBr_4) in CH_3CN at 15 ºC.

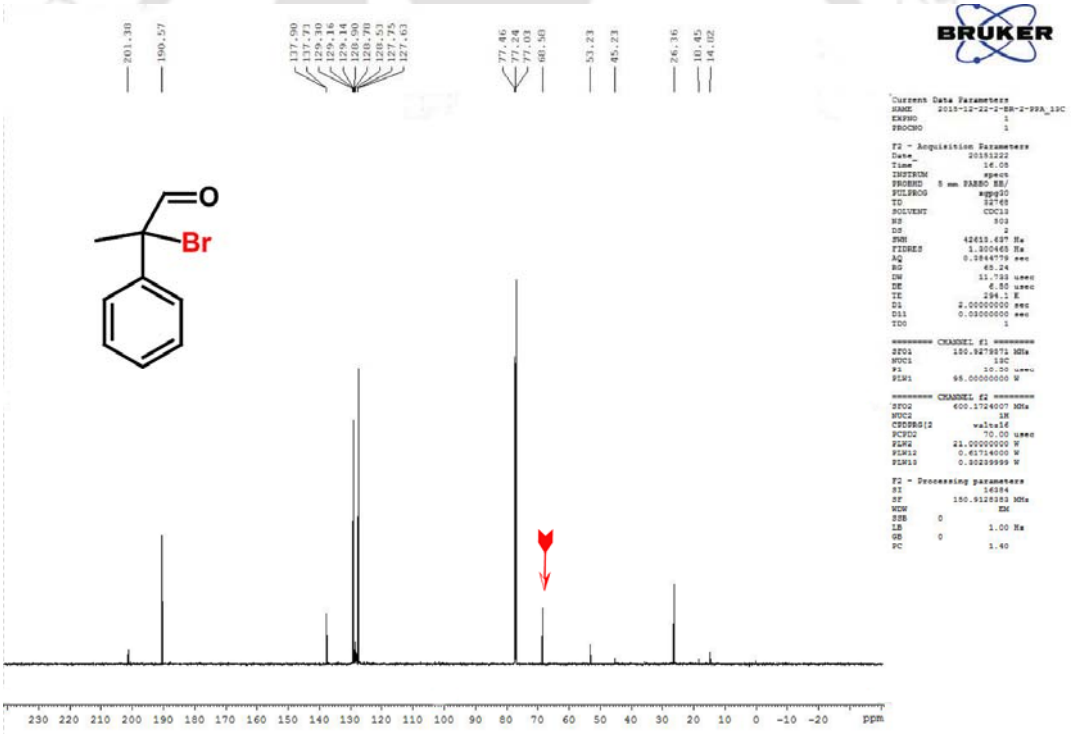

Figure 4.5. ^{13}C spectrum of 2-bromo-2-phenylpropionaldehyde. The product was formed by the addition of 2–phenylpropionaldehyde to intermediate **5** in the presence of excess CCl_3Br (or CBr_4) in CH_3CN at 15 ºC.

Table 4.1. Second order rate constants of the reaction of **5** with 2-PPA and α-[D_1]-2-phenylpropionaldehyde at 15 ºC.

Catalyst	k_2 (2-PPA) 15 ºC	k_2 (α-[D_1]-2-phenylpropionaldehyde) 15 ºC
5	2.74(1) x 10^{-2} M^{-1} s^{-1}	5.05(3) x 10^{-3} M^{-1} s^{-1}

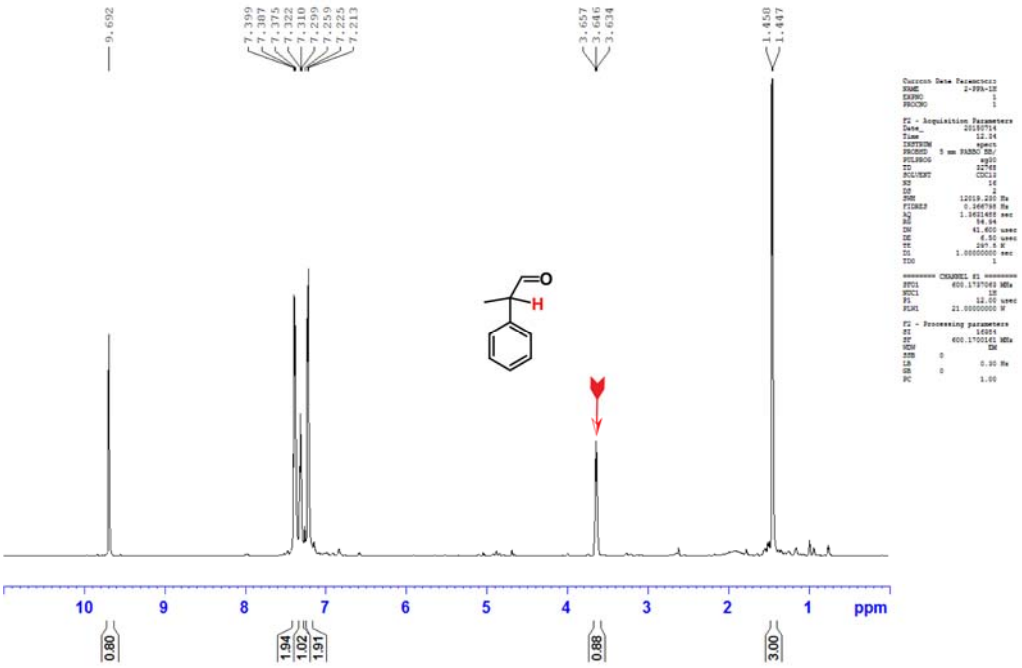

Figure 4.6. ^{1}H NMR spectrum of 2-phenylpropionaldehyde.

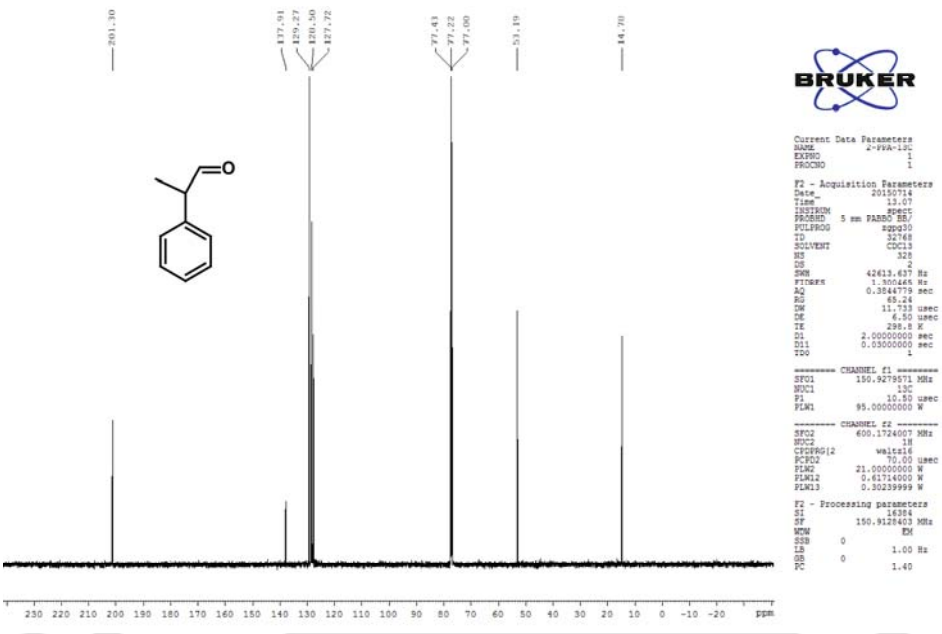

Figure 4.7. ^{13}C NMR spectrum of 2-phenylpropionaldehyde.

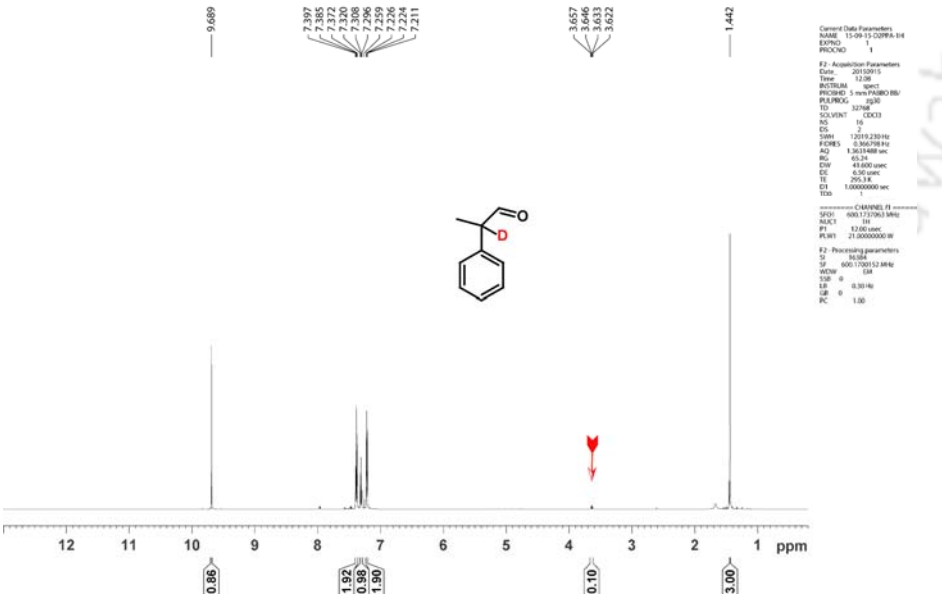

Figure 4.8. ^{1}H NMR spectrum of α-[D_1]-2-phenylpropionaldehyde.

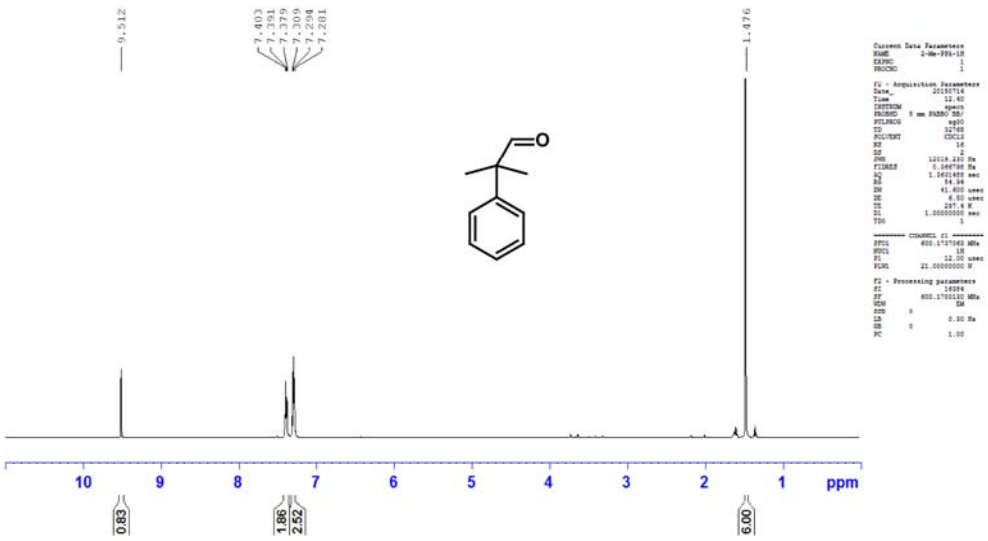

Figure 4.9. ^{1}H NMR spectrum of 2-methyl-2-phenylpropionaldehyde.

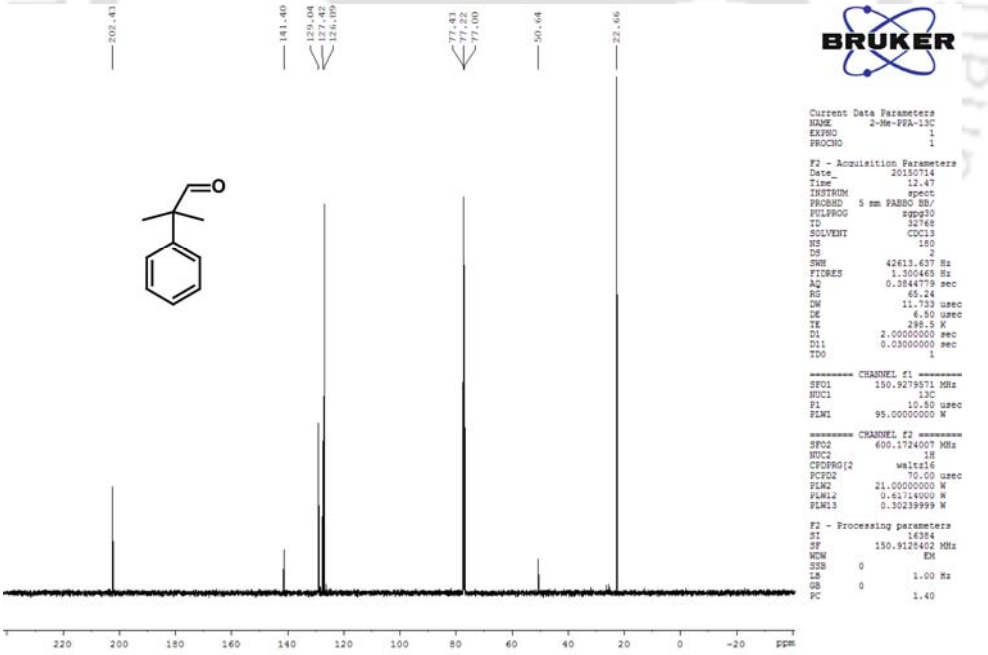

Figure 4.10. ^{13}C NMR spectrum of 2-methyl-2-phenylpropionaldehyde.

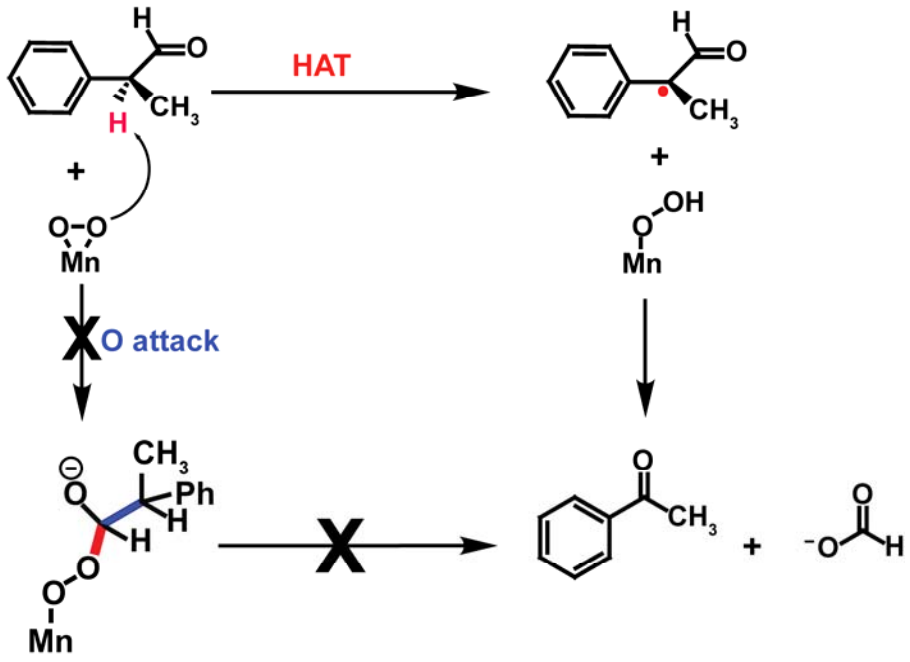

Scheme 4.3. Proposed mechanism for the deformylation reaction of 2-PPA by manganese(III)-peroxo complex.

4.4 Conclusion

Manganese(III)-peroxo complex with a pentadentate bispidine ligand system has been synthesized and characterized and studied its reactivity with aldehydes. Manganese(III)-peroxo can react through hydrogen atom abstraction reactions instead of the commonly proposed nucleophilic addition reaction. Evidence of the mechanism comes from experiments which identify a primary kinetic isotope effect of 5.4 for the deformylation reaction. For the help of density functional theory (DFT), found that the side-on manganese-peroxo with bispidine ligand system will preferentially react via hydrogen atom abstraction rather than nucleophilic addition with aldehydes through its availability of low-energy metal 3d orbitals that can pick up an electron from the peroxo group.[42]

4.5 References

1. *Biomimetic Oxidations Catalyzed by Transition Metal Complexes* (Ed.: B. Meunier), Imperial College Press, London, **2000**.
2. *Cytochrome P450: Structure, Mechanism, and Biochemistry*, 3rd ed. (Ed.: P. R. Ortiz de Montellano), Kluwer Academic/Plenum Publishers, New York, **2005**.
3. D. J. Vinyard, G. M. Ananyev, G. C. Dismukes, *Annu. Rev. Biochem.* **2013**, *82*, 577–606.
4. G. Renger, T. Renger, *Photosynth. Res.* **2008**, *98*, 53–80.
5. J. Barber, *Quart. Rev. Biophys.* **2003**, *36*, 71–89.
6. P. E. M. Siegbahn, *Chem. Eur. J.* **2008**, *14*, 8290–8302.
7. T. A. Jackson, T. C. Brunold, *Acc. Chem. Res.* **2004**, *37*, 461–470.
8. B. R. Streit, B. Blanc, G. S. Lukat–Rodgers, K. R. Lukat-Rodgers, J. L. Dubois, *J. Am. Chem. Soc.* **2010**, *132*, 5711–5724.
9. S. Hofbauer, C. Gruber, K. F. Pirker, A. Sündermann, I. Schaffner, C. Jakopitsch, C. Oostenbrink, P. G. Furtmüller, C. Obinger, *Biochemistry* **2014**, *53*, 3145–3157.
10. M. Costas, M. P. Mehn, M. P. Jensen, L. Que Jr., *Chem. Rev.* **2004**, *104*, 939–986.
11. P. C. A. Bruijnincx, G. van Koten, R. J. M. Klein Gebbink, *Chem. Soc. Rev.* **2008**, *37*, 2716–2744.
12. M. M. Abu-Omar, A. Loaiza, N. Hontzeas, *Chem. Rev.* **2005**, *105*, 2227–2252.
13. S. V. Kryatov, E. V. Rybak–Akimova, S. Schindler, *Chem. Rev.* **2005**, *105*, 2175–2226.

14. G. Roelfes, V. Vrajmasu, K. Chen, R. Y. N. Ho, J.–U. Rohde, C. Zondervan, R. M. la Crois, E. P. Schudde, M. Lutz, A. L. Spek, R. Hage, B. L. Feringa, E. Münck, L. Que Jr., *Inorg. Chem*. **2003**, *42*, 2639–2653.
15. J. Annaraj, Y. Suh, M. S. Seo, S. O. Kim, W. Nam, *Chem. Commun*. **2005**, 4529–4531.
16. A. Thibon, J.–F. Bartoli, S. Bourcier, F. Banse, *Dalton Trans*. **2009**, 9587–9584.
17. A. Mukherjee, M. A. Cranswick, M. Chakrabarti, T. K. Paine, K. Fujisawa, E. Münck, L. Que Jr., *Inorg. Chem*. **2010**, *49*, 3618–3628.
18. J. Cho, S. Jeon, S. A. Wilson, L. V. Liu, E. A. Kang, J. J. Braymer, M. H. Lim, B. Hedman, K. O. Hodgson, J. S. Valentine, E. I. Solomon, W. Nam, *Nature* **2011**, *478*, 502–505.
19. J. Annaraj, J. Cho, Y.–M. Lee, S. Y. Kim, R. Latifi, S. P. de Visser, W. Nam, *Angew. Chem. Int. Ed*. **2009**, *48*, 4150–4153.
20. D. F. Leto, S. Chattopadhyaay, V. W. Day, T. A. Jackson, *Dalton Trans*. **2013**, *42*, 13014–13025.
21. M. Zlatar, M. Gruden, O. Y. Vassilyeva, E. A. Buvaylo, A. N. Ponomarev, S. A. Zvyagin, J. Wosnitza, J. Krzystek, P. Garcia-Fernandez, C. Duboc, *Inorg. Chem*. **2016**, 1192–1201.
22. C.–M. Lee, C.–H. Chuo, C.–H. Chen, C.–C. Hu, M.–H. Chiang, Y.–J. Tseng, C.–H. Hu, G.–H. Lee, *Angew. Chem. Int. Ed*. **2012**, *51*, 5427–5430.
23. W. Nam, *Acc. Chem. Res*. **2007**, *40*, 522–531.
24. M. K. Coggins, J. A. Kovacs, *J. Am. Chem. Soc*. **2011**, *133*, 12470–12473.

25. M. K. Coggins, V. Martin–Diaconescu, S. DeBeer, J. A. Kovacs, *J. Am. Chem. Soc*. **2013**, *135*, 4260–4272.
26. H. E. Colmer, A. W. Howcroft, T. A. Jackson, *Inorg. Chem*. **2016**, *55*, 2055–2069.
27. Y. Goto, S. Wada, I. Morishima, Y. Watanabe, *J. Inorg. Biochem*. **1998**, *69*, 241–247.
28. P. Comba, M. Kerscher, W. Schiek, *Prog. Inorg. Chem*. **2007**, *55*, 613–704.
29. P. Comba, S. Fukuzumi, H. Kotani, S. Wunderlich, *Angew. Chem. Int. Ed*. **2010**, *49*, 2622–2625.
30. L^1 = (dimethyl-2,4-di(2-pyridyl)3-(pyridin-2-ylmethyl)-7-benzyl-3,7-diaza-bicyclo[3.3.1] nonan-9-one-1,5-dicarboxylate).
31. P. Barman, A. K. Vardhaman, B. Martin, S. J. Wörner, C. V. Sastri, P. Comba, *Angew. Chem. Int. Ed*. **2015**, *54*, 2095–2099.
32. M. S. Seo, J. Y. Kim, J. Annaraj, Y. Kim, Y.–M. Lee, S.–J. Kim, J. Kim, W. Nam, *Angew. Chem. Int. Ed*. **2007**, *46*, 377–380.
33. R. A. Geiger, S. Chattopadhyay, V. W. Day, T. A. Jackson, *Dalton Trans.* **2011**, *40*, 1707–1715.
34. Y. Goto, S. Wada, I. Morishima, Y. Watanabe, *J. Inorg. Biochem*. **1998**, *69*, 241–247.
35. J. Cho, R. Sarangi, J. Annaraj, S. Y. Kim, M. Kubo, T. Ogura, E. I. Solomon, W. Nam, *Nat. Chem*. **2009**, *1*, 568–572.
36. R. L. Shook, W. A. Gunderson, J. Greaves, J. W. Ziller, M. P. Hendrich, A. S. Borovik, *J. Am. Chem. Soc*. **2008**, *130* , 8888–8889.
37. J. Cho, R. Sarangi, H. Y. Kang, J. Y. Lee, M. Kubo, T. Ogura, E. I. Solomon, W. Nam, *J. Am. Chem. Soc*. **2010**, *132*, 16977–16986.

38. R. V. Ottenbacher, D. G. Samsonenko, E. P. Talsi, K. P. Bryliakov, *ACS Catal*. **2016**, *6*, 979–988.
39. J. A. Kovacs, *Acc. Chem. Res*. **2015**, *48*, 2744–2753.
40. J. T. Groves, T. E. Nemo, *J. Am. Chem. Soc.* **1983**,*105*, 6243–6248.
41. S. Rana, A. Dey, D. Maiti, *Chem. Commun.* **2015**, *51*, 14469–14472.
42. P. Barman**,** P. Upadhyay, A. S. Faponle, J. Kumar, S. S. Nag, D. Kumar, C. V. Sastri, S. P. de Visser, *Angew. Chem. Int. Ed*. **2016**, *55*, 11091–11095.

CHAPTER-V

Influence of Ligand Architecture in Tuning Reaction Bifurcation Pathways for Chlorite Oxidation by Non-Heme Iron Complexes

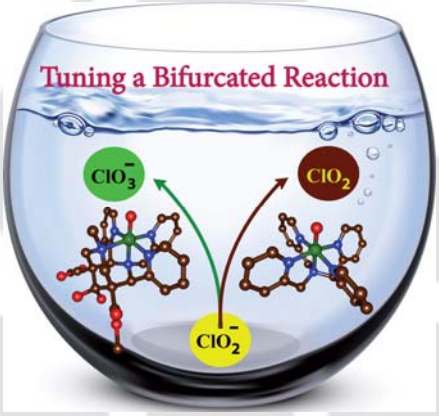

Inorg. Chem. **2016**, *55*, 10170–10181.

5.1 Introduction

Iron is ubiquitous in life and has a relatively high abundance. Nature has developed many iron complexes for a multitude of functions ranging from electron transfer and oxygen transport to oxidation catalysis. Therefore, iron enzymes are involved in vital biosynthesis and biodegradation processes in the body.[1-3] There are two classes, the heme and non-heme iron enzymes. The former have an array of biochemical functions ranging from enzymatic catalysis (monoxygenases, e.g., the cytochromes P450),[4-9] and detoxification by peroxidases and catalases,[10-14] to oxygen transport (hemoglobin)[15, 16] and electron transfer (e.g., cytochrome *c*).[17-22] Non-heme iron proteins acts as dioxygenases in the metabolism of cysteine,[23-26] DNA base repair[27-31] and biosynthesis pathways,[32-34] e.g., hydroxyproline. Finally, metal clusters, such as iron-sulfur clusters, are involved in electron transfer, whereby they relay electrons between a redox partner to a catalytically active site of an enzyme.[35, 36] Often iron containing biomolecules can react via several possible reaction channels leading to bifurcation pathways of which the product distributions are dependent on the structure and chemical properties of the metal centre.

A common approach in mechanistic bioinorganic chemistry is to synthesize a biomimetic model that shares key structural and electronic features and study short-lived intermediates relevant to the enzymatic catalytic cycle,[37-41] to probe the effects of the protein, the local environment and the nature of the transition metal center.[42-44] A common problem associated with biomimetic oxidants is that they may react via multiple reaction channels leading to bifurcation pathways. In biotechnology, bifurcation often is to be avoided and hence, understanding the chemical origin and nature of bifurcation pathways is essential.

Several examples on modifying bifurcation mechanisms and their corresponding product distributions and regioselectivities have been described. For instance, Fukuzumi and co-workers[45] investigated the electron transfer versus oxygen atom transfer mechanisms of a non-heme iron(IV)-oxo complex and found the former to be enhanced by the addition of perchloric acid. Nam et al.[46] showed that by replacing the axial ligand in an iron(IV)-oxo porphyrin cation radical model, a regioselectivity change from aromatic to aliphatic hydroxylation of ethylbenzene occurred. Clearly, subtle changes to the active oxidant or its environment affect the regioselectivity and bifurcation of the reaction processes and consequently the product distributions.

Investigated a biomimetic non-heme iron model, $[Fe^{II}(N4Py)]^{2+}$ with N4Py = N,N-bis(2-pyridylmethyl)-bis(2-pyridyl)methylamine (Figure 1), and reacted it with terminal oxidants to form the corresponding iron(IV)-oxo and iron(IV)-tosylimido complexes very recently.[47, 48] It was shown that the system reacted by competitive electron transfer or atom transfer with substrates. To gain further insight into bifurcation pathways between electron and atom transfer processes, decided to look into an environmentally relevant reaction, namely the detoxification of ClO_2^- in drinking water. Chlorine oxides (ClO_x^-) are used extensively for cleaning and health care purposes with functions ranging from bleaching to disinfection. The high solubility of chlorine oxides in water and their long lifetime in the environment, however, has resulted in major ecological problems, specifically with drinking water. From an environmental perspective the bioremediation of ClO_x^- from water supplies is performed efficiently by perchlorate respiring bacteria. These achieve this reactivity using two enzymes, perchlorate reductase, which catalyzes the conversion of perchlorate to chlorate and subsequently to chlorite, and chlorite dismutase that converts chlorite to chloride (Cl^-) and molecular oxygen (O_2).[49-53] Chlorite dismutase, however, is an

iron-heme enzyme and little is known of non-heme iron centers for the activation of chlorine oxides. Therefore, decided to investigate non-heme iron complexes and their reactivity with ClO_2^-. To further understand the nature of bifurcation pathways, two types of iron(II) precatalysts with N4Py as well as a pentadentate bispidine as ligands (dimethyl 2,4-di(2-pyridyl)3-(pyridin-2-ylmethyl)-7-methyl-3,7-diazabicyclo [3.3.1]nonan-9-one-1,5-dicarboxylate, L^1) has been used.[54] $[Fe^{II}(L^1)]^{2+}$ complex because it is known to react efficiently with thioanisoles to form sulfoxides with rate constants considerably faster than those obtained for $[Fe^{II}(N4Py)]^{2+}$.[55] Experimental (kinetics and spectroscopy) study using these iron(IV)-oxo complexes shows dramatic differences in electron transfer versus oxygen atom transfer reactivities. These differences are analyzed in detail and approaches are proposed as to how to modify these oxidants further to target specific products.

5.2 Experimental Section

The ligands (N4Py, L^1 and L^2 = dimethyl 2,4-di(2-pyridyl)-3-methyl-7-(pyridin-2-ylmethyl)-3,7-diazabicyclo[3.3.1] nonan-9-one-1,5-dicarboxylate) were prepared by literature procedures.[56-58] The corresponding $[Fe^{II}(N4Py)(NCCH_3)](OTf)_2$, $[Fe^{II}(L^1)](BF_4)_2$ and $[Fe^{II}(L^2)](BF_4)_2$ were prepared and characterized by purified procedures (Figure 2.2, 2.3 and 2.4).[47, 56, 58] Formation of chlorine dioxide(ClO_2) from sodium chlorite($NaClO_2$) was monitor by the change in absorption spectrum.

5.3 Results and discussions

The disproportionation of ClO_2^-, under the influence of iron(II) complexes, in water was studied with the focus on the product distributions as a function of the ligand structure and electronic characteristics. ClO_2^- can react via

any of several reaction pathways, and as such a variety of products can be expected, including ClO_2 and ClO_3^-. The reactivities of the iron(II) complexes with ClO_2^-, and subsequently characterize short-lived intermediates formed during the reactions, determine reaction products and identify rate-limiting steps. Computational modeling of the reaction mechanisms and reactivity patterns was performed to rationalize the product distributions and understand the chemical differences between the oxidations.

The reactivity of sodium chlorite with non-heme iron(II) complexes with pentadentate ligands N4Py, L^1 and L^2 was investigated in acetate buffer (50 mM) at pH 5.0 at 25 °C (Figure 5.1).

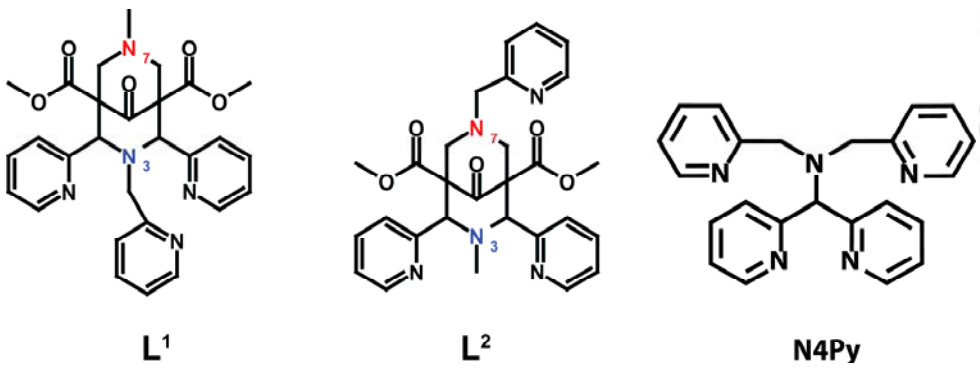

Figure 5.1. Ligands investigated in this work.

Addition of the iron(II) complexes to solutions of sodium chlorite ($NaClO_2$), there is an increase in absorbance at 360 nm, characteristic for the formation of chlorine dioxide.[59] Figure 5.2a shows the spectral changes for the reaction of $[Fe^{II}(L^1)]^{2+}$ with ClO_2^-, whereas those involving the $[Fe^{II}(L^2)]^{2+}$ and $[Fe^{II}(N4Py)]^{2+}$ complexes are given in the Figures 5.3, 5.4 and 5.5, where the same spectral changes are observed. The consumption of chlorite in the process is

monitored by the decrease in absorbance at 260 nm ($\varepsilon_{260} \approx 154\ M^{-1}\ cm^{-1}$) as well as the concomitant formation of ClO_2 as measured through the increase in absorption at 360 nm ($\varepsilon_{360} \approx 1250\ M^{-1}\ cm^{-1}$).

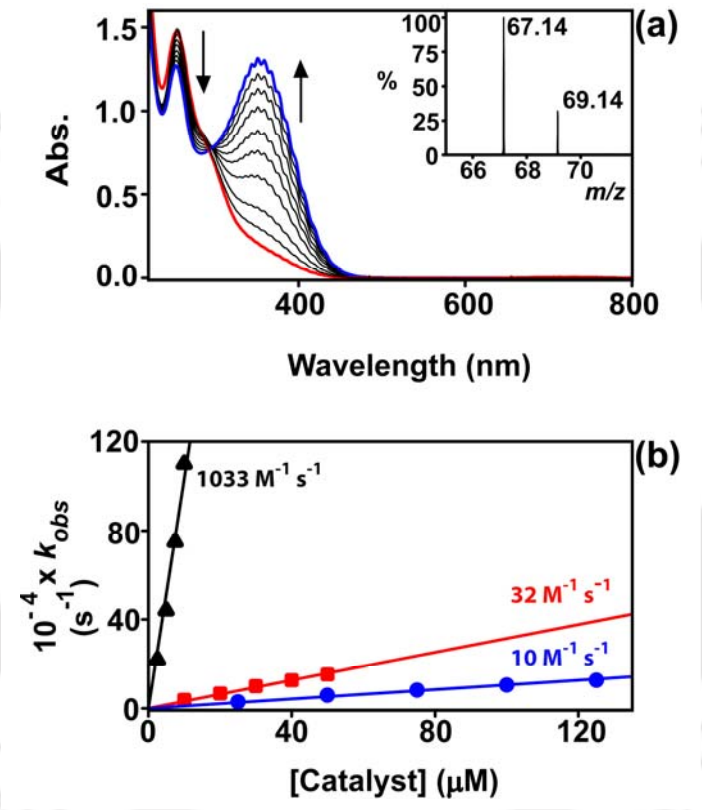

Figure 5.2. Spectroscopic and kinetics studies for the reaction of iron(II) complexes with ClO_2^-. (a) Changes in the UV/Vis absorption spectra at a scan interval of every 180 s upon the addition of 8.0 mM $NaClO_2$ to 50 μM $[Fe^{II}(L^1)]^{2+}$ in an acetate buffer at 25 °C. Inset shows ESI-MS of products obtained. (b) Second order rate constants obtained for the reaction of ClO_2^- with $[Fe^{II}(N4Py)]^{2+}$ (▲), $[Fe^{II}(L^1)]^{2+}$ (●) and $[Fe^{II}(L^2)]^{2+}$ (■).

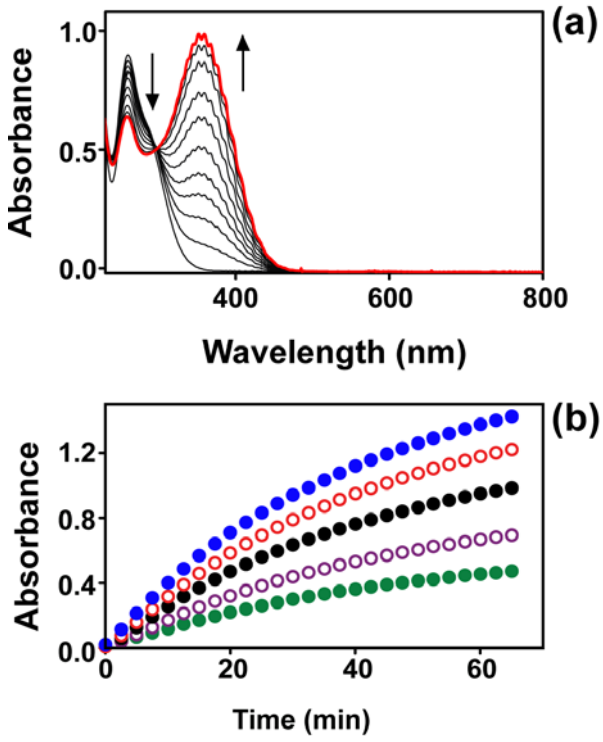

Figure 5.3. a) UV/Vis spectral changes for the reaction of 10 μM $[Fe^{II}(L^2)]^{2+}$ with 8.0 mM $NaClO_2$. Inset shows the time trace for the formation of ClO_2 at 25 °C and pH = 5.0 in acetate buffer. Scan interval was 120 s. (b) Absorbance changes at 360 nm as a function of time. Reaction conditions: $[Fe^{II}(L^2)]^{2+}$ = 10 μM; $[ClO_2^-]$ = 12.0, 10.0, 8.0, 6.0, 4.0 mM (top to bottom).

Negative ion mode ESI-MS of a diethyl ether extract of the reaction mixture (Inset of Figure 5.2a) shows a signal with an isotopic pattern consistent with ClO_2 formation (*m/z* = 67.14). The reaction reaches a maximum in conversion within 40 min with oxidant loading of 10 μM at 25 ºC and pH=5.0.

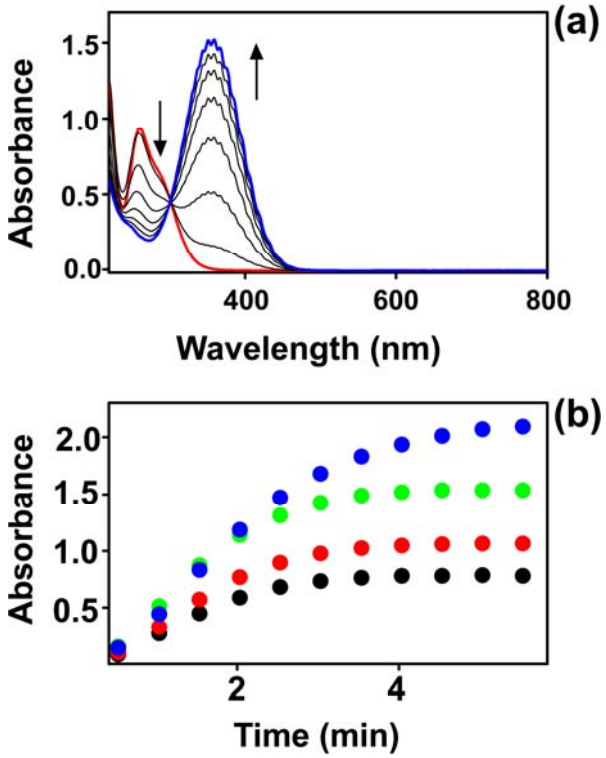

Figure 5.4. a) UV/Vis spectral changes for the reaction of 10 μM $[Fe^{II}(N4Py)]^{2+}$ with 8.0 mM $NaClO_2$. Inset shows the time trace for the formation of ClO_2 at 25 °C and pH = 5.0 in acetate buffer. Scan interval was 30 s. (b) Formation of ClO_2 versus time. Experimental conditions: $[Fe^{II}(N4Py)]^{2+}$ = 10 μM; $[ClO_2^-]$ = 10.0, 8.0, 6.0, and 4.0 mM (top to bottom).

The first-order rate constants as a function of oxidant concentration (Figure 5.2b, Table 5.1) for the reaction of ClO_2^- with $[Fe^{II}(N4Py)]^{2+}$, $[Fe^{II}(L^1)]^{2+}$ and $[Fe^{II}(L^2)]^{2+}$ were determined. The second-order rate constants of k_2 = 10 M^{-1} s^{-1} and 32 M^{-1} s^{-1}, respectively, for $[Fe^{II}(L^1)]^{2+}$ and $[Fe^{II}(L^2)]^{2+}$ (Figure 5.2b) were determined from the dependence of the rate of generation of ClO_2 on the initial concentrations of the iron(II) complexes. These reaction rates correspond to a

maximum yield of 13 and 10 % with respect to iron for $[Fe^{II}(L^1)]^{2+}$ and $[Fe^{II}(L^2)]^{2+}$, respectively. Our results contradict previous substrate sulfoxidation studies by $[Fe^{II}(L^1)]^{2+}$ and $[Fe^{II}(L^2)]^{2+}$, in which the latter was 100 times more reactive, whereas it reacts 40 times faster in hydrogen atom abstraction reactions.[55]

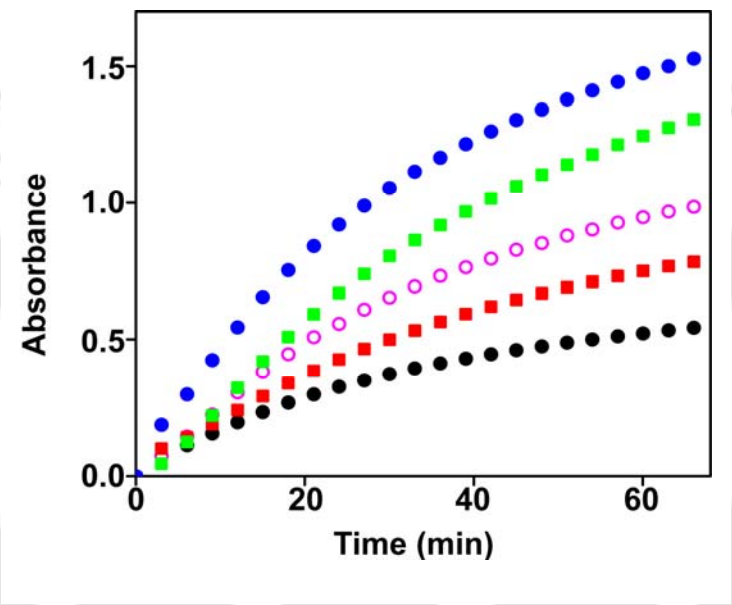

Figure 5.5. Formation of ClO_2 versus time. Experimental conditions: $[Fe^{II}(L^1)]^{2+}$ = 50 μM; $[ClO_2^-]$ = 10.0, 8.0, 6.0, 4.0, and 2.0 mM (top to bottom).

Table 5.1. kinetic and efficiency data for the oxidation of ClO_2^- in aqueous acetate buffer at 25 ºC.

Complex	k_2 ($M^{-1}s^{-1}$)	% ClO_2	TON
$[Fe^{II}(L^1)]^{2+}$	10	13	300
$[Fe^{II}(L^2)]^{2+}$	32	10	775
$[Fe^{II}(N4Py)]^{2+}$	1033	16	2796

In comparison to the bispidine-type complexes, addition of 10 μM $[Fe^{II}(N4Py)]^{2+}$ to chlorite (4 mM) resulted in the immediate appearance of an absorption band at 360 nm; characteristic of the formation of chlorine dioxide. The absorbance at 360 nm reaches a maximum with a second order rate constant of 1033 M^{-1} s^{-1} and an overall yield of 16% of ClO_2. As such, the $[Fe^{II}(N4Py)]^{2+}$ complex reacts with rate constants that are at least 30 times higher than the fastest reacting bispidine complex. The yield of the ClO_2 obtained here is in the line with previous studies of analogous manganese and ruthenium catalysts.[60-62]

Identification of the formation of intermediates such as $Fe^{IV}(O)$ species could provide insight into the reaction mechanism between the iron(II) complexes with ClO_2^-. Recent studies on the reactivity of non-heme manganese(II) complexes with ClO_2^- showed that oxygen atom transfer occurred to form a manganese(IV)-oxo species and ClO^-. The corresponding iron(IV)-oxo complexes $[Fe^{IV}(O)(L^1)]^{2+}$, $[Fe^{IV}(O)(L^2)]^{2+}$ and $[Fe^{IV}(O)(N4Py)]^{2+}$ have been

characterized previously with UV/Vis absorption, resonance Raman, EPR and mass spectrometric methods.[63,64]

Figure 2.10 and 2.16 shows the UV/Vis absorption and mass spectrometric characterization of the iron(IV)-oxo species $[Fe^{IV}(O)(L^1)]^{2+}$, and the corresponding spectra for the systems with ligands L^2 and N4Py are given in the Figures 2.11, 2.12, 2.17 and 2.18.[55]

Addition of 1.2 equiv of $NaClO_2$ to 1 mM solutions of the iron(II) complexes results in a change in the UV/Vis absorption spectra is observed with a NIR absorption band characteristic of iron(IV)-oxo complexes in near quantitative yields, which was confirmed by ESI-MS analysis: $[Fe^{IV}(O)(L^1)]^{2+}$, $[Fe^{IV}(O)(L^2)]^{2+}$ and $[Fe^{IV}(O)(N4Py)]^{2+}$ with *m/z* values close to the theoretical values were observed. Note that under stoichiometric conditions, the iron(IV)-oxo complex is the sole product of the reaction and ClO_2 is not detected.

The data in Figure 2.10 and 2.16, therefore, provides evidence that the reaction of the iron(II) complexes with ClO_2^- proceeds through the formation of an iron(IV)-oxo intermediate (Eq 1). This iron(IV)-oxo species was characterized for all three pentacoordinated ligand systems and subsequently reacts with another molecule of chlorite through either electron transfer or oxygen atom transfer to form the final products and hence the overall reaction of two molecules of ClO_2^- per iron center.

$$[Fe^{II}]^{2+} + ClO_2^- \rightarrow [Fe^{IV}(O)]^{2+} + ClO^- \qquad \text{(Eq 1)}$$

The reaction of an iron(IV)-oxo species with excess ClO_2^- can leads to products resulting from either electron transfer or oxygen atom transfer, Eq 2 and 3.

$$[Fe^{IV}(O)]^{2+} + ClO_2^- \rightarrow [Fe^{III}(O)]^{+} + ClO_2 \qquad \text{(Eq 2)}$$

$$[Fe^{IV}(O)]^{2+} + ClO_2^- \rightarrow [Fe^{II}]^{2+} + ClO_3^- \qquad \text{(Eq 3)}$$

The ClO_2 content of the reaction mixture after reaction with $[Fe^{II}(L^1)]^{2+}$, $[Fe^{II}(L^2)]^{2+}$ and $[Fe^{II}(N4Py)]^{2+}$ was determined by extraction with diethyl ether followed by ESI-MS analysis.

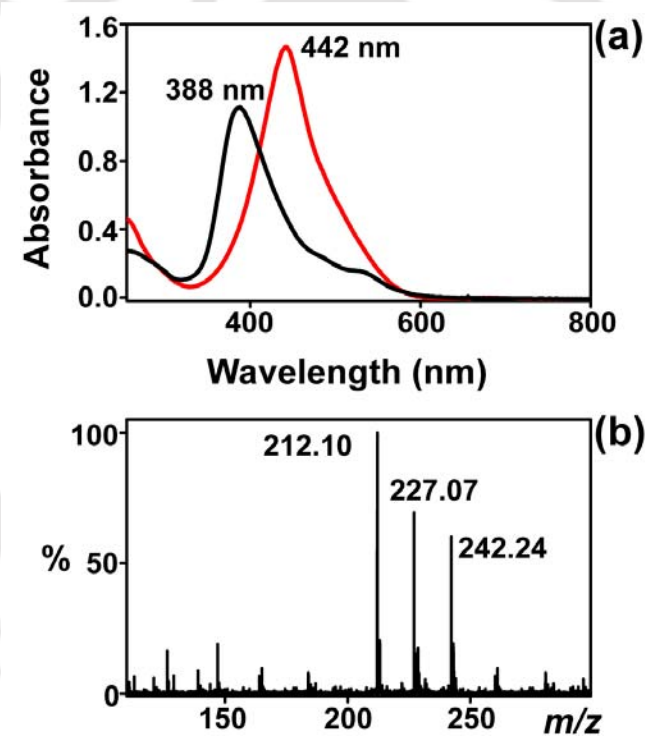

Figure 5.6. (a) UV/Vis absorption spectra of $[Fe^{II}(N4Py)]^{2+}$ (10 μM, 388 nm) and $[Fe^{II}(L^2)]^{2+}$ (10 μM, 442 nm) after reaction with 4.0 mM $NaClO_2$ with *o*-tolidine (40 μM) in acetate buffer. (b) ESI-MS spectra of products obtained from the reaction of $NaClO_2$ with $[Fe^{II}(L^2)]^{2+}$.

The content of ClO_3^- in the product mixture was determined using *o*-tolidine, as described elsewhere.[65] It should be noted that *o*-tolidine reacts with ClO_3^- but not with either ClO_2^- or ClO_2. Reaction of the iron(II) bispidine complexes with $NaClO_2$ in acetate buffer in the presence of *o*-tolidine at ambient temperature results in the appearance of a band at 442 nm corresponding to 3,3′-dimethyl-4-amino-4′-nitrobiphenyl (Figure 5.6a). The ESI-MS spectrum (after extraction) shows a signal at m/z 242.24 corresponding to the oxidized product. In addition, a signal at *m/z* = 227.07 corresponding to the partially oxidized nitroso intermediate is observed (Figure 5.6b). The reactions involved and products obtained are summarized in Scheme 5.1.

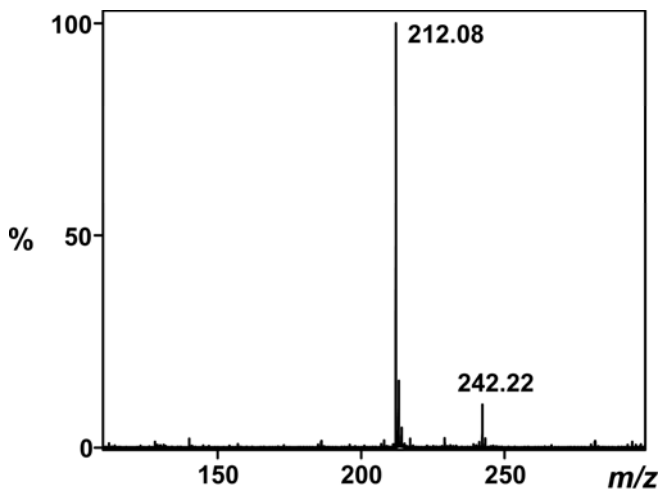

Figure 5.7. ESI-MS spectra of products obtained from the reaction of $NaClO_2$ with $[Fe^{II}(N4Py)]^{2+}$ in presence of *o*-tolidine.

In contrast, the reaction with $[Fe^{II}(N4Py)]^{2+}$ did not result in the formation of products associated with the reaction of *o*-tolidine with ClO_3^-. Instead a peak at 388 nm was observed in the UV/Vis absorption spectrum indicating the presence of ferric species.[22] ESI-MS analysis of the organic extracted phase did not show significant formation of the nitro derivate, which may be a consequence of subsequent reaction in the oxidation of ClO_2^-(Figure 5.7). Hence, the bispidine based complexes, $[Fe^{II}(L^1)]^{2+}$ and $[Fe^{II}(L^2)]^{2+}$, react via oxygen atom transfer processes with the formation of ClO_3^- products as the dominant pathway, whereas $[Fe^{II}(N4Py)]^{2+}$ reacts to yield ClO_2 and related products through a one-electron transfer process.

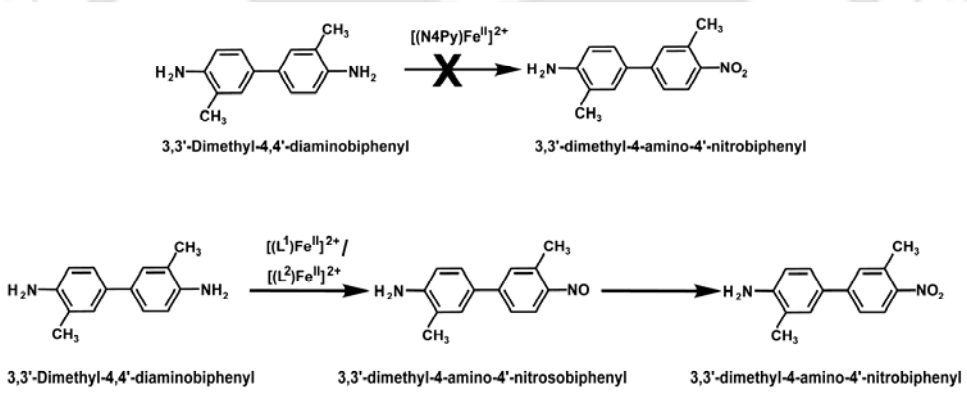

Scheme 5.1. Reaction of *o*-tolidine with iron(II) complexes.

5.4 Conclusion

In summary, first experimental results of detoxification of chlorite to chlorine dioxide selectively has been studied. With the help of Density functional theory, found that the reaction can proceed via competitive pathways (oxygen atom transfer as well as proton coupled electron transfer), whereby the nature of the ligand system and its binding affinity of ClO_x^- substrates determine the driving force of each reaction step.There is a iron(IV)-oxo formation in the first step, which can go further reaction with two pathways either oxygen atom transfer or proton coupled electron transfer to give chlorine dioxide. In $[(N4Py)Fe^{II}]^{2+}$ its going mainly via proton coupled electron transfer (PCET) pathway but $[(L^1)Fe^{II}]^{2+}$ and $[(L^2)Fe^{II}]^{2+}$ going via oxygen atom transfer pathway.[66]

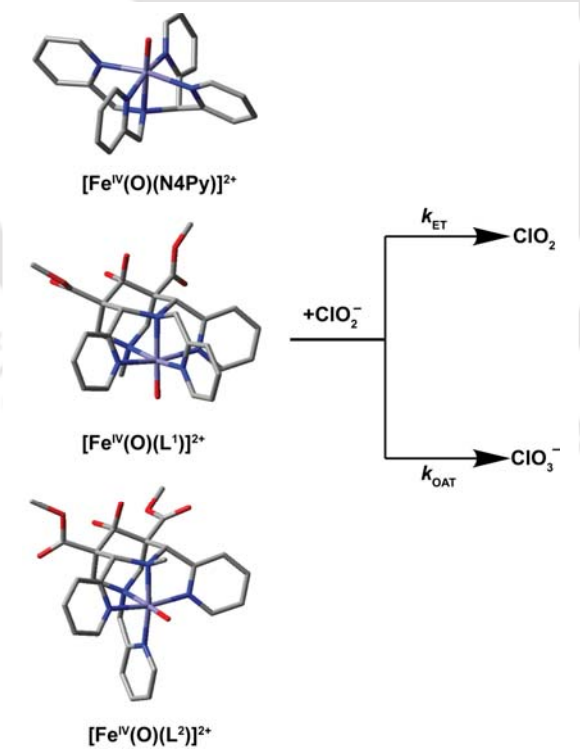

5.5 References

1. D. A. Kraut, K. S. Carroll, D. Herschlag, *Annu. Rev. Biochem*. **2003**, *72*, 517–571.
2. P. W. Atkins, L. Jones, *Chemical Principles*, W. H. Freeman and Co., New York, **2010**.
3. L. A. Moran, H. R. Horton, K. G. Scrimgeour, M. D. Perry, *Principles of Biochemistry*, 5th Ed., Pearson, Boston, **2012**.
4. M. Sono, M. P. Roach, E. D. Coulter, J. H. Dawson, *Chem. Rev*. **1996**, *96*, 2841–2888.
5. J. T. Groves, *Proc. Natl. Acad. Sci. USA* **2003**, *100*, 3569–3574.
6. B. Meunier, S. P. de Visser, S. Shaik, *Chem. Rev*. **2004**, *104*, 3947–3980.
7. *Cytochrome P450: Structure, Mechanism, and Biochemistry*, 3rd ed. (Ed.: P. R. Ortiz de Montellano), Kluwer Academic/Plenum Publishers, New York, **2005**.
8. A. W. Munro, H. M. Girvan, K. J. McLean, *Nat. Prod. Rep*. **2007**, *24*, 585–609.
9. G. Grogan, *Curr. Opin. Chem. Biol.* **2011**, *15*, 241–248.
10. E. L. Raven, *Nat. Prod. Rep*. **2003**, *20*, 367–381.
11. M. Alfonso–Prieto, X. Biarnés, P. Vidossich, C. Rovira, *J. Am. Chem. Soc*. **2009**, *131*, 11751–11761.
12. J. Colin, B. Wiseman, J. Switala, P. C. Loewen, A. Ivancich, *J. Am. Chem. Soc*. **2009**, *131*, 8557–8563.
13. *Handbook of Porphyrin Science* (Ed.: K. M. Kadish, K. M. Smith, R. Guilard), World Scientific Publishing Co., New Jersey, **2010**.
14. T. L. Poulos, *Chem. Rev*. **2014**, *114*, 3919–3962.

15. B. Giardina, I. Messana, R. Scatena, M. Castagnola, *Crit. Rev. Biochem. Mol. Biol.* **1995**, *30*, 165–196.
16. C. Rivetti, A. Mozzarelli, G. L. Rossi, E. R. Henry, W. A. Eaton, *Biochemistry* **1993**, *32*, 2888–2906.
17. H. B. Gray, J. R. Winkler, *Annu. Rev. Biochem*. **1996**, *65*, 537–561.
18. L. Quintanar, C. Stoj, A. B. Taylor, P. J. Hart, D. J. Kosman, E. I. Solomon, *Acc. Chem. Res*. **2007**, *40*, 445–452.
19. P. E. M. Siegbahn, M. R. A. Blomberg, *Chem. Rev*. **2010**, *110*, 7040–7061.
20. D. R. Weinberg, C. J. Gagliardi, J. F. Hull, C. F. Murphy, C. A. Kent, B. C. Westlake, A. Paul, D. H. Ess, D. G. McCafferty, T. J. Meyer, *Chem. Rev*. **2012**, *112*, 4016–4093.
21. Y.–L. P. Ow, D. R. Green, Z. Hao, T. W. Mak, *Nature Mol. Cell Biol.* **2008**, *9*, 532–542.
22. S. Yoshikawa, A. Shimada, *Chem. Rev*. **2015**, *115*, 1936–1989.
23. G. D. Straganz, B. Nidetzky, *Chem. Bio. Chem.* **2006**, *7*, 1536–1548.
24. *Iron-Containing Enzymes: Versatile Catalysts of Hydroxylation Reaction in Nature*, (Ed.: S. P. de Visser, D. Kumar), RSC Publishing, Cambridge, UK, **2011**.
25. M. R. A. Blomberg, T. Borowski, F. Himo, R.–Z. Liao, P. E. M. Siegbahn, *Chem. Rev*. **2014**, *114*, 3601–3658.
26. E. P. Tchesnokov, M. Fellner, E. Siakkou, T. Kleffmann, L. W. Martin, S. Aloi, I. L. Lamont, S. M. Wilbanks, G. N. L. Jameson, *J. Biol. Chem*. **2015**, *290*, 24424–24437.
27. S. C. Trewick, T. F. Henshaw, R. P. Hausinger, T. Lindahl, B. Sedgwick, *Nature* **2002**, *419*, 174–178.
28. P. Ø. Falnes, R. F. Johansen, E. Seeberg, *Nature* **2002**, *419*, 178–182.

29. P. J. O'Brien, *Chem. Rev*. **2006**, *106*, 720–752.
30. C. Yi, C. G. Yang, C. He, *Acc. Chem. Res*. **2009**, *42*, 519–529.
31. H. Liu, J. Llano, J. W. Gauld, *J. Phys. Chem. B* **2009**, *113*, 4887–4898.
32. M. Wu, H.–S. Moon, T. P. Begley, J. Myllyharju, K. I. Kivirikko, *J. Am. Chem. Soc*. **1999**, *121*, 587–588.
33. L. M. Hoffart, E. W. Barr, R. B. Guyer, J. M. Bollinger Jr., C. Krebs, *Proc. Natl. Acad. Sci. USA* **2006**, *103*, 14738–14743.
34. A. Seifert, D. M. Katschinski, S. Tonack, B. Fischer, A. N. Santos, *Chem. Res. Toxicol*. **2008**, *21*, 341–348.
35. D. C. Johnson, D. R. Dean, A. D. Smith, M. K. Johnson, *Annu. Rev. Biochem.* **2005**, *74*, 247–281.
36. A. N. Volkov, *Acc. Chem. Res*. **2015**, *48*, 3036–3043.
37. M. Costas, *Coord. Chem. Rev*. **2011**, *255*, 2912–2932.
38. P. C. A. Bruijnincx, G. van Koten, R. J. M. Klein Gebbink, *Chem. Soc. Rev*. **2008**, *37*, 2716–2744.
39. S. V. Kryatov, E. V. Rybak–Akimova, S. Schindler, *Chem. Rev*. **2005**, *105*, 2175–2226.
40. A. R. McDonald, L. Que Jr., *Coord. Chem. Rev*. **2013**, *257*, 414–428.
41. W. Nam, Y.–M. Lee, S. Fukuzumi, *Acc. Chem. Res*. **2014**, *47*, 1146–1154.
42. T. H. Parsell, M.–Y. Yang, A. S. Borovik, *J. Am. Chem. Soc*. **2009**, *131*, 2762–2763.
43. P. Comba, M. Kerscher, *Coord. Chem. Rev*. **2009**, *253*, 564–574.
44. D. Sil, F. S. T. Khan, S. P. Rath, *Inorg. Chem*. **2014**, *53*, 11925–11936.
45. J. Park, Y. Morimoto, Y.–M. Lee, W. Nam, S. Fukuzumi, *J. Am. Chem. Soc*. **2012**, *134*, 3903–3911.

46. W. J. Song, Y. O. Ryu, R. Song, W. Nam, *J. Biol. Inorg. Chem*. **2005**, *10*, 294–304.
47. A. K. Vardhaman, P. Barman, S. Kumar, C. V. Sastri, D. Kumar, S. P. de Visser, S. P. *Angew. Chem. Int. Ed*. **2013**, *52*, 12288–12292.
48. E. J. Klinker, T. A. Jackson, M. P. Jensen, A. Stubna, G. Juhász, E. L. Bominaar, E. Münck, L. Que Jr., *Angew. Chem. Int. Ed*. **2006**, *45*, 7394–7397.
49. K. S. Bender, C. Shang, R. Chakraborty, S. M. Belchik, J. D. Coates, L. A. Achenbach, *J. Bacteriol*. **2005**, *187*, 5090–5096.
50. L. M. Steinberg, J. J. Trimble, B. E. Logan, *FEMS Microbiol. Lett*. **2005**, *247*, 153–159.
51. J. A. Mayfield, B. Blanc, K. R. Rodgers, G. S. Lukat–Rodgers, J. L. DuBois, *Biochemistry* **2013**, *52*, 6982–6994.
52. S. Hofbauer, I. Schaffner, P. G. Furtmüller, C. Obinger, *Biotechnol. J.* **2014**, *9*, 461–473.
53. L. M. Dassama, T. H. Yosca, D. A. Conner, M. H. Lee, B. Blanc, B. R. Streit, M. T. Green, J. L. DuBois, C. Krebs, J. M. Bollinger Jr., *Biochemistry* **2012**, *51*, 1607–1616.
54. P. Comba, M. Kerscher, W. Schiek, *Prog. Inorg. Chem*. **2007**, *55*, 613–704.
55. D. Wang, K. Ray, M. J. Collins, E. R. Farquhar, J. R. Frisch, L. Gömez, T. A. Jackson, M. Kerscher, A. Waleska, P. Comba, M. Costas, L. Que Jr., *Chem. Sci.* **2013**, *4*, 282–291.
56. M. Lubben, A. Meetsma, E. C. Wilkinson, B. Feringa, L. Que Jr., *Angew. Chem. Int. Ed. Engl.* **1995**, *34*, 1512–1514.

57. H. Börzel, P. Comba, K. S. Hagen, Y. D. Lampeka, A. Lienke, G. Linti, M. Merz, H. Pritzkow, L. V. Tsymbal, *Inorg. Chim. Acta.* **2002**, *337*, 407–419.

58. M. R. Bukowski, P. Comba, C. Limberg, M. Merz, L. Que Jr., T. Wistuba, *Angew. Chem. Int. Ed*. **2004**, *43*, 1283–1287.

59. T. W. Clapper, W. A. Gale, *Encyclopedia of Chemical Technology*, 2nd Ed. (Ed.: R. E. Kirk, D. F. Othmer), Wiley, New York, **1964**.

60. S. D. Hicks, D. Kim, S. Xiong, G. A. Medvedev, J. Caruthers, S. Hong, W. Nam, M. M. Abu−Omar, M. M. *J. Am. Chem. Soc*. **2014**, *136*, 3680−3686.

61. S. D. Hicks, J. L. Petersen, C. J. Bougher, M. M. Abu−Omar, *Angew. Chem. Int. Ed*. **2011**, *50*, 699–702.

62. Z. Hu, H. Du, W.−L. Man, C.−F. Leung, H. Liang, T.−C. Lau, *Chem. Commun*. **2012**, *48*, 1102–1104.

63. J. Kaizer, E. J. Klinker, N. Y. Oh, J.–U. Rohde, W. J. Song, A. Stubna, J. Kim, E. Münck, W. Nam, L. Que, Jr., *J. Am. Chem. Soc.* **2004**, *126*, 472–473.

64. G. Roelfes, M. Lubben, K. Chen, R. Y. N. Ho, A. Meetsma, S. Genseberger, R. M. Hermant, R. Hage, S. K. Mandal, V. G. Young Jr., Y. Zang, H. Kooijman, A. L. Spek, L. Que Jr., B. L. Feringa, *Inorg. Chem*. **1999**, *38*, 1929–1936.

65. P. Urone, E. Bonde, *Anal. Chem*. **1960**, *32*, 1666–1668.

66. P. Barman, A. S. Faponle, A. K. Vardhaman, D. Angelone, A.–M. Rensland, W. R. Browne, P. Comba, C. V. Sastri, S. P. de Visser, *Inorg. Chem.* **2016**, *55*, 10170–10181.

CHAPTER-VI

Long-Range Electron Transfer Triggers Mechanistic Differences between Iron(IV)-Oxo and Iron(IV)-Imido Oxidants

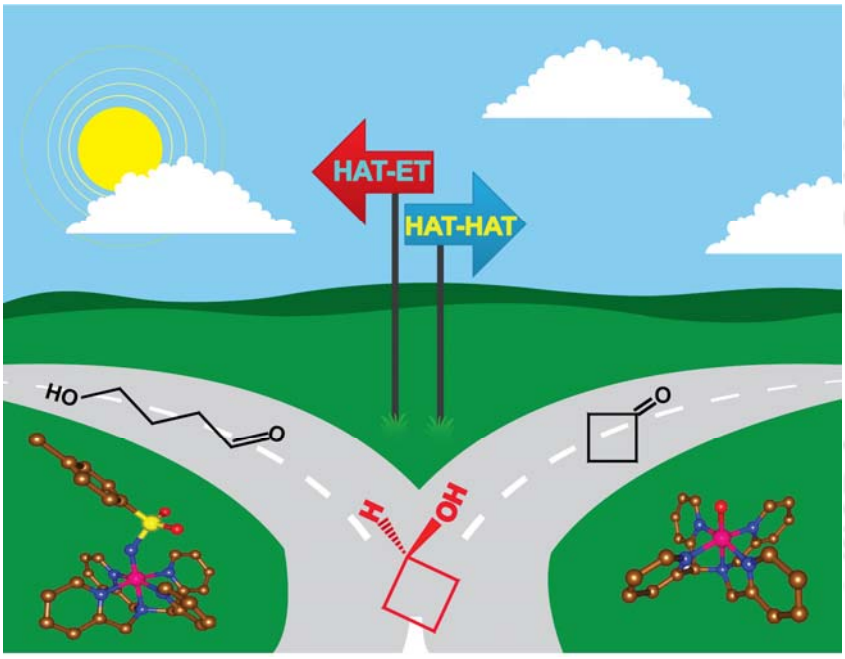

J. Am. Chem. Soc. **2014**, *136*, 17102–17115.

6.1 Introduction

Nature often utilizes molecular oxygen for oxidation reactions through monoxygenases and dioxygenases. In many of these systems a high-valent iron(IV)-oxo active species is found. In recent years evidence has accumulated of possible iron(IV)-imido and iron(V)-nitrido intermediates in enzymatic catalysis, although little is known on their activity.

Monoxygenases and dioxygenases are common enzymes in biology that utilizes molecular oxygen usually on a transition metal center that can either be bound into a heme or non-heme environment.[1-17] A well-studied class of monoxygenases are the cytochromes P450 (P450s) that are found in all forms of life and catalyze the regioselective and stereospecific hydroxylation and epoxidation of substrates. These reactions have important functions in biology that include the biosynthesis of hormones in the liver, as well as the detoxification of metabolites and xenobiotics, such as drug molecules, in the body.[18,19] As such there is interest in understanding their function and mechanism from a pharmaceutical as well as biotechnological viewpoint. The P450s form a high-valent iron(IV)-oxo heme cation radical species in the catalytic cycle that is called Compound I (Cpd I),[20, 21] which is a highly reactive oxidant that reacts with substrates through aliphatic and aromatic hydroxylation, *N*-dealkylation and sulfoxidation reactions.[22, 23]

Despite the fact that lots of research has been devoted to P450 catalysis and synthetic model complexes there are still major gaps in our understanding of its catalytic mechanism and function. For instance, why does nature use molecular oxygen in the catalytic cycle of P450 enzymes and not, for instance, nitrogen, which is more abundant in the atmosphere? Technically, an iron(IV)-imido (Fe^{IV}=NR, R = alkyl) or iron(V)-nitrido (Fe^{V}≡N) complex should be stable intermediates in P450 catalyzed reactions. Moreover, an iron(IV)-imido or

iron(V)-nitrido could be reactive in NR group reactivity to substrates in analogy to Cpd I. Indeed, over the years several examples in P450 catalysis, e.g. in aziridation and imidation reactions, have been reported that include an iron(IV)-nitrido intermediate.[24-26] For an example, the reaction of iron(III)-porphyrin complexes with *N*-tosyliminophenyliodinane (PhINTs) in the presence of olefins led to efficient aziridination of the substrate. More recent work on the amination of substrates by engineered $P450_{BM3}$ enzymes gave several examples of efficient nitrogen group transfer reactions.[27, 28]

Despite being relatively rare in enzymology, actually in inorganic chemistry there are many examples of high-valent metal-imido and metal-nitrido complexes, where they have been shown to be reactive in various processes.[29-31] Bioinspired P450 analogues have been developed to understand the chemical and physical properties of the active species of P450 enzymes.[32-35] In a number of these synthetic complexes an iron-nitrido or iron-imido complex could be formed, spectroscopically characterized and studied for reactivity with selected substrates.[36-39] In addition, studies have been reported on high-valent ruthenium-nitrido porphyrin complexes, which were shown to efficiently activate sp^3 hybridized C–H bonds of substrates.[40]

In more recent work, attention has shifted to non-heme iron and ruthenium based nitrido and imido complexes. These structures range from pentacoordinated to heptacoordinated iron complexes and have been spectroscopically characterized.[41-46] The studies showed that aliphatic substrates with a C–H bond strength similar to that of cyclohexane could be activated efficiently. In addition to mononuclear iron and ruthenium complexes, evidence of diiron(III,IV)-tosylimido complexes has also been reported.[47] Thus, Latour and co-workers observed hydrogen atom abstraction and nitrene transfer reactions by the diiron(III,IV)-tosylimido complex efficiently, whereby the sulfimidation of

para-substituted thioanisoles was found to correlate linearly with the Hammett constant in an electrophilic pathway. The iron(IV)-tosylimido (NTs) complex with pentadentate N4Py ligand (N4Py = *N*,*N*-bis(2-pyridylmethyl)-*N*-bis(2-pyridyl) methylamine) was synthesized by Klinker et al. and spectroscopically characterized with UV/Vis, NMR, EPR, EXAFS and Mössbauer spectroscopies.[48] As the analogous iron(IV)-oxo species is also known, we used the opportunity to study the reactivity of $[Fe^{IV}(O)(N4Py)]^{2+}$ (**6**) versus $[Fe^{IV}(NTs)(N4Py)]^{2+}$ (**7**), against selected substrates.[49] It is found that the iron(IV)-oxo oxidant is more effective in hydrogen atom abstraction reactions, but the iron(IV)-tosylimido species, surprisingly, it is seen to be much more reactive with sulfides. The intricate details of the catalysts that are responsible for these reactivity differences between **6** and **7** could not be established in detail.

6.2 Experimental Section

High-valent iron(IV)-oxo and iron(IV)-imido complexes were generated *in-situ* from 1 mM solution of respective iron(II) complexes. The iron(IV)-oxo complex (**6)** was prepared using 1.5 equiv. of iodosylbenzene (PhIO) as an oxidant in acetonitrile solution at 25 °C. The iron(IV)-imido complex (**7)** was generated in an acetonitrile solution *in-situ* using 1.5 equiv. of PhINTs as tosylimido donor using procedures reported before.[48, 50, 51] Oxidation reactions of benzyl alcohol were followed by monitoring the change in absorption spectrum of the intermediates using UV/Vis spectrophotometer. Second order rate constants were determined by varying the concentration of substrates.

6.3 Results and discussions

$[Fe(N4Py)CH_3CN)](CF_3SO_3)_2$ complex was prepared and characterized as reported earlier.[52] The complex gave ESI-MS peak at *m/z* = 572.03 corresponding to $[Fe^{II}(N4Py)CF_3SO_3]^+$ (Figure 2.4). Intermediates **6** and 7 were generated in an acetonitrile solution *in-situ* using either PhINTs as tosylimido donor or PhIO as oxygen atom donor using procedures reported before.[48, 50, 51] Iron(IV)-oxo complex **6** was confirmed by visible features at low energy 695 nm ($\varepsilon \approx 400\ M^{-1}\ cm^{-1}$) arises from ligand field transitions, which were characteristic for *S* = 1 iron(IV) complexes (Figure 2.18). Electron spray ionization mass spectra (Figure 2.12) shows a major peak at *m/z* = 588.01 which corresponds to $\{[Fe^{IV}(O)N4Py](OTf)\}^+$, an appropriate isotope pattern matched with theoretically stimulated distribution. The identity of iron(IV)-imido complex **7** was confirmed by visible features with an intense LMCT band at 445 nm ($\varepsilon \approx 2700\ M^{-1}\ cm^{-1}$) and a low energy band at 660 nm ($\varepsilon = 250\ M^{-1}\ cm^{-1}$), arises from ligand field transitions characteristic for *S* = 1 iron(IV) complexes (Figure 2.18). The electron spray ionization mass spectrum (Figure 2.13) shows a major peak at *m/z* = 741.07 assigned as $\{[Fe^{IV}(NTs)N4Py](OTf)\}^+$, an appropriate isotope pattern matched with theoretically stimulated distribution.

The reactivity of high-valent iron(IV)–oxo complexes has been extensively studied over the past few decades,[9-17, 32-35, 53] but, by contrast, only very few studies have been reported on its closely related iron(V)–nitrido ($Fe^V{\equiv}N$) or the iron(IV)–imido ($Fe^{IV}{=}NR$) species. The origin and chemical details of the reaction mechanism of iron(IV)–oxo in relation to iron(IV)–imido with substrates are poorly understood, therefore, decided to do a comparative kinetics study on the two complexes. One of the most common reaction mechanisms found for enzymatic iron(IV)–oxo intermediates is hydrogen atom

abstraction (HAT), therefore, studied the reactivity of **6** and **7** with *para*-X-benzyl alcohol.

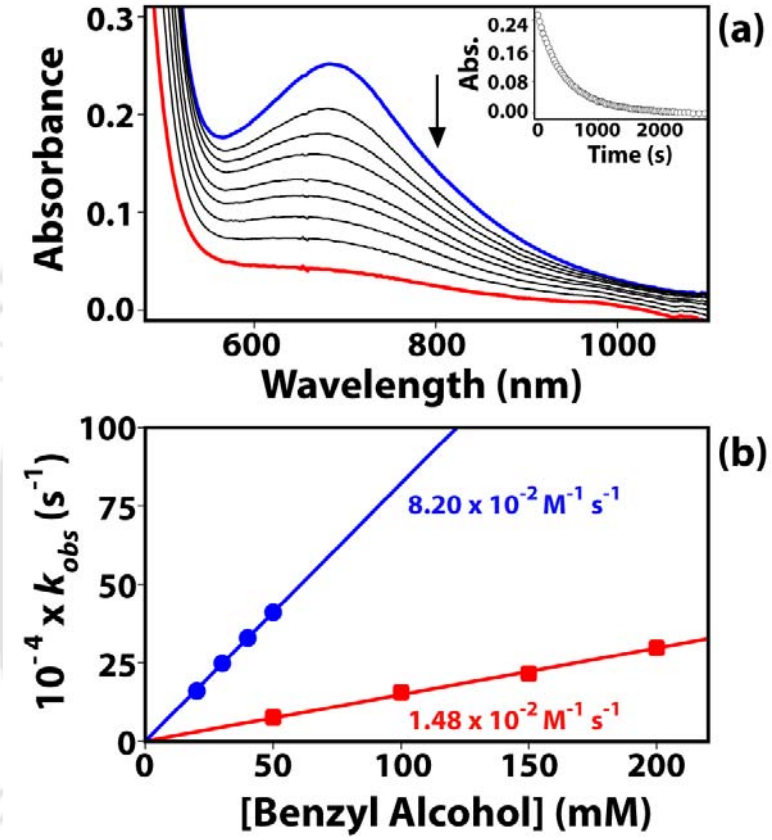

Figure 6.1. UV/Vis spectral changes of **7** (1 mM, blue line) upon the addition of *para*-H-benzyl alcohol (150 equiv. diluted in 50 μL of CH_3CN) in CH_3CN at 25 °C. Inset shows decay profile of 660 nm band. (b) Second-order rate constants determined in the reactions of 1 mM of **6** (●) and **7** (■) in CH_3CN solution against various concentrations of benzyl alcohol at 25 °C.

Complexes **6** and **7** were generated in an acetonitrile solution *in situ* and subsequently substrate was added. Upon addition of substrate to a solution of **6**

and **7**, the intermediates decayed by pseudo-first-order kinetics and the d-d transitions were monitored at 660 nm in the UV/Vis spectrum (Figure 6.1a). The first order rate constants were then plotted as a function of substrate concentration to obtain the second-order rate constants (k_2) of which show the example for *para*-H-benzyl alcohol in Figure 6.1b.

The second order rate constant, k_2, obtained for benzyl alcohol at 25 °C was determined to be 1.48×10^{-2} M^{-1} s^{-1} for $[Fe^{IV}(NTs)(N4Py)]^{2+}$, whereas a value of 8.20×10^{-2} M^{-1} s^{-1} was found for $[Fe^{IV}(O)(N4Py)]^{2+}$. Therefore, the $[Fe^{IV}(O)(N4Py)]^{2+}$ complex reacts with benzyl alcohol with rate constants that are almost six times larger than those found for the $[Fe^{IV}(NTs)(N4Py)]^{2+}$ complex. Similar rate enhancements were found for, e.g., fluorene by **6** and **7**.[49] As such the rate enhancement is not dependent on the HAT donor in these cases and most likely proceeds via the same mechanism.

To gain more insight into the details of the hydrogen atom abstraction mechanism, repeated the experiments with benzyl alcohol-d_7 ($C_6D_5CD_2OH$) and give the comparative second-order rate plots in Figure 6.2. These studies established a kinetic isotope effect (KIE) of 7.0, which is relatively low for typical hydrogen atom abstraction reactions but can still be considered as a rate determining HAT step in the reaction mechanism. In the case of HAT of fluorene by **6** and **7**, also a KIE = 7 for the iron(IV)-tosylimido complex was established, whereas a value of 30 was obtained for the iron(IV)-oxo species. Clearly, there are fundamental differences in reactivity between iron(IV)-oxo and iron(IV)-tosylimido that lead to this dramatic lowering of the kinetic isotope effects. Our studies, reported here are in line with those reported on hydrogen atom abstraction from benzyl alcohol by $[Fe^{IV}(O)(N4Py)]^{2+}$ that also found a large KIE of 48 at 0 °C.[54]

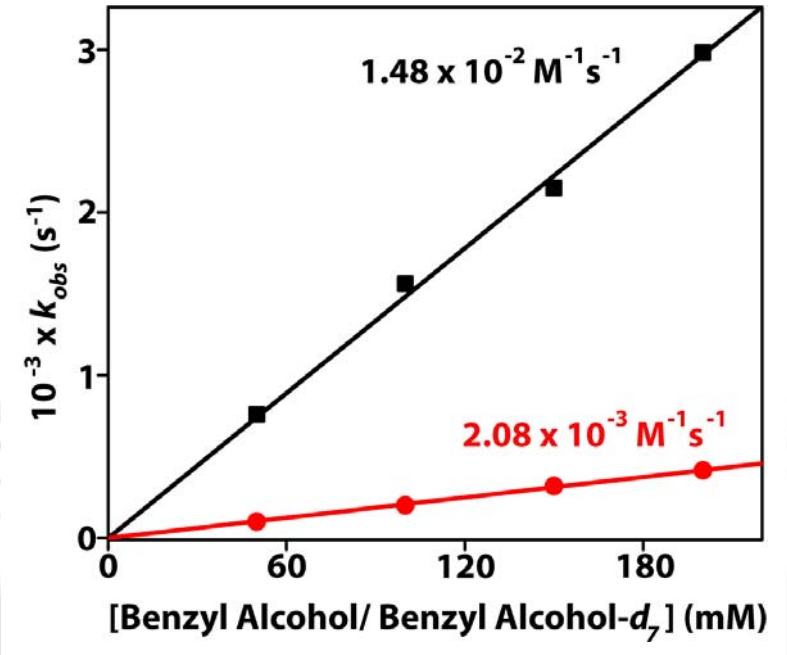

Figure 6.2. Second-order rate constants determined in the reactions of 1 mM $[Fe^{IV}(NTs)(N4Py)]^{2+}$ with benzyl alcohol (■) and benzyl alcohol-d_7 (●) in CH_3CN at 25 °C.

To gain insight into the intrinsic details of the reaction mechanism of benzyl alcohol with **6** and **7**, decided to study *para* substituted benzyl alcohols and create a Hammett plot, see Figure 6.3 and Table 6.1. Reaction of $[Fe^{IV}(O)(N4Py)]^{2+}$ with *para* substituted benzyl alcohol indicates that the reaction rates are not greatly dependent on the *para* substituent and either electron-withdrawing or electron-donating group give similar reaction rates (Figure 6.5). Plot the reaction rate as a function of σ_P of the substituent a small Hammett ρ value ~ –0.1 is found.[54] This clearly indicates that there is no substituent effect in the reaction of $[Fe^{IV}(O)(N4Py)]^{2+}$ with benzyl alcohol.

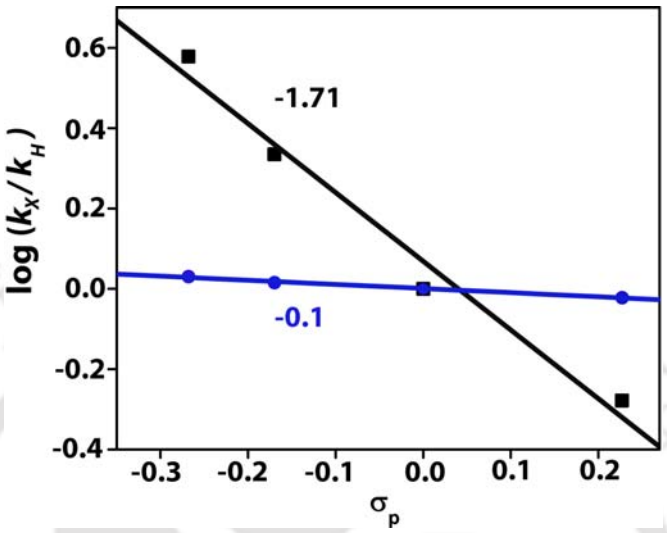

Figure 6.3. Plot of log(k_X/k_H) against σ_p values of *para*-X-benzyl alcohol in reaction with **6** (●) and **7** (■) at 25 °C. The k_X and k_H are the pseudo first order rate constants of *para*-X-benzyl alcohol at 25 °C.

Table 6.1. Pseudo first order rate constants determined reactions of **6** and **7** (1 mM solution) in the presence of *para*-X benzyl alcohol at 25 °C in CH_3CN.

Substituent of *para*-X-Benzyl Alcohol	**σ_p**	**Intermediates**			
		(6)		**(7)**	
		k_2 ($M^{-1} s^{-1}$)	**log(k_X/k_H)**	**k_2 ($M^{-1} s^{-1}$)**	**log(k_X/k_H)**
CH_3O–	–0.268	8.8×10^{-2}	0.031	5.6×10^{-2}	0.577
CH_3–	–0.170	8.5×10^{-2}	0.016	3.2×10^{-2}	0.335
H–	0.0	8.2×10^{-2}	0.00	1.48×10^{-2}	0.00
Cl–	0.227	7.8×10^{-2}	-0.022	7.8×10^{-3}	-0.278

By contrast to the reaction of **6** with benzyl alcohol, the same reaction with **7** gives a dramatic change in substituent effect with a Hammett ρ value of ~ –1.71 (Figure 6.3 and figure 6.4). This large Hammett value indicates that during the hydrogen atom abstraction from the substrate there is a considerable amount of positive charge built-up in the transition state. Most likely it originates from additional stabilization of positive charge on the substrate in the transition state by electron-donating groups in the *para*-position of benzyl alcohol and thereby enhances the overall rate of oxidation. The large Hammett value and low KIE indicates that there is large amount of charge transfer in the rate determining step.[55]

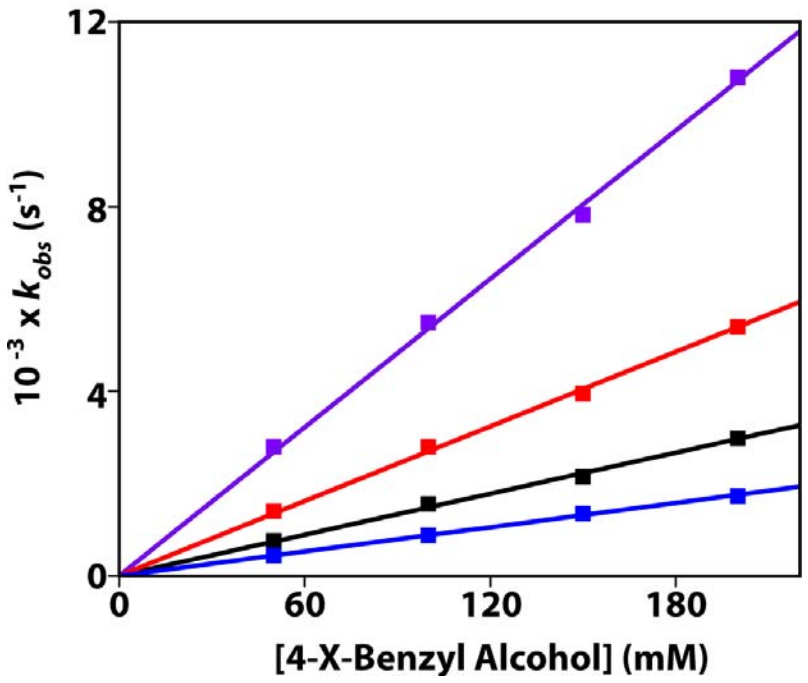

Figure 6.4. Plot of k_{obs} against *para*-X-benzyl alcohol concentration to determine second-order rate constants in the reactions of $[Fe^{IV}(NTs)(N4Py)]^{2+}$ (1 mM) with 4-methoxybenzyl alcohol (Purple), 4-methylbenzyl alcohol (red), benzyl alcohol (black) and 4-chlorobenzyl alcohol (blue) in CH_3CN at 25 °C (from top to bottom).

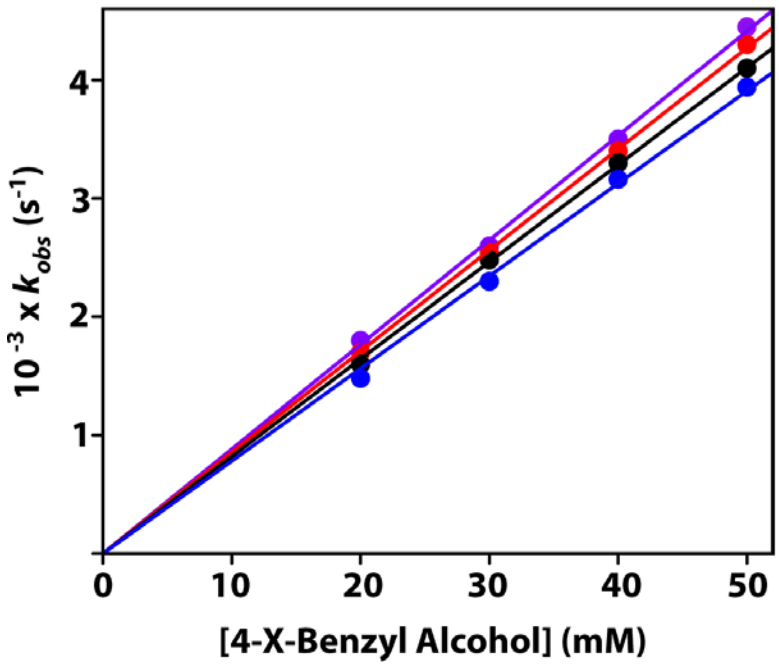

Figure 6.5. Plot of k_{obs} against *para*-X-benzyl alcohol concentration to determine second-order rate constants in the reactions of $[Fe^{IV}(O)(N4Py)]^{2+}$ (1 mM) with *para*-methoxybenzyl alcohol (purple), *para*-methylbenzyl alcohol (red), benzyl alcohol (black) and *para*-chlorobenzyl alcohol (blue) in CH_3CN at 25 °C (from top to bottom).

To unequivocally establish that the rate determining step is indeed one-electron transfer did a subsequent set of experiments with cyclobutanol as mechanistic probe. It has been shown previously that the oxidation of cyclobutanol proceeds through either an initial one-electron or two-electron transfer process, which leads to different products.[54,56-58] Thus, the one-electron transfer reaction is followed by ring-opening of the substrate to give 4-hydroxybutyraldehyde products, whereas the reaction initiated by a two-electron transfer results in the formation of cyclobutanone products (Scheme 6.1). In the

oxidation of cyclobutanol by **7** observed 4-hydroxybutyraldehyde as the major products; hence the reaction of **7** with aliphatic substrates proceeds via a dominant radical pathway. By contrast, cyclobutanol reacts with **6** to yield cyclobutanone products after a specific C–H bond cleavage.[54] This observation in agreement with our earlier observation for the oxidation reaction of fluorene by **6** and **7**, where the latter gives 9,9'-bifluorene as the major product, while with the former fluorenone was obtained.[49]

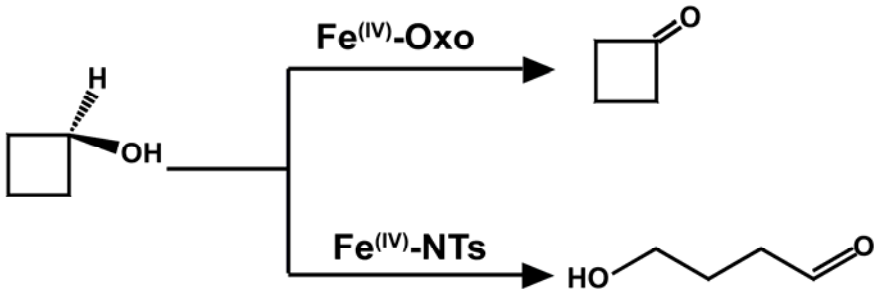

Scheme 6.1. Oxidation of cyclobutanol by $[Fe^{IV}(O)(N4Py)]^{2+}$ (**6**) and $[Fe^{IV}(NTs)(N4Py)]^{2+}$ (**7**) complexes.

6.4 Conclusion

In summary, this chapter present here the first comparative study on the reactivity patterns of non-heme iron(IV)-oxo versus iron(IV)-imido. This chapter explained that due to the larger electron affinity of the oxidant the iron(IV)-imido is a better oxidant of sulfoxidation reactions than iron(IV)-oxo. By contrast, these trends are reversed for stepwise one-electron transfer reactions, such as, hydrogen atom abstraction reactions where stereochemical interactions upon substrate approach determine the relative rate constants. However, the opposite trend is found for HAT reactions from, e.g. *para*-X-benzyl alcohol and fluorene. Subsequent DFT calculations confirmed the experimentally observed trends and gave smaller barriers for HAT by iron(IV)-oxo complexes relative to iron(IV)-imido, whereas the reverse trend is found for heteroatom transfer. The origin of the rate reversal was investigated through a thermochemical analysis of the bond breaking and electron transfer processes. It was found that the electron affinity of $[Fe^{IV}(NTs)(N4Py)]^{2+}$ is so high that it accepts electrons from HAT substrates at a large distance, which was due to differences in orbital interactions as compared to the iron(IV)-oxo species.[59]

6.5 References

1. M. Sono, M. P. Roach, E. D. Coulter, J. H. Dawson, *Chem. Rev*. **1996**, *96*, 2841–2888.
2. J. T. Groves, *Proc. Natl. Acad. Sci. USA* **2003**, *100*, 3569–3574.
3. *Cytochrome P450: Structure, Mechanism, and Biochemistry*, 3rd ed. (Ed.: P. R. Ortiz de Montellano), Kluwer Academic/Plenum Publishers, New York, **2005**.
4. I. G. Denisov, T. M. Makris, S. G. Sligar, I. Schlichting, *Chem. Rev*. **2005**, *105*, 2253–2277.
5. *Handbook of Porphyrin Science*, (Ed.: K. M. Kadish, K. M. Smith, R. Guilard), World Scientific, New Jersey, **2010**.
6. P. R. Ortiz de Montellano, *Chem. Rev*. **2010**, *110*, 932–948.
7. E. O'Reilly, V. Koehler, S. Flitsch, N. Turner, *Chem. Commun*. **2011**, *47*, 2490–2501.
8. G. Grogan, *Curr. Opin. Chem. Biol*. **2011**, *15*, 241–248.
9. E. I. Solomon, T. C. Brunold, M. I. Davis, J. N. Kemsley, S.–K. Lee, N. Lehnert, F. Neese, A. J. Skulan, Y.–S. Yang, J. Zhou, *Chem. Rev*. **2000**, *100*, 235–349.
10. T. D. H. Bugg, *Curr. Opin. Chem. Biol*. **2001**, *5*, 550–555.
11. M. Costas, M. P. Mehn, M. P. Jensen, L. Que Jr., *Chem. Rev*. **2004**, *104*, 939–986.
12. P. C. A. Bruijnincx, G. van Koten, R. J. M. Klein Gebbink, *Chem. Soc. Rev*. **2008**, *37*, 2716–2744.
13. T. D. H. Bugg, S. Ramaswamy, *Curr. Opin. Chem. Biol*. **2008**, *12*, 134–140.
14. M. M. Abu–Omar, A. Loaiza, N. Hontzeas, *Chem. Rev*. **2005**, *105*, 2227–2252.

15. S. V. Kryatov, E. V. Rybak–Akimova, S. Schindler, *Chem. Rev*. **2005**, *105*, 2175–2226.
16. E. G. Kovaleva, J. D. Lipscomb, *Nat. Chem. Biol*. **2008**, *4*, 186–193.
17. P. He, G. R. Moran, *Curr. Opin. Chem. Biol*. **2009**, *13*, 443–450.
18. F. P. Guengerich, *Chem. Res. Toxicol*. **2001**, *14*, 611–650.
19. A. W. Munro, H. M. Girvan, K. J. McLean, *Nat. Prod. Rep*. **2007**, *24*, 585–609.
20. J. Rittle, M. T. Green, *Science* **2010**, *330*, 933–937.
21. *Iron-Containing Enzymes: Versatile Catalysts of Hydroxylation Reaction in Nature*, (Ed.: S. P. de Visser, D. Kumar), RSC Publishing, Cambridge, UK, **2011**.
22. J. T. Groves, *J. Inorg. Biochem*. **2006**, *100*, 434–447.
23. B. Meunier, S. P. de Visser, S. Shaik, *Chem. Rev*. **2004**, *104*, 3947–3980.
24. R. E. White, M. B. McCarthy, *J. Am. Chem. Soc*. **1984**, *106*, 4922–4926.
25. E. W. Svastits, J. H. Dawson, R. Breslow, S. H. Gellman, *J. Am. Chem. Soc*. **1985**, *107*, 6427–6428.
26. J.–P. Mahy, G. Bedi, P. Battioni, D. Mansuy, *J. Chem. Soc. Perkin Trans. II* **1988**, 1517–1524.
27. J. A. McIntosh, P. S. Coelho, C. C. Farwell, Z. J. Wang, J. C. Lewis, T. R. Brown, F. H. Arnold, *Angew. Chem. Int. Ed*. **2013**, *52*, 9309–9312.
28. R. Singh, M. Bordeaux, R. Fasan, *ACS Catal*. **2014**, *4*, 546–552.
29. R. A. Eikey, M. M. Abu–Omar, *Coord. Chem. Rev*. **2003**, *243*, 83–124.
30. J. F. Berry, *Comments Inorg. Chem*. **2009**, *30*, 28–66.
31. C. T. Saouma, J. C. Peters, *Coord. Chem. Rev*. **2011**, *255*, 920–937.
32. M. R. Bukowski, K. D. Koehntop, A. Stubna, E. L. Bominaar, J. A. Halfen, E. Münck, W. Nam, L. Que Jr., *Science* **2005**, *310*, 1000–1002.

33. J.–U. Rohde, J.–H. In, M. H. Lim, W. W. Brennessel, M. R. Bukowski, A. Stubna, E. Münck, W. Nam, L. Que Jr., *Science* **2003**, *299*, 1037–1039.
34. M. Martinho, F. Banse, J.–F. Bartoli, T. A. Mattioli, P. Battioni, O. Horner, S. Bourcier, J.–J. Girerd, *Inorg. Chem*. **2005**, *44*, 9592–9596.
35. C. V. Sastri, M. S. Seo, M. J. Park, K. M. Kim, W. Nam, *Chem. Commun*. **2005**, 1405–1407.
36. C.–M. Che, V. K.–Y. Lo, C.–Y. Zhou, J.–S. Huang, *Chem. Soc. Rev*. **2011**, *40*, 1950−1975.
37. H. Lu, X. P. Zhang, *Chem. Soc. Rev*. **2011**, *40*, 1899−1909.
38. Z. Long, D. Liang, *Chin. Science Bull*. **2012**, *57*, 2352–2360.
39. M. J. Zdilla, J. L. Dexheimer, M. M. Abu–Omar, *J. Am. Chem. Soc*. **2007**, *129*, 11505–11511.
40. P. Zardi, A. Caselli, P. Macchi, F. Ferretti, E. Gallo, *Organometallics* **2014**, *33*, 2210–2218.
41. J. J. Scepaniak, R. P. Bontchev, D. L. Johnson, J. M. Smith, *Angew. Chem. Int. Ed*. **2011**, *50*, 6630–6633.
42. J. Hohenberger, K. Ray, K. Meyer, *Nat. Comm*. **2012**, *3*, 1–13.
43. J. Torres–Alacan, U. Das, A. C. Filippou, P. Vöhringer, *Angew. Chem. Int. Ed*. **2013**, *52*, 12833–12837.
44. Y. Liu, X. Guan, E. L.–M. Wong, P. Liu, J.–S. Huang, C.–M. Che, *J. Am. Chem. Soc*. **2013**, *135*, 7194–7204.
45. W.–L. Man, J. Xie, Y. Pan, W. W.Y. Lam, H.–K. Kwong, K.–W. Ip, S.–M. Yiu, K.–C. Lau, T.–C. Lau, *J. Am. Chem. Soc*. **2013**, *135*, 5533–5536.
46. W.–L. Man, W. W. Y. Lam, H.–K. Kwong, S.–M. Yiu, T.–C. Lau, *Angew. Chem. Int. Ed*. **2012**, *51*, 9101–9104.

47. E. Gouré, F. Avenier, P. Dubourdeaux, O. Sénèque, F. Albrieux, C. Lebrun, M. Clémancey, P. Maldivi, J.–M. Latour, *Angew. Chem. Int. Ed*. **2014**, *53*, 1580–1584.
48. E. J. Klinker, T. A. Jackson, M. P. Jensen, A. Stubna, G. Juhász, E. L. Bominaar, E. Münck, L. Que Jr., *Angew. Chem. Int. Ed*. **2006**, *45*, 7394–7397.
49. A. K. Vardhaman, P. Barman, S. Kumar, C. V. Sastri, D. Kumar, S. P. de Visser, *Angew. Chem. Int. Ed*. **2013**, *52*, 12288–12292.
50. J. Kaizer, E. J. Klinker, N. Y. Oh, J.–U. Rohde, W, J. Song, A. Stubna, J. Kim, E. Münck, W. Nam, L. Que Jr., *J. Am. Chem. Soc*. **2004**, *126*, 472–473.
51. A. K. Vardhaman, C. V. Sastri, D. Kumar, S. P. de Visser, *Chem. Commun*. **2011**, *47*, 11044–11046.
52. M. Lubben, A. Meetsma, E. C. Wilkinson, B. Feringa, L. Que Jr., *Angew. Chem. Int. Ed. Engl.***1995**, *34*, 1512–1515.
53. W. Nam, Y.–M. Lee, S. Fukuzumi, *Acc. Chem. Res*. **2014**, *47*, 1146–1154.
54. N. Y. Oh, Y. Suh, M. J. Park, M. S. Seo, J. Kim, W. Nam, *Angew. Chem. Int. Ed*. **2005**, *44*, 4235–4239.
55. W.–C. Cheng, W.–Y. Yu, C.–K. Li, C.–M. Che, *J. Org. Chem*. **1995**, *60*, 6840–6846.
56. K. Meyer, J. Roček, *J. Am. Chem. Soc*. **1972**, *94*, 1209–1214.
57. O. Pestovsky, A. Bakac, *J. Am. Chem. Soc*. **2004**, *126*, 13757–13764.
58. S. K. Hanson, R. T. Baker, J. C. Gordon, B. L. Scott, L. A. Silks, D. L. Thorn, *J. Am. Chem. Soc*. **2010**, *132*, 17804–17816.
59. S. Kumar, A. S. Faponle, P. Barman, A. K. Vardhaman, C.V. Sastri, D. Kumar, S. P. de Visser, *J. Am. Chem. Soc.* **2014**, *136*, 17102–17115.

Curriculum Vitae

Prasenjit Barman was born at Nadia, West Bengal. His secondary and higher secondary education were at Bethuadahari J. C. M. High School. He obtained his B.Sc (Hons) degree in Chemistry from Kalna College under The University of Burdwan and M.Sc degree in Chemistry from Indian Institute of Technology Guwahati. Under the tutelage of Dr. C. V. Sastri at Indian Institute of Technology Guwahati, he pursued his research exploring the reactivity and mechanistic pathways of high-valent metal intermediates using biomimetic models.